INVESTIGATION OF ACTIVATED WATER HYACINTH (*Eichhornia crassipes*) - BASED ADSORBENTS FOR REMOVAL OF SELECTED HEAVY METALS IN WASTEWATERS FROM THE NAKAWA INDUSTRIAL AREA, KAMPALA

BY

ATUMANYE CLAIRE

22/U/GMCH/091/PE

A DISSERTATION SUBMITTED TO THE DIRECTORATE OF RESEARCH AND GRADUATE TRAINING IN PARTIAL FULFILLMENT OF THE REQUIREMENTS FOR THE AWARD OF DEGREE OF MASTER OF SCIENCE IN CHEMISTRY OF KYAMBOGO UNIVERSITY

APRIL, 2025

DECLARATION

I, **ATUMANYE CLAIRE** hereby declare that this dissertation titled "***INVESTIGATION OF ACTIVATED WATER HYACINTH (Eichhornia crassipes)-BASED ADSORBENTS FOR REMOVAL OF SELECTED HEAVY METALS IN WASTEWATERS FROM THE NAKAWA INDUSTRIAL AREA, KAMPALA***" is my original work and has never been presented for a degree in any other university.

Signature ……..... Date ……

ATUMANYE CLAIRE**.**

APPROVAL

We as supervisors confirm that the dissertation titled "***INVESTIGATION OF ACTIVATED WATER HYACINTH (Eichhornia crassipes)-BASED ADSORBENTS FOR REMOVAL OF SELECTED HEAVY METALS IN WASTEWATERS FROM THE NAKAWA INDUSTRIAL AREA, KAMPALA***" has been done by the candidate under our supervision.

1. **ASSOC. PROF. JUSTUS KWETEGYEKA**

   Department of Chemistry

   Kyambogo University

   Signature: ..... Date: .....

1. **DR. HAKIMU NSUBUGA**

   Department of Chemistry

   Muni University

   Signature: ..... Date: .....

DEDICATION

This work is dedicated to my parents who have instilled in me the value of hard work and perseverance and all the people who have supported me throughout my education.

ACKNOWLEDGEMENT

First, my sincere gratitude goes to God for the continued blessings. Secondly, I acknowledge my supervisors Assoc. Professor Justus Kwetegyeka and Dr. Hakimu Nsubuga for their enormous support and guidance during the research period. Without their help; this project would not have been a success. My heartfelt thanks also go to Ivan Kiganda for his cooperation and assistance in ensuring that I kept the focus. Furthermore, I acknowledge the laboratory personnel, staff and students of the Chemistry department at Kyambogo University for their academic and emotional support.

TABLE OF CONTENTS

LIST OF TABLES

LIST OF FIGURES

LIST OF ABBREVIATIONS

USEPA	United States Environmental Protection Agency
WHO	World Health Organization
H_3PO_4	Phosphoric Acid
EU	European Union
pH	Potential Hydrogen
NEMA	National Environmental Management Authority
$PbSO_4$	Lead Sulphate
PbS	Lead Sulfide
PbCO3	Lead Carbonate
NaOH	Sodium Hydroxide
ppm	Parts per Million
mg g^{-1}	Milligram per Gram
mg L^{-1}	Milligram per Litre
ANOVA	Analysis of Variance
q_e	Measured Adsorbate Concentration at Equilibrium
°C	Degrees Centigrade
H_2SO_4	Sulphuric Acid

ABSTRACT

Industrial activities in the Nakawa Industrial Area, Kampala, have led to the discharge of toxic heavy metals, including Copper (Cu), lead (Pb), cadmium (Cd), chromium (Cr), and Zinc (Zn) into local wastewater streams, posing significant environmental and public health threats. These metals are non-biodegradable, highly toxic, and tend to accumulate in living organisms, leading to long-term health risks. Conventional methods for heavy metal removal, such as chemical precipitation and ion exchange, are often cost-prohibitive, particularly for developing regions, and are ineffective at low metal concentrations. This study investigated the feasibility of using chemically activated water hyacinth (*Eichhornia crassipes*) biomass, an invasive aquatic plant, as a cost-effective and environmentally sustainable adsorbent for the removal of heavy metals from industrial wastewater. Water hyacinth biomass was subjected to chemical activation using both eggshell powder and 0.5 M phosphoric acid (H_3PO_4) followed by thermal treatment in a muffle furnace. Characterization of the activated adsorbent was performed using Fourier Transform Infrared Spectroscopy (FTIR) to identify the surface functional groups and Scanning Electron Microscopy (SEM) to observe the surface morphology, elemental composition and porosity of the adsorbent. The results indicated that chemical activation significantly enhanced the surface properties of the water hyacinth, increasing its porosity and introducing functional groups capable of binding heavy metals. Batch adsorption experiments were conducted to evaluate the adsorbent's capacity for removing Cu, Pb, Cd, Cr and Zn from both synthetic and real industrial wastewater samples. Optimal adsorption conditions were determined by varying key parameters, including particle size, solution pH, contact time and adsorbent mass. The optimal pH for metal removal was found to range from 4.0 to 5.0, with a contact time of 90 minutes and an adsorbent dosage of 1.0 g. Under these conditions, the maximum adsorption capacities for Pb, Cd, Cu, Cr and Zn were 7.26 mg/g, 10.21 mg/g, 5.33 mg/g, 1.04 mg/g and 8.36 mg/g, respectively. Kinetic studies revealed that the adsorption process for Cd^{2+}, Zn^{2+} and Cr^{3+} ions followed a pseudo-second-order kinetic model, indicating chemisorption as the rate-limiting step while, the kinetics of Pb^{2+} and Cu^{2+} were better expressed by the pseudo first order model. The equilibrium data were best described by the Freundlich isotherm model, suggesting multilayer adsorption on heterogeneous surfaces with maximum adsorption occurring at specific sites. When tested with real wastewater samples from the Nakawa Industrial Area, the adsorbent exhibited slightly reduced adsorption efficiencies, with capacities of 7.01 mg/g for Pb, 9.93 mg/g for Cd, 5.20 mg/g for Cu, 1.02 mg/g for Cr and 8.06 mg/g for Zn due to the complex composition of the industrial effluent, which contained competing ions and organic matter. This study demonstrates the effectiveness of activated water hyacinth as a low-cost, sustainable adsorbent for the removal of toxic heavy metals from industrial wastewater. The findings provide a practical solution for addressing both environmental contamination and the management of water hyacinth, which is a persistent invasive species in many parts of the world.

CHAPTER ONE

INTRODUCTION

1.1 Background

Emission of hazardous heavy metals into the biosphere is the outcome of rapid industrialization and urbanization. In underdeveloped nations, industrial effluents are frequently dumped into water bodies without being treated for the contaminants or inorganic elements that are embedded in the majority of wastewater (Zhou *et al*., 2020). Heavy metals are defined as naturally occurring metals with an elemental density of more than 5 g cm^{-3} and an atomic number above 20 (Ali & Khan, 2018). According to Mishra *et al*. (2019), cadmium (Cd), chromium (Cr), copper (Cu), lead (Pb), nickel (Ni), and zinc (Zn) are some of the most typical heavy metal contaminants. Several of these metals are potentially harmful even at extremely low concentrations of ppm posing a major threat to aquatic ecosystems. In addition, heavy metals do not biodegrade and tend to accumulate in living things. Therefore, they can seriously harm both human health and wildlife (Garba *et al*., 2016).

Leaching from waste dumps, contaminated soils, and contaminated water causes these metals to get mobilized and transported into the food chain. The concentration of these metals rises as the food chain moves up, a process known as bio-magnification (Shi *et al*., 2019). When in touch with living beings, heavy metals cause problems and changes in the chemical processes of metabolism that are correlated with the length of exposure and the concentration. For instance, long-term zinc intake can result in hypocupremia, anemia, neutropenia, and leukopenia (Guo & Katta, 2017). Therefore, heavy metal removal is essential to protecting and restoring the ecosystem.

In Uganda, attaining sustainable development goals heavily relies on environmental sustainability and integrity. Several industries fail to properly treat their effluent before releasing it into the

environment, despite legal requirements to do so. This leads to the release of certain pollutants into nearby land and water bodies (NEA, 2019). Thus, adequate wastewater treatment is required to prevent the release of heavy metals and other pollutants. Physical and chemical treatment methods such as ion exchange, membrane filtration, electrochemical treatment, chemical precipitation, coagulation and flocculation are the most widely used conventional processes for the removal of heavy metals. However, these techniques have substantial drawbacks that render them commercially unviable (Kansara *et al*., 2016).

Researchers have recently made an effort to use readily available, reasonably priced industrial solid waste products and biomaterials such as cereal husks, coconut shells and plants in the creation of activated carbon due to its suitability for use as an adsorbent (Acevedo & Barriocanal, 2015; Barakat, 2011). As a result, the effectiveness of water hyacinth as a cost-effective activated adsorbent in the removal of certain heavy metal ions from industrial wastewaters was evaluated in this study. The reason for its use in adsorbent preparation is its high bioaccumulation capability (Rezania *et al*., 2015). Bioaccumulation is known as the net uptake of a pollutant from the environment (Maher *et al*., 2016). The use of water hyacinth for removal of heavy metals in waste water from the Nakawa industrial area is crucial due to the severe health and environmental risks posed by the persistent pollutants in industrial wastewaters, which can accumulate in the ecosystem and harm both humans and aquatic life.

1.2 Problem statement

Metal-contaminated wastewater containing heavy metals like Cd, Cu, Pb, Zn and Cr poses severe health risks, including cancer, growth inhibition, organ and nervous system damage, autoimmune disorders, and developmental issues, necessitating strict treatment measures to protect the environment and future generations. Physical and chemical treatment methods, including chemical

precipitation, gravity settling, flotation, filtration, sorption (e.g., adsorption and ion exchange), membrane processes, electrolytic recovery, and liquid-liquid extraction, are frequently employed for the removal of heavy metals from wastewater. However, these methods can exhibit significant limitations, such as incomplete removal of contaminants, high energy consumption, and the generation of toxic sludge. Among these methods, adsorption is favored due to its simplicity, convenience, and high removal efficiency. Therefore, there is increasing interest in developing adsorbents from various biomaterials for efficient and cost-effective removal of metals from water and wastewater. The utilization of water hyacinth leverages readily available biological material from the environment. This material, requiring minimal to no additional treatment, can significantly contribute to the achievement of the Millennium Development Goals (MDGs), particularly those related to sustainability and environmental preservation, while also serving as a cost-effective adsorbent. Nakawa Industrial area is one of the prominent industrial hubs in Kampala, Uganda characterized by a diverse range of manufacturing industries such as pharmaceutical industries, plastics, mattresses, paints which use heavy metal-based materials in the manufacturing and processing activities. This causes the surrounding areas to be subjected to severe environmental pollution and health risks if the generated wastewater from these industries is released into the environment untreated.

1.3 Objectives

1.3.1 General objective

To investigate the efficiency of water hyacinth-based adsorbents in the removal of selected heavy metals from wastewater collected from the Nakawa industrial area.

1.3.2 Specific objectives

i). To synthesize and characterize various water hyacinth-based adsorbents using Fourier Transform Infrared analysis, Scanning Electron Microscopy and Scanning Electron Microscopy – Energy Disperse X-ray Spectroscopy.

ii). To determine the concentration of selected heavy metals in the wastewater samples

iii). To determine the optimum adsorption conditions for the removal of selected heavy metals (Cd, Cu, Pb, Zn, and Cr) in the wastewater samples.

iv). To determine the adsorption kinetics and isotherm models of Cd, Cu, Pb, Zn, and Cr using the optimized parameters in (iii).

1.4 Justification of the study

The research findings will contribute to the development of cost-effective and sustainable adsorbents for the removal of heavy metals from wastewater. The use of water hyacinth, an abundant and renewable resource, as an adsorbent can also help in mitigating the environmental impact of this invasive aquatic weed thus, putting to usage what has otherwise been condemned. Additionally, water hyacinth being a locally available raw material, it will help in saving the country from expenses associated with the importation of technology and materials for pollution control. One of the activators that was used in this study is eggshell powder and eggshells are readily available in abundance.

CHAPTER TWO

LITERATURE REVIEW

2.1 Overview of water pollution

Water pollution is the introduction of substances or energy forms into a water body that alters its natural characteristics directly or indirectly negatively affecting its lawful usage (Oliveira *et al*., 2021; WHO, 2017). High temperatures, dissolved chemicals, colloidal suspensions, and an unpleasant stench are some of the forms of water pollution (Kant, 2012).

Industrial activities are among the major contributors to water pollution, releasing various pollutants that affect both local and global environments. On a global scale, water pollution remains a pressing issue, posing significant threats to ecosystems, human health, and the sustainability of natural resources (Siddiqua *et al*., 2022). The comprehensive study of river and lake water bodies from 1972 to 2017 highlights the growing concern surrounding heavy metal pollution on a global scale, emphasizing the need for sustained monitoring and intervention (Zhou *et al*., 2020). The local ramifications of water pollution by industries are equally profound.

Industrial processes often release organic and inorganic compounds into effluent water, which eventually contaminates freshwater sources. These compounds can persist in the environment due to their stability and non-biodegradable nature, leading to severe ecological impacts (Shi *et al*., 2019). Among the various pollutants, heavy metals have emerged as some of the most harmful and widespread contaminants. The most common heavy metal pollutants in water bodies include; chromium, lead, zinc, cadmium, copper, mercury, nickel and arsenic (Garai *et al*., 2021).

The health implications of water pollution are extensive and varied. Chemical contamination, like being in contact with heavy metals and organic pollutants, can cause acute and chronic health effects (Mamba & Mishra, 2016). Exposure to contaminated water is also linked to respiratory

diseases, developmental issues in children, and various cancers (Gopinathan, 2023). Furthermore, the health risks are influenced by factors like the concentration of pollutants, duration of exposure, and individual susceptibility (Obinna & Ebere, 2019).

In Uganda, the accelerated industrialization has resulted in heightened water pollution levels, particularly in urban areas where industrial discharges are rampant. The interplay between industrial growth and environmental degradation is a critical area of concern, as the country's water bodies increasingly face contamination from effluents and runoff (Walakira & Okot-Okumu, 2011). According to a study conducted by the Lake Victoria Environmental Management Project's (LVEMP, 2005), Management of Industrial and Municipal Effluents and Urban Run-off component, the majority of factories in Uganda lack effluent treatment plants, and those that do have them are typically poorly built and designed. Few, if any, of the companies with wastewater treatment plants under investigation were meeting effluent discharge regulations.

The study was therefore undertaken to investigate the use of water hyacinth-based adsorbents for removal of selected heavy metals in wastewaters from the Nakawa Industrial area so that remediation measures can be undertaken.

2.2 Heavy metals in wastewater

Heavy metals enter the aquatic environment either naturally, through chemical reactions such as weathering and leaching, or through human activity (Ogunkunle *et al*., 2020). Additionally, the majority of the heavy metal wastes that need to be handled have traditionally been disposed off in the soil, where they can either be absorbed by plants, increasing their chances of making it into the food chain, or they may exist as organic or inorganic metal ligands, or as free ions (Aboulroos *et al*., 2006). These poisonous compounds, according to Jaishankar *et al*. (2014), can remain on the rocks, be buried beneath organic materials, or be carried through the soil to ground water.

Metals may experience complexation, chelation, and hydrolysis once they are in the environment, which modify their availability and distribution (Tchounwou *et al*., 2012). The toxic and accumulative properties of heavy metals affect aquatic species and cause ecosystem disruption (Garba *et al*., 2016; Govind & Madhuri, 2014). They also pose a major risk to human health once they enter the body through the biological chain (Kim *et al*., 2017). Permanent damage is brought about by internal heavy metal stimulation, which produces reactive oxygen species and has a number of negative effects on the body, such as mutation and variation in genes, mercaptoprotein consumption, and lipid peroxidation (Morcillo *et al*., 2016).

This study covered the following metals which are commonly found in industrial wastewater:

2.2.1 Cadmium

According to Murithi *et al*. (2014), the mineral greenockite (CdS) is the primary form in which cadmium is found. It is a frequent environmental pollutant that mostly results from a variety of industrial processes like printing, mining, smelting, electroplating, and dyeing (Gong *et al*., 2018; Kim *et al*., 2016). Cadmium is one of the most poisonous metals in the environment and cannot be eliminated alone by relying on the capacity of the natural environment to purify itself (Mohan *et al*., 2007). This is a significant issue that requires immediate attention. Cd primarily accumulates in organisms through interaction with Cd-binding proteins like metallothionein (Gaete Olivares *et al*., 2016). Additionally, it can affect hormone production and secretion, causing endocrine disruptive toxicity, oxidative stress, and mitochondrial malfunction (Gaete Olivares *et al*., 2016).

2.2.2 Chromium

The sixth most abundant element in the Earth's crust, ferro-chromite ($Fe_2Cr_2O_4$), is one of the main natural sources of chromium that pollutes the environment (Augustynowicz *et al*., 2010). Other sources include chromium-using industries like metallurgical, chemical, and refractory (heat-

resistant) industries (V. K. Gupta & Ali, 2004). There are various oxidation states in which chromium can occur, although the metal stage (Cr0), trivalent stage (Cr^{3+}), and hexavalent stage (Cr^{6+}) are the most prevalent. It can be found in the form of ions as $HCrO_4$, CrO_7, and CrO_4 in industrial effluent. When compared to chromium (III), chromium (VI) is 500 times more hazardous (Sen & Ghosh Dastidar, 2010). Chromium(VI) is persistent, which causes it to build up in the food chain and reach dangerous levels (0.050 ppm), which can lead to major health risks such as stomach and lung irritation, gastrointestinal cancer, stunted plant development, and animal mortality (Shanker *et al*., 2005).

2.2.3 Lead

Lead is a silvery metal that is extremely hazardous and can harm every area of the body. Storage batteries, soldering supplies, coatings, cable cladding, and weaponry like lead bullets are the main uses for lead. $PbSO_4$, PbS, and $PbCO_3$ are its natural forms (Wuana & Okieimen, 2011). Lead poisoning due to lead exposure is known to induce symptoms like nausea, brain damage, headaches, mortality, abdominal discomfort, and swelling of the optic nerve (Jaishankar *et al*., 2014). In children, it decreases IQ and produces convulsions, while in adults, it causes memory loss, renal damage, nephropathy, sleeplessness, anorexia, abdominal pain, and high blood pressure (Wuana & Okieimen, 2011).

2.2.4 Zinc

In nature, zinc is found as a mineral. Due to the burning of coal and the making and processing of steel, its concentration has increased. By stimulating T-cells, zinc ions play a crucial role in immune system regulation (Deshpande *et al*., 2013). A slight zinc shortage in our bodies can lead to disorders like memory loss, hair loss, infertility, and diabetes because zinc is also essential for hormonal balance and functions as an antioxidant in the body (Guo & Katta, 2017). However, an

excess of zinc (5.000 ppm) in our systems can lead to headaches, nausea, vomiting, loss of appetite, and heavy metal toxicity, stomach problems, disorientation, reduced immunological function and kidney stones, an accumulation of minerals in the kidney, which can cause excruciating discomfort and clog the ureter (Plum *et al*., 2010; Tang *et al*., 2010).

2.2.5 Copper

Copper has been largely disregarded as a factor in a number of health issues. However, it has been claimed that the heavy metal copper is a cause of anorexia, exhaustion, premenstrual syndrome, melancholy, headaches and migraines, allergies, and hyperactivity in children (Sud *et al*., 2008). Although humans can tolerate relatively high copper concentrations, excessive copper (2.000 ppm) can nonetheless have serious negative effects on health such as anaemia, intestinal distress, and damage to the heart, kidney, liver, pancreas, and brain (Al-Rub *et al*., 2006). Metal fume fever may develop as a result of occupational exposure to copper fumes, dusts, or mists, and nasal mucous membranes may atrophically change. Wilson's disease is the result of persistent copper poisoning (Miraj & Rao, 2020).

Table 2.1 below lists the recommended standards for drinking water as determined by national and internal organizations.

Table 2.1 Recommended standards for drinking water

Parameters	Maximum permissible levels in mg/L			
	NEMA	WHO	EU	USEPA
Cadmium	0. 005	0. 005	0. 005	0. 005
Chromium	NA	0. 050	0. 050	0. 100
Lead	0. 050	0. 010	0. 100	0. 010
Zinc	5. 000	5. 000	NA	5. 000
Copper	0. 100	2. 000	2. 000	1. 300

NA: Not available

Source: (Mebrahtu & Zerabruk, 2002)

2.3 Water hyacinth as an environmental concern

The scientific name of water hyacinth is *Eichhornia crassipes*. It is considered as the world's most noxious, dreadful, and aquatic invasive weeds producing $14x10^7$ daughter plants yearly and covering water area of 1.4 km^2 with an amount of fresh biomass containing $28x10^3$ tons (Ruan *et al*., 2016). The implications of water hyacinth proliferation extend beyond simple ecological disruption. Abba & Sankarannair (2024) highlight how alterations in hydrology due to this invasive species can lead to significant changes in riverine ecosystems. This disruption is particularly evident in regions like Uganda, where water resources are critical for both biodiversity and human livelihoods.

Water hyacinth is associated with the accumulation and concentration of pollutants in aquatic ecosystems. Its dense mats can trap contaminants, including heavy metals and agricultural runoff, exacerbating water quality issues (Bashir *et al*., 2020; Stehle & Schulz, 2015). Consequently, the presence of water hyacinth may lead to increased toxicity in freshwater environments, posing risks to both aquatic life and human health.

Water hyacinth can also significantly alter water clarity, which in turn decreases phytoplankton production and negatively impacts dissolved oxygen levels (Gallardo & Aldridge, 2018). The nonlinear effects of these changes can lead to reduced abundance and diversity of aquatic invertebrates and fish populations. This alteration of ecological communities indicates a cascading effect on the entire aquatic ecosystem, which may disrupt the food web dynamics essential for maintaining ecological balance (Havel *et al*., 2015).

Its decayed roots, stems, and leaves impair the growth of other aquatic creatures if timely salvage treatment is not applied (Duan *et al*., 2020). The plant also makes good breeding grounds for mosquitoes and other insects, therefore, locations where it is abundant generally experience an increase in several diseases including skin rash, cough, malaria, encephalitis, gastrointestinal problems, and bilharzia.

Nevertheless, water hyacinth has garnered significant attention for its applications in environmental phytoremediation due to its superior bioaccumulation capabilities compared to most other aquatic macrophytes (Rezania *et al*., 2015). While its rapid growth in freshwater ecosystems often leads to ecological disruption, innovative research has highlighted its potential for pollution control and resource utilization. Güereña *et al* (2015) assert that the utilization of water hyacinth can transform waste into valuable resources, providing both economic and

ecological advantages. The authors emphasize that harnessing this invasive species can lead to improved biodiversity conservation efforts in areas where water hyacinth often proliferates.

2.4 Conventional Methods for Heavy Metal Removal

Various methods have been developed in the recent years to remove heavy metals from the waste water effluents and drinking water to improve the quality. These methods include ion exchange, electrochemical treatment, membrane filtration, chemical precipitation, coagulation and flocculation among others (Mohammad , 2017).

2.4.1 Ion exchange

Ion exchange involves the interchange of ions from a nearby medium. Concurrently, this action can be used to manage a fairly large amount and eliminate low levels of pollutants (Kansara *et al*., 2016). Ion exchange resins made of synthetic organic materials are important matrices. Sulphonic acid, which is a component of these resins, accelerates the physico-chemical process denoted by: (Chisti, 2018),

$$\mathrm{nRSO_3^- - H^+ + M^{n+} \leftrightharpoons nRSO_3^- - M^{n+} + nH^+}$$

The anionic group from the resin is represented by $nRSO_3^-$, and the metal cation is represented by M^{n+}; n is the coefficient of the reaction component that depends on the oxidation state of the metal ions. The method is relatively expensive and unable to withstand large metal ion concentrations since the surrounding medium is contaminated by waste water pollutants (Kansara *et al*., 2016). The technique also calls for the removal of suspended materials using additional techniques prior to the ion exchange process (Liu *et al*., 2015).

2.4.2 Membrane filtration

This method includes filtration procedures like ultrafiltration (UF), microfiltration (NF), and reverse osmosis (RO) which can be used, depending on the particle size that needs to be removed. Membrane filtration methods, particularly ultrafiltration and microfiltration, achieve high removal efficiencies of contaminants, making membrane technologies an attractive option for various applications, including heavy metal removal from wastewater (Qasem *et al*., 2021; Vieira *et al*., 2020). One of the significant drawbacks of membrane filtration is the tendency for membranes to foul over time, leading to reduced performance and increased maintenance requirements (Zhang *et al*., 2016). This not only affects the efficiency of the filtration process but also necessitates regular cleaning and replacement of membranes, contributing to higher operational costs. Reverse osmosis (RO) systems often require significant energy input, making them less sustainable in terms of operational efficiency (Zheng *et al*., 2018).

2.4.3 Electrochemical treatment

Electrochemical processes encompass a range of techniques including electrochemical oxidation, electrochemical reduction, electrocoagulation, electrocoagulation/flotation, electrodialysis, and electrochemical advanced oxidation processes (EAOP). These methods are particularly effective in eliminating or converting environmental pollutants into non-toxic materials (Rashid *et al*., 2021). The core principle behind many of these methods is the generation of reactive species such as hydroxyl radicals, which are powerful oxidants that efficiently mineralize pollutants found in wastewater (Feng *et al*., 2016).

The robustness, flexibility, and ease of operation of electrochemical methods make them suitable for managing fluctuating wastewater streams (Barrera-Díaz *et al*., 2014). Despite their advantages, electrochemical treatment methods also present several challenges. One primary concern is the

requirement for nontoxic, inexpensive, and high-surface-area electrodes. The development and maintenance of these electrodes can incur significant costs and may hinder the widespread adoption of electrochemical technologies (Liu *et al*., 2021).

2.4.4 Chemical precipitation

Chemical precipitation involves the addition of reagents to wastewater, leading to the formation of insoluble precipitates that can be removed from the liquid phase. This method is particularly effective for treating wastewater containing heavy metals, as it can achieve high removal efficiencies with relatively low operational costs (Benalia *et al*., 2022). The effectiveness of the chemical precipitation process largely depends on the choice of precipitating agents, pH levels, and other operational conditions (Zhang & Duan, 2020).

The method typically involves straightforward processes such as mixing, settling, and filtration, which can be implemented on a large scale (Donkadokula *et al*., 2020). This accessibility allows even smaller industries to adopt this treatment method without facing prohibitive costs. Chemical precipitation also enables the recovery of valuable materials. For instance, certain contaminants can be precipitated and later recovered for reuse in other processes, thus promoting sustainability (Haleem *et al*., 2023). One significant limitation associated with this method is the production of sludge, which requires further treatment and disposal (Benalia *et al*., 2022).

2.4. 5 Coagulation and flocculation

The coagulation-flocculation process involves the addition of coagulants to wastewater, which helps aggregate suspended particles and heavy metals into larger flocs that can be easily removed. This method is particularly effective for industrial wastewaters due to its straightforward execution and high efficiency (Teh *et al*., 2016). Despite the effectiveness of coagulation-flocculation, the long-term environmental impacts of residual coagulants and the management of sludge generated

from the treatment process may exacerbate pollution other than alleviating it (Bazrafshan *et al*., 2015).

2.5 Emerging adsorbents

The use of adsorbents is one of the most common and appealing processes for removing heavy metal ions and other contaminants.

2.5.1 Nanomaterials

Most of the emerging adsorbents are in the form of nanomaterials. Nanomaterials are defined as materials with at least one dimension in the nanoscale range (1–100 nm) (Sannino, 2021). Nanomaterials have emerged as a critical solution for the removal of heavy metals and other pollutants from contaminated water, primarily due to their high surface area and reactivity, which enhances their adsorption capabilities (Voisin *et al*., 2017). The unique properties exhibited by these materials do not only facilitate the effective treatment of polluted water but also demonstrate significant advantages over traditional adsorbents (Yang *et al*., 2019a). They include;

2.5.1.1 Nanobiomaterials

Recently, there has been a lot of interest in the creation of low-cost adsorbents made of different types of biomaterials for the removal of metals from water and wastewater (Malik *et al*., 2017). \The main benefits of adsorbents from biomass material include; short operation times, no generation of potentially harmful secondary compounds, enhanced selectivity for specific metals of interest, low operating costs, the potential for metal recovery and reuse, the reusability of biomaterial, and the removal of heavy metals from effluent independent of toxicity (Hossain *et al*., 2018).

Biomaterials, particularly those engineered at the nanoscale, have emerged as effective solutions for heavy metal removal due to their high surface area and reactivity (Zou *et al*., 2016). Similarly,

biochar has gained attention as a low-cost adsorbent in wastewater treatment, demonstrating effective removal of heavy metals through multiple mechanisms such as electrostatic attraction, ion exchange, and complexation. The porous structure of biochar contributes to its high adsorption capacity, making it an attractive option for large-scale applications (Inyang *et al*., 2016).

2.5.1.2 Zeolites

Zeolites are crystalline aluminosilicates with a three-dimensional framework structure, characterized by their porous nature (Ngah *et al*., 2013; Wu *et al*., 2019). This structure facilitates their role as effective adsorbents (Cychosz *et al*., 2017; Slater & Cooper, 2015). The extensive porosity and tunable surface properties of zeolites allow for selective adsorption, making them ideal for various applications, including gas separation and environmental remediation (Nugent *et al*., 2013). In a study by Kansara *et al*. (2016), cinoptilolite, an example of a zeolite was able to successfully remove heavy metals from aqueous solutions.

2.5.1.3 Silica gel

Silica gel, composed primarily of silicon dioxide (SiO_2), is widely recognized for its high surface area and porosity, making it a prominent candidate in various adsorption applications, particularly in environmental remediation (Al-Tohamy *et al*., 2022). The combination of silica gel with other materials has been shown to enhance its adsorptive properties. Li *et al*. (2018) reviewed metal-organic framework-based materials, highlighting that when silica gel is modified or combined with metal-organic frameworks, its capacity to adsorb toxic and radioactive metal ions improves substantially. This suggests that there is potential for hybrid materials that leverage the strengths of silica gel alongside other innovative materials.

2.5.1.4 Biopolymers and hydrogels

Biopolymers, derived from natural sources, offer a sustainable alternative to synthetic polymers, while hydrogels provide unique properties such as high water retention and tunable mechanical strength. The versatility of biopolymer-based hydrogels, particularly those derived from cellulose and chitosan has been highlighted in recent studies. These hydrogels can be fabricated through crosslinking with synthetic polymers, resulting in enhanced mechanical, biological, and physicochemical properties (Tran *et al*., 2018). The combination of natural and synthetic components allows for the customization of hydrogels to meet specific adsorption needs. For instance, the GAD beads, which are cross-linked with biopolymers, exhibited impressive adsorption capacities for heavy metal ions (Cu^{2+} and $Cr_2O_7^{2-}$), outperforming other adsorbents (Sun *et al*., 2015).

2.5.1.5 Metal Oxides

The synthesis of ordered mesoporous metal oxides has been highlighted for its impact on textural properties, which directly influence the adsorption performance (Liu *et al*., 2017). For instance, magnesium oxide nanoparticles have been highlighted for their efficacy in adsorbing lead (Pb) from aqueous solutions, showcasing the potential of specific nanomaterials in targeting particular contaminants (Yaqoob *et al*., 2020). Similarly, iron oxide nanoparticles have proven effective in remediating water contaminated with heavy metals, with surface modification strategies further enhancing their performance (Guerra *et al*., 2018).

2.5.1.6 Modified clay minerals

The inherent properties of clay minerals, such as their high cation exchange capacity and swelling capabilities, are crucial for their function as adsorbents. Ruiz-Hitzky *et al*. (2010) explored hybrid

materials based on clays, noting their potential for environmental and biomedical applications. These hybrid materials can be engineered to enhance adsorption capacities, providing a versatile platform for pollutant removal. Gu *et al*. (2019) provided a comprehensive review of clay mineral adsorbents specifically for heavy metal removal, emphasizing their effectiveness and the mechanisms involved, which include ion exchange and adsorption processes. The application of clay minerals for remediation purposes is also an eco-friendly approach (Otunola & Ololade, 2020).

2.6 Preparation of adsorbents from water hyacinth

The conversion of water hyacinth (*Eichhornia crassipes*) into adsorbents has garnered significant attention due to its potential for addressing water pollution and waste management (Madikizela, 2021). Traditional methods, such as chemical precipitation and membrane filtration, are often costly and generate hazardous waste, leading to a search for alternative solutions (Afroze *et al*., 2016). Water hyacinth, in particular, has been identified as an efficient and economical adsorbent for treating industrial wastewaters. Priya & Selvan (2017) highlighted its sustainability and availability, attributing its effectiveness to its high surface area and porosity, which facilitate the adsorption process. This aligns with findings from Lim & Aris (2014), who noted that conventional methods often lack cost-effectiveness, making non-conventional, biomass-based adsorbents like water hyacinth a preferable alternative.

Sabir, (2015) also discussed the economic challenges associated with commercial activated carbon and advocated for low-cost alternatives derived from bio-waste, reinforcing the cost advantages of materials like water hyacinth. Moreover, the development of bio-hybrid materials, including hydrogels and aerogels from water hyacinth, presents new avenues for enhancing adsorbent efficiency while maintaining cost-effectiveness. These materials offer a renewable alternative for

water purification that can potentially outcompete conventional adsorbents in terms of cost and performance (Guragain *et al*., 2011)

The process of converting water hyacinth into adsorbents involves various methods, including physical, chemical, and thermal activation to enhance the adsorption properties of biochar and activated carbon derived from this aquatic plant (Oumam *et al*., 2020).

2.6.1 Physical activation methods

Physical activation typically involves the use of high temperatures and gases such as steam or carbon dioxide to enhance the porosity and surface area of the adsorbent. According to Sajjadi *et al*. (2019), this method effectively increases the surface area and porosity of biochar, which is critical for adsorption applications. Furthermore, studies by Torres-Perez *et al*. (2012) indicated that agricultural residues, including water hyacinth, can be converted into activated carbons through physical methods, demonstrating significant potential for water purification, specifically in removing arsenate.

The effectiveness of physical activation can be further improved through the application of thermal treatment. de Carvalho *et al*. (2022), highlighted that thermal treatment not only enhances the pore size but also increases the surface area of activated carbons, which directly correlates with their adsorption capacity. This finding underscores the importance of optimizing thermal conditions during the physical activation process.

2.6.2 Chemical activation methods

Chemical activation typically involves the use of chemical agents such as phosphoric acid, potassium hydroxide, or zinc chloride to enhance the surface characteristics of activated carbons. Zotov *et al*. (2018) reported that chemical modifications significantly enhance the adsorption

capacity of activated carbon derived from water hyacinth, making it suitable for applications in water treatment. Additionally, a study by Manfrin *et al*. (2020) emphasized the utility of chemical activation in the production of activated biochar from various biomass sources, revealing that optimal conditions can lead to the effective removal of heavy metals from contaminated waters.

The integration of chemical treatment with physical methods can be used to maximize adsorbent performance. Riyanto & Prabalaras (2019) conducted a study on the adsorption kinetics of activated carbon from water hyacinth, illustrating that chemical activation can lead to improved kinetics and isotherm characteristics, thus enhancing the overall efficiency of the adsorbent in removing Co (II) ions from aqueous solutions.

2.6.3 Thermal activation methods

Thermal activation involves heating the biomass in the absence or limited presence of oxygen, which allows for the formation of a porous structure. Baghirzade *et al*. (2021) explored the thermal regeneration of spent granular activated carbon, indicating that thermal processes can also be applied to regenerate used adsorbents, potentially increasing the sustainability of water treatment systems. The regeneration of activated carbon is crucial in reducing waste and improving economic feasibility in water treatment applications.

Additionally, El-Bery *et al*. (2022) demonstrated that activated carbon derived from lignocellulosic agricultural wastes, including water hyacinth, exhibited high adsorption capacities for pollutants such as phenol and methylene blue. This finding is significant as it not only highlights the versatility of thermal activation but also points to the potential for using agricultural waste as a resource for producing effective adsorbents.

2.7 Optimization of process parameters for maximum adsorption efficiency

Various studies have focused on optimizing process parameters for water hyacinth-based adsorbents to enhance adsorption capacity for different contaminants, including heavy metals and organic dyes. The effectiveness of these adsorbents can be significantly influenced by optimizing various process parameters, including pH, contact time, adsorbent dosage, and initial concentration of contaminants.

Huang *et al*. (2014) investigated the adsorption characteristics of lead ions on mesoporous activated carbons derived from water hyacinth. Their study showed the significance of adsorption kinetics and isotherms, establishing that activated carbon from water hyacinth exhibits a considerable adsorption capacity for Pb (II). The authors noted that the optimal conditions for maximizing adsorption were related to both the surface area of the activated carbon and the specific interaction mechanisms between the adsorbate and the adsorbent. In another study by Xu *et al*. (2016), the enhancement of methylene blue adsorption through citric acid modification of biochar from water hyacinth was explored. This modification significantly increased the surface functionality and, consequently, the adsorption capacity (395mg g^{-1}). The study highlighted that the adsorption of methylene blue was influenced by the initial dye concentration and biochar dosage, suggesting that process parameter optimization could lead to higher remediation efficiency.

Mahamadi & Nharingo (2010) conducted a detailed analysis of the removal efficiencies of various heavy metals, including zinc, cadmium, and lead using water hyacinth. Their findings indicated that the initial metal ion concentration and adsorbent dose were critical parameters affecting the adsorption process. Specifically, they determined that an optimal initial Zn (II) concentration of 43.18 mg/L, an adsorbent dose of 0.062 g, and a temperature of 313.5 K resulted in an 85%

removal efficiency. This study highlights the potential for using response surface methodology in optimizing adsorption processes.

Further emphasizing this approach, Biswas *et al*. (2019) utilized response surface methodology (RSM) to optimize Zn (II) adsorption on a biochar-alginate composite derived from water hyacinth and achieved a removal efficiency of 85% under optimum conditions of system temperature of 313.5 K, initial metal ion concentration of 43.18 mg/L, and the adsorbent dosage of 0.062 g. Langeroodi *et al*. (2018) also utilized RSM to optimize the removal of Fe (III) ions using a metal oxide nanocomposite, finding that pH and initial ion concentration were the most critical parameters for maximizing adsorption. The optimization of these parameters is therefore crucial for practical applications in wastewater treatment.

2.8 Properties of water hyacinth-based Adsorbents

The unique physicochemical properties of water hyacinth-based adsorbents make them particularly advantageous compared to conventional adsorbents. These properties are responsible for its capacity to adsorb contaminants from water.

One of the most significant properties of water hyacinth-based adsorbents is their high surface area and porosity. The natural structure of water hyacinth fibers, combined with treatments like carbonization or activation, enhances the surface area available for adsorption (Zhuang *et al*., 2020). The increased porosity allows for greater pollutant capture like heavy metals and organic dyes, making these adsorbents more efficient than many traditional materials. Huang *et al*. (2014) demonstrated that activated carbons derived from water hyacinth exhibit significant surface areas (up to 325 m^2/g) and high carbon content (82-84%) while maintaining low ash content (4-5%). These characteristics suggest that water hyacinth-derived adsorbents possess a favorable structure for pollutant adsorption, particularly for metal ions.

Water hyacinth also contains a variety of functional groups, such as hydroxyl, carboxyl, and amine groups, which can interact with pollutants through mechanisms like ion exchange, complexation, and hydrogen bonding. These functional groups enhance the adsorptive capacity of water hyacinth-based adsorbents in removing pollutants from wastewater (Salahuddin *et al*., 2021; Zhang *et al*., 2020) The presence of these groups makes water hyacinth-based adsorbents more versatile and effective across different types of contaminants compared to adsorbents like activated carbon or synthetic polymers.

Additionally, Water hyacinth is a readily available and low-cost material, especially in regions where it is considered a nuisance. The conversion of this invasive plant into adsorbents provides a sustainable solution by turning an environmental problem into a resource. This cost-effectiveness, combined with the low energy requirements for processing, gives water hyacinth-based adsorbents a significant economic advantage over other adsorbents such as activated carbon, which can be expensive to produce (Pal *et al*., 2023).

Unlike synthetic adsorbents, water hyacinth-based materials are also biodegradable and environmentally friendly. After use, these adsorbents can be safely disposed of or even used as a soil amendment, adding further value to their application. This contrasts with synthetic adsorbents, which may pose disposal challenges and environmental risks (Guna *et al*., 2017).

Water hyacinth-based adsorbents have demonstrated high adsorptive capacities for a range of pollutants, including heavy metals like lead and cadmium, as well as organic pollutants like dyes and pesticides. The adsorption performance often surpasses that of conventional adsorbents, largely due to the combined effects of high surface area, porosity, and the abundance of functional groups (Bapat & Jaspal, 2020). This makes them highly effective in diverse environmental remediation applications. Da Silva *et al*. (2018) investigated the use of piassava, banana peels,

coffee grinds, eucalyptus bark, coconut shells, and water hyacinth in the adsorption of Pb^{2+} and Ni^{2+} ions in water. They discovered that water hyacinth had a greater ability for adsorption than the rest of the studied adsorbents.

2.9 Adsorption mechanisms

Adsorption is a process that involves contaminants from the matrix adhering to the active sites of the adsorbent until equilibrium is reached (Fu & Wang, 2011). The possible adsorption mechanisms of metal ions relevant to water hyacinth-based adsorbents are physical adsorption, and chemisorption which involves electrostatic interactions, hydrogen bonding, pi-pi interactions, and precipitation.

2.9.1 Physical adsorption

Physical adsorption happens when there are weak attractive forces like Van der Waals forces are present between the adsorbate and adsorbent. It is a non-chemical process that involves the diffusion and deposition of heavy metal ions in the pores of the adsorbent material. The increase of micropores and mesopores can increase surface area and facilitate contaminant diffusion, which can promote physical adsorption and accelerate adsorption kinetics (Yang *et al*., 2019b). For instance, Fahmi *et al* (2018) in their study about the adsorption performance of grated empty fruit bunch BC, they discovered that more exposed microporous and bigger surface area can enhance Pb(II) adsorption ability.

2.9.2 Ion exchange

Ion exchange often takes place between the proton of oxygen-containing functional groups (-COOH, -OH) and divalent metal cations (M^{2+}). An indication of this is cation exchange capacity (Yang *et al*., 2019b). According to Lai *et al* (2019), this removal mechanism greatly aids in the adsorption of heavy metals by activated carbon and biochar.

2.9.3 Electrostatic interaction

When positive or negative charges are present on the surface of the adsorbent, electrostatic attraction will contribute to the process of adsorption between the adsorbent and the opposing charged ions. One of the processes for the heavy metal adsorption by activated carbon, biochar, carbon nanotubes, and graphene is electrostatic interaction (Yang *et al*., 2019b). Most carbon-based materials including water hyacinth biochar have variable charges on their surfaces, and the electrostatic interaction can be influenced by the solution pH and pH_{pzc} of adsorbents. Additionally, on the surface of carbon-based adsorbents, there may be interactions between protonated or deprotonated functional groups and heavy metal ions, such as the electrostatic attraction between protonated $-NH_3^+$ and $HCrO_4$, $Cr_2O_7^{2-}$, and CrO_4^{2-} (Wang *et al*., 2014).

2.9.4 Precipitation/ coprecipitation

To separate from water, heavy metal ions can coprecipitate on an adsorbent surface to create solid precipitates or to generate solid precipitates alone. Coprecipitation can be observed in adsorption systems with high concentrations of heavy metal ions, and it can occur repeatedly on carbon-based adsorbent surfaces (Liu *et al*., 2020; Yang *et al*., 2019b). For instance, the precipitation or coprecipitation of $CdCO_3$, $Cd_3(PO_4)_2$, and $Cd(OH)_2$ on B_2O_3 is an example of this (Zhang *et al*., 2015).

2.9.5 Surface complexation

For the purpose of enriching heavy metals from aqueous solution, functional groups (such as -OH, -COOH, -O, and CO-NH-) react with heavy metal ions or complexes on the surface of adsorbents (Li *et al*., 2017). Surface complexation also produces multiatom structures during reaction processes (Yang *et al*., 2019a). The possibility of Cd^{2+}, Cu^{2+}, and Ni^{2+} complexing with -OH and -COOH has been highlighted in numerous papers (Deng *et al*., 2019; Faheem *et al*., 2018; Zhan *et*

al., 2018). Furthermore , Li *et al*. (2017) discovered that surface complexation, which was contributed by OH or COOH on biochar surface, may have been a significant process in Cd, Pb, and Hg removal.

2.10 Factors influencing adsorption

2.10.1 Effect of pH

Ion exchange and electrostatic interaction in adsorption are significantly impacted by H^+ concentration. The pH value at which the zeta potential of adsorbents reaches zero also known as pH_{pzc}, is varied for different carbon-based materials (Ahmad *et al*., 2020). In addition to more H^+ being able to exchange with heavy metal cations when the pH is lower than pH_{pzc} value, a high concentration of H^+ will also protonate the surface functional groups such as -NH_2, -OH of carbon-based materials, increasing the quantity of surface positive charges (Ma *et al*., 2019; Yang *et al*., 2019b). The adsorption of heavy metal cations would then experience a decrease in water due to electrostatic repulsion, whereas the adsorption impact of anions such as $HCrO_4$ would improve (Wang *et al*., 2014).

2.10.2 Effect of initial concentration

When the carbon-based adsorbent has not reached saturation, the adsorption capacity for heavy metals within a specific concentration range keeps rising with an increase in starting concentration. According to Hayati *et al*. (2017), one explanation for this is that higher initial concentration improves the transfer power from solution to surfaces made of carbon-based materials. However, if the initial concentration is placed at a higher level, all adsorption sites would be taken up by the initially adsorbed heavy metal ions, and/or the adsorbent surface would be completely covered (Man Mohan & Gajalakshmi, 2024).

2.10.3 Effect of contact time

According to Osasona *et al*. (2014), contact time is another crucial parameter that has a significant impact on the adsorption process and kinetics. Until an equilibrium is reached, the amount of contaminants removed often rises as contact duration increases. The existence of free active sites on the adsorbent's surface that can bind contaminants is what causes the initial high rate of metal ion adsorption. The rate of metal ion adsorption then reduces along with the reduction in accessible sites as contact time is increased. According to a study by Li *et al*. (2015), the absorption of metal ions (Cd(II), Pb(II), and Cu(II)) onto chitosan/sulfydryl-functionalized graphene oxide composite (CS/GO-SH) increased quickly in the first 10 minutes and reached an equilibrium value after about 30 minutes.

Additionally, for various adsorbents, different values for adsorption equilibrium exist and different metal ions also differ in their equilibrium adsorption time. For example; In a study by Changmai *et al*. (2018), the authors found the equilibrium times for three different bio-adsorbents, that is; cabbage waste, tomato waste, and polyethylene terephthalate acid to be approximately 75, 99, and 99 minutes respectively. In another study by Lee & Choi (2018), the adsorption equilibrium was detected after 4 hours for the hazardous cadmium, copper, and lead ions and one hour for the lead ions in the adsorption of these ions onto the adsorbent surface.

2.10.4 Surface area

Normally, the amount of adsorbent absorbed correlates with a particular surface area. According to Alslaibi *et al*. (2013), specific surface area is the portion of the total surface area available for adsorbate uptake. When there is more adsorption completed per unit weight of adsorbent, the solid

is likely to be more porous and finely split, which means there are more active sites accessible for adsorption (Bazrafshan *et al*., 2016).

2.10.5 Temperature

Since both chemical and physical adsorption are often exothermic, a drop in temperature typically results in an increase in the amount of adsorbate absorption (Bazrafshan *et al*., 2016). Heavy metal uptake is typically favored only up to a certain level at high temperatures until it progressively declines. Over the majority of the temperature range typically seen in wastewaters, the effects of temperature on adsorption equilibrium are not particularly noticeable. As a result, little temperature changes have no appreciable impact on the adsorption process (Bernard *et al*., 2013)

2.10.6 Mass of the adsorbent

Adsorption occurs on the adsorbent's surface, therefore the quantity of active sites available and the bulk of the adsorbent affect how many adsorbates may be adsorbed and, in turn, how effective adsorption is (Fu & Wang, 2011). According to a study by Abdelkreem (2013), there was an increase in phenol uptake to 85% from 52% when the dosage of olive milk waste was increased to 1.0 g from 0.25 g. Ghaedi *et al*. (2011) observed similar findings in their assessment of the applicability efficiency and performance of gold nanoparticle loaded activated carbon for remove the Congo red from wastewater.

2.10.7 Adsorbent and adsorbate nature

Owing to the greater solute-solvent bond that is established, which influences the adsorption process, adsorption reduces as solute solubility increases. Thus, the adsorption on the adsorbent decreases with increasing solute solubility in the solvent and vice versa (Alslaibi *et al*., 2013). However, when some surface functional groups, such as carboxyl or carbonyl, are present, the

adsorbent's physiochemical characteristics can affect both the adsorption capacity and rate. Concentrating appropriate functional groups on the adsorbent surface can accomplish this (Aravindhan *et al*., 2009).

2.11 Industrial wastewater characteristics in Nakawa

The Nakawa Industrial Area in Kampala, Uganda, has emerged as a significant industrial hub, particularly characterized by a diverse range of manufacturing and processing industries, including food and beverage industries, pharmaceutical industries, plastics, mattresses, paints and corrugated iron sheets industries. Nonetheless, this rapid industrialization has raised concerns regarding environmental sustainability, particularly in relation to wastewater management and effluent discharge. This is because a diverse range of industrial activities contribute significantly to the generation of industrial wastewater which often lacks proper treatment before being discharged, leading to severe environmental pollution which is likely to affect the water quality of the receiving streams (Paul, 2011).

Recent studies have provided valuable insights into the physicochemical properties of industrial effluents in Nakawa. Walakira & Okot-Okumu (2011) examined the impacts of industrial effluents on water quality in streams receiving discharges from various industries in the Nakawa-Ntinda area. They reported pH levels ranging from 3.68 to 12.41 mg/L, electrical conductivity (EC) between 212 and 4633 µS/cm, turbidity levels from 20.9 to 715.9 NTU, and biochemical oxygen demand (BOD) values varying from 16.4 to 325.5 mg/L. Chemical oxygen demand (COD) was found to range from 39 to 1351 mg/L, indicating a significant level of organic pollution. Additionally, total nitrogen (TN) and total phosphorus (TP) were assessed, with TN levels ranging from 0.45 to 32.63 mg/L and TP from 0.078 to 1.674 mg/L, revealing nutrient loading issues.

The study further highlighted noncompliance with national regulations regarding heavy metal discharge from chemical and pharmaceutical industries. The absence of wastewater treatment facilities across these industries underscores a critical gap in environmental management practices. Fuhrimann *et al*. (2015) conducted a study on microbial and chemical contamination in the Nakivubo wetland area, which receives water from the Nakawa streams. They reported high levels of microbial pathogens, which pose significant health risks to the local population. The presence of these pathogens is exacerbated by the lack of proper wastewater treatment, leading to increased disease transmission risk.

The assessment of heavy metals by Sekabira *et al*. (2010) in the Nakivubo urban stream revealed concerning concentrations of lead (Pb), copper (Cu), and cadmium (Cd). Their findings indicate that the industrial discharges contribute significantly to the heavy metal contamination of local water sources, which poses not only environmental risks but also threats to public health through bioaccumulation in the food chain.

2.12 Suitability of water hyacinth-based adsorbents for Nakawa wastewaters

The use of natural adsorbents, such as water hyacinth-based adsorbents has emerged as a promising approach for wastewater treatment due to its high adsorption capacity and cost-effectiveness (Crini *et al*., 2019). The efficacy of water hyacinth-based adsorbents for treating various types of wastewaters, focusing on their potential applications in Nakawa wastewaters can be evidenced by the previous findings that studied its ability to remove pollutants from wastewater.

In a study by Saha *et al*. (2017), water hyacinth was utilized for the phytoremediation of industrial mine wastewater, achieving an impressive 99.5% removal of chromium (Cr VI) over 15 days. This finding emphasizes the plant's potential for heavy metal removal, essential for treating contaminated waters in Nakawa.

Another study demonstrated that functionalizing water hyacinth biochar with nanoscale zero-valent iron and chitosan significantly enhances its adsorptive capacity for hexavalent chromium. This approach not only utilizes the invasive species but also provides a sustainable solution for wastewater treatment, illustrating how this biomass waste can be converted into valuable resources (Chen *et al*., 2019).

Priya & Selvan (2017) highlighted its efficiency as the adsorbent for textile effluent treatment, indicating its economic viability as a sustainable solution in wastewater management. Furthermore, its high biomass production provides a continuous supply of raw materials for adsorbent production.

The potential of adding value to biomass waste through application in environmental treatment was studied by Dinari *et al*. (2017) . Their study emphasizes the importance of developing modified adsorbents, such as mesoporous silica composites, which can effectively remove trace heavy metals like Cr (VI) from contaminated water. This indicates a significant advancement in the field of environmental engineering, where waste materials are repurposed for pollution mitigation. The findings suggest that the valorization of biomass waste, including water hyacinth, can lead to innovative materials that address both pollution and water management challenges.

Akinbile & Yusoff (2012) demonstrated the capability of water hyacinth in effectively removing nutrients from aquaculture wastewater, suggesting that it can also address nutrient loading in domestic and industrial effluents. The reduction of nutrients is crucial for preventing eutrophication, a common issue in polluted water bodies.

Despite the existing literature, there is limited research specifically addressing the effectiveness of water hyacinth-based adsorbents in the unique context of Ugandan wastewater, particularly

concerning local industrial effluents and domestic wastewater compositions. This study therefore investigated the effectiveness of water hyacinth based adsorbents as a cheap, viable adsorbent in remediation of selected heavy metals.

2.13 Use of eggshell powder for activating water hyacinth-based adsorbents

Calcium carbonate crystals make up 94% to 97% of the eggshell; organic materials and eggshell pigment make up the remaining material (Koelkebeck, 2014). As a result, it is anticipated that egg shells are a perfect calcium source. According to Fahmi Khairol *et al*. (2019), calcium is a non-toxic, ecologically friendly modifier that is abundant in nature. During calcination, the specific surface area and pore volume of the crushed eggshells and seashells biomaterials increases, as the calcination temperature increases. This is because of the evolution of porosity within the material as a result of the release of CO_2 from $CaCO_3$, leading to the formation of CaO (Hart & Onyeaka, 2020). Numerous materials such as clinoptilolite, sludge, and biochar treated by a Ca source have been identified in some investigations to have high adsorption capabilities for the contaminants from water (Mitrogiannis *et al*., 2017).

2.14 Modelling of adsorption

2.14.1 Equilibrium adsorption models

Adsorption is explained using a variety of adsorption isotherms, which are typically used to determine the adsorbent's adsorption capacity expressed in mgg^{-1} or $mgmg^{-1}$. The most often utilized isotherms for solid-solution adsorption in wastewater treatment and water purification are the Freundlich and Langmuir models. For a given initial concentration, these models aid in clarifying the adsorption capacity of adsorbents at equilibrium (Sutherland, 2010).

2.14.1.1 Freundlich isotherm

According to Afroze *et al* (2016), the Freundlich adsorption isotherm model (Freundlich 1906) takes into account a heterogeneous adsorption surface with unequally distributed accessible sites and various adsorption energies. Therefore, it explains the equilibrium on heterogeneous surfaces. The Freundlich theory states that the adsorption isotherm changes from being linear at n = 1 to being favorable at n < 1 and unfavorable at n > 1 (Tran *et al*., 2017). The value of the R^2 correlation coefficient for linear regression typically indicates which model should be picked to provide the greatest fit.

The linear form of Freundlich isotherm is shown in Equation 2.1

$$\log q_e = {}^{1}/_{n} \log C_e + \log K_f \qquad \text{(Equation 2.1)}$$

Where;

q_e (Mg/g) - Amount of the heavy metal ion adsorbed per unit weight of activated water hyacinth bio-material.

Ce (mg/L) - the amount of unadsorbed solute in the solution.

K_f - a constant indicating adsorption capacity.

n- Adsorption intensity

The adsorption intensity (n) defines the adsorbent heterogeneity and affinity (Foo & Hameed, 2010). A stronger bond between the adsorbate and the adsorbent is indicated by a greater value of n (or a lower value of 1/n).

2.14.1.2 Langmuir Isotherms

According to the Langmuir model, a single molecule can be adsorbed by an adsorbent surface active sites, where it binds until it is desorbed. Adsorbate generates a uniform monomolecular

layer at equilibrium throughout the adsorption process, suggesting that there is no interaction between the metal ions adsorbed (Rahimi & Vadi, 2014).

The linear form of Langmuir isotherm is shown in equation

$$\frac{1}{q_e} = \left(\frac{1}{q_{mb}}\right) \times \frac{1}{C_e} + \frac{1}{q_m} \qquad \text{(Equation 2.2)}$$

Where;

q_e - equilibrium adsorption capacity measured in mg/g.

C_e - the equilibrium concentration of adsorbed solute measured in mg/L.

q_m - the highest concentration of the solute ion per unit weight of water hyacinth measured in mg/g.

b - the Langmuir constant measured in l/mg

The following three assumptions underlie Langmuir isotherms: a solution containing an adsorbate that is strongly attracted to the surface is in contact with the surface of the adsorbent; the surface has a particular number of sites where the solute molecules can be adsorbed; and monolayer adsorption, in which just one layer of molecules is attached to the surface (Febrianto *et al*., 2009; Ghaedi *et al*., 2012).

2.14.2 Kinetic adsorption models

Adsorption kinetic studies focus specifically on the rate at which adsorbate molecules adhere to the surface of an adsorbent. These studies are important in understanding how quickly a substance can be removed from a solution or gas phase by an adsorbent material. Both pseudo-first-order and pseudo-second-order models can be used to assess and quantitatively determine the rate of adsorption. Scale-up trials can benefit from this information for future system design.

2.14.2.1 The pseudo first-order equation

The reversibility of the equilibrium between the solid and liquid phases is described by the pseudo-first-order equation model, which is based on the assumption that the metal cation binds to only one sorption site on the sorbent surface (Vijaya *et al*., 2008). The following equation represents the pseudo-first-order Lagergren model (Wan Ngah & Hanafiah, 2008).

$$\log(q_e - q_t) = \log(q_e) - \frac{K_1}{2.303} t \qquad \text{(Equation 2.3)}$$

Where:

K_1 is the pseudo-first-order adsorption rate constant (min^{-1}),

t is the contact time (min),

q_t and q_e are the adsorption capacities at time t and at equilibrium, respectively (mg g^{-1}).

The values of k_1 and qe are determined by the slope and intercept of a linear plot of log (q_e-q_t) vs. t. The first-order kinetics model is applied when log (q_e-q_t) vs. t forms a straight line. Log q_e ought to be equal to the intercept of the plot of log (q_e-q_t) against t in a genuine first-order process.

2.14.2.2 The pseudo second-order equation

The pseudo-second-order equation postulates that chemical adsorption may be the cause of the rate-limiting step. This model suggests that there are two binding sites on the adsorbent surface where metal cations can bind. Aurich *et al*. (2017) developed the linearized form of the equation for the Lagergren pseudo-second-order adsorption kinetic, which is:

$$\frac{t}{q_t} = \frac{1}{k_2 {q_e}^2} + \frac{t}{q_e} \qquad \text{(Equation 2.4)}$$

Where:

K_2 ($gmg^{-1}min^{-1}$) denotes the pseudo-second-order adsorption rate constant

q_e (mg g^{-1}) is the amount of the solute adsorbed at equilibrium,

q_t (mg g^{-1}) denotes the amount of solute adsorbed at time t,

It is possible to derive the rate constant K_2 (g mg min^{-1}), initial sorption rate h (mgg $^{-1}min^{-1}$), and qe (mg g) from a plot of t/q_t vs. t. The second-order kinetic theory should be applicable if a plot of t/q_t against t shows a linear connection.

2.15. Principle and mode of operation of an Atomic Absorption spectrometer (AAS)

AAS is an analytical method that uses the light radiation absorbed by free atoms in the gaseous phase to determine the elements in a sample quantitatively. The principle of AAS according to Nollet (2012) is based on the fact that; an atom is composed of a positively charged nucleus that is surrounded by a number of negatively charged particles called electrons that are required to provide neutrality. The energy levels that these electrons occupy are distinct and energy can be introduced to shift an electron between levels. As the excited atoms return to their ground state, they emit characteristic wavelengths of light. Each element emits light at specific wavelengths, which are unique to that element and correspond to its electronic structure.

The AAS approach uses the free atoms of the analyte to absorb radiant light at a wavelength specific to that element of interest, which allows the concentration of that particular element to be quantified (Helaluddin *et al*., 2016). The relationship between the analyte absorbance and the associated concentration is ascertained during analysis using standard series with known concentrations. Analyte samples are atomized throughout the analysis process, and by absorbing light at certain wavelengths that correspond to the analyte's electronic transition, the corresponding electrons in the sample analyte are excited to higher energy levels. Energy from the radiation source passes via a monochromator, which only allows radiation that is particular to the element

under consideration to be selected. Consequently, the radiation flux in the standards and sample in the flame or electro-thermal atomizers is measured using a detector by utilizing the Beer-Lambert Law to convert the analyte's absorbance to concentration (Helaluddin *et al*., 2016).

Beer-Lambert law states that the length of the light path through the analyte solution and the analyte's corresponding concentration are directly correlated with the amount of light absorbed by the analyte.

$A = \varepsilon\, l\, c$ ..... Equation 2.2

Where;

A is Absorption

ε = Coefficient of molar absorption

l = Light radiation path length

C = Analyte concentration

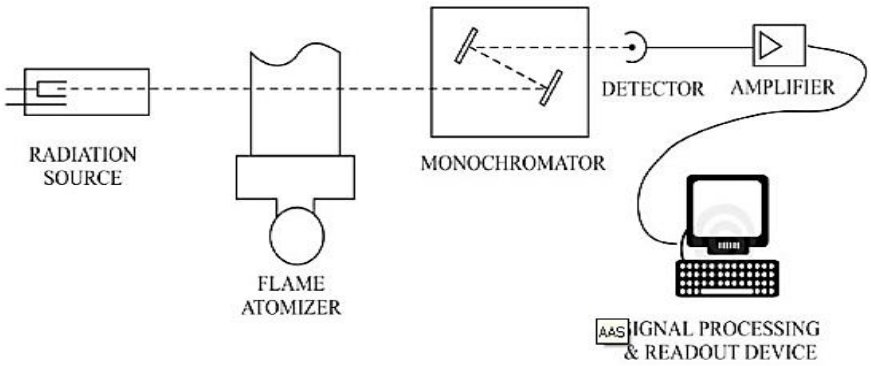

Figure 2.1: Principal sketch of AAS. Source: (Novi ., 2018)**.**

Several adsorption studies about the use of AAS for determination of heavy metals in wastewater have been done. In this study, a new adsorbent synthesized from water hyacinth and dual-activated with both eggshell powder and phosphoric acid was used for the adsorption of selected heavy metals and their concentration determined using AAS.

CHAPTER THREE

MATERIALS AND METHODS

3.1 Materials

3.1.1 Reagents

All reagents used in the study were of analytical grade and they were obtained from Labx Chemical Suppliers Uganda Limited. They included: Ethylenediaminetetraacetic acid, Cadmium sulphate ($3CdSO_4.8H_2O$), copper (II) sulphate ($CuSO_4.5H_2O$), Chromium nitrate ($Cr(NO_3)_3.9H_2O$), lead (II) nitrate [$Pb(NO_3)_2$], Zinc (II) sulphate ($ZnSO_4.7H_2O$), nitric acid (HNO_3), phosphoric acid, Sodium hydroxide (NaOH). All dilutions were done using distilled water.

3.1.2 Equipment

Atomic Absorption Spectrometry (GF-AAS, Model Shimadzu AA-6300, Japan Model, was used to determine heavy metal concentrations in the wastewater samples. A Zeiss Sigma 300 VP Gemin 1 (Germany), scanning electron microscopy (SEM) was used to examine the surface morphology and Energy-dispersive X-ray Spectroscopy was used to determine the elemental composition of the adsorbent. Fourier transform infrared spectrophotometer (FTIR Bruker Alpha II) in the range of 500 to 4,000 cm^{-1} was used to record the FT-IR spectrum of the activated adsorbent before and after heavy metal adsorption. An OHAUS Aquasearcher Multimeter for pH/EC/Temperature was used to determine the corresponding physico-chemical parameters of the wastewater samples. An EC/ TDS/Turbidity meter was used to determine TDS and Turbidity. All sonication was done by an Athena Digital ATS-15 ultrasonicator. Other materials included an oven, plastic bags, mortar, pestle, refrigerator, egg shells, water hyacinth, waste water samples, 300 µm and 425 µm mesh sieves, aluminium foil, a stainless-steel knife and an analytical balance.

3.2. Methods

3.2.1 Water Hyacinth collection and preparation

The water hyacinth used in this study was collected along the shores of Lake Victoria in Jinja, Uganda on 2nd February, 2024 and washed on site to remove mud, dust and any other foreign material and packaged in plastic bags for transportation. The method by Monowara *et al*. (2021) with some modifications was followed to prepare the water hyacinth powder as summarized. The water hyacinth plant material was transported to the Kyambogo University laboratory and re-washed several times with distilled water to remove any other remaining mud and unwanted material. The water hyacinth was cut into small pieces (2-3 cm in length) and the obtained pieces spread on an aluminium foil. This was followed by drying in an oven at 120 ^{0}C for 12 hours to reduce the moisture content. The dried water hyacinth was allowed to cool and soaked in 0.25 M ethylenediaminetetraacetic acid (Sigma-Aldrich, 99.0%) (at pH 10) for 24 h to dissolve Hg^{2+}, Pb^{2+}, and Cd^{2+} ions present on the plant tissues and then washed with distilled water severally till the pH of the rinse was nearly 7.0. This was followed by oven drying at 110 ^{o}C for 12 hours. The plant material was left to cool and then crushed using a mechanical grinder to obtain a fine powder. The powder was sieved through a 425 µm mesh sieve to ensure uniform particle size. The material was then kept in a plastic self-sealing bag for subsequent use.

3.2.2. Preparation of the activating agent from chicken egg shells

The egg shells (500g) were obtained from a local egg rolex vendor in Nakawa-Ntinda, Kampala. The preparation of egg shell activating agent was done following the procedure by Zhang *et al*. (2019) which is summarized as follows: The obtained egg shells were washed thoroughly under running tap water to remove any membrane and organic residue. The cleaned egg shells were rinsed with distilled water, spread on aluminium foil and oven dried at 120 ^{0}C overnight. The dried

egg shells were allowed to cool at room temperature and then ground using a mechanical grinder to obtain a fine powder. The powder was sieved through a 425 µm mesh sieve to ensure uniform particle size. The obtained powder was then kept in a zip-lock plastic bag for further use.

3.2.3. Preparation of phosphoric acid for use as an activating agent

Analytical grade concentrated phosphoric acid with an 85% concentration was obtained from Labx Chemical Suppliers, Uganda limited. For the activation process, 100 mL of 50% phosphoric acid solution was prepared in a 100 mL volumetric flask by mixing 50 mL of phosphoric acid (85%) with 50 mL of distilled water in a fume hood.

3.2.4. Collection of wastewater samples

Wastewater samples were collected at the release tube exits from selected Industries of the Nakawa Industrial area. Nakawa industrial area, is located on the eastern edge of the city of Kampala which is the largest city in Uganda. The GPS coordinates of Nakawa are $0^0 19^I 59.0^{II}$N and $32^0 37^I 05.0^{II}$E. Its latitude is 0.333055, and its longitude is 32.618066, with an average elevation of 1178 meters. The wastewater samples in the study were collected at the exit tubes in three different industries which included; a Pharmaceutical Products industry (Site 1), a Paints Manufacturing Industry (Site 2) and a Batteries Manufacturing Industry (Site 3). The samples (5 litres each) were collected in clean polyethylene bottles that had been cleaned with distilled water, rinsed with nitric acid and labelled 1, 2 and 3 respectively corresponding to each of the sampling sites. The collected samples were stored in a refrigerator to maintain sample integrity for subsequent use.

3.2.5. Determining the physicochemical parameters of wastewater samples

The selected physico-chemical parameters (Temperature, pH, Electrical conductivity, Total Dissolved Solids, Turbidity, Dissolved Oxygen, chlorides and Total Hardness) were determined using the methods suggested by Lukubye & Andama (2017).

3.2.6 Preparation of activated water hyacinth-Based Biochar

3.2.6.1 Synergistic activation of water hyacinth-based biochar with eggshell powder and phosphoric acid

This was done following the procedure by Zięzio *et al*. (2020) with a few changes as summarized; To 50 grams of eggshell powder, 50 grams of water hyacinth powder was added and mixed in a 1:1 ratio by weight in a large beaker. Phosphoric acid solution (50 %) was slowly added to the mixture while stirring continuously with a glass rod until a homogeneous slurry was formed. The mixture was then stirred for an additional 30 minutes to ensure that it was well impregnated with the acid solution. Following this, the beaker was covered with parafilm and the slurry left to sit at room temperature for 24 hours to allow proper impregnation.

3.2.6.2 Carbonization of the water hyacinth-based biochar

For carbonization, the method by Danish *et al*. (2018) was followed with some slight modification whereby; the impregnated mixture was transferred into glazed porcelain silica crucibles. The crucibles were covered and placed in a Nabertherm muffle furnace. The temperature of the muffle furnace was set to 600°C and the temperature maintained for 6 hours. After carbonization, the furnace was turned and allowed to cool down to room temperature naturally. Once cooled, the crucibles were carefully removed from the furnace using tongs and the carbonized material transferred into a large beaker, washed with distilled water several times, stirring with a glass rod,

until the pH of the wash water was neutral (pH 7). The washed material was filtered using filter paper and a funnel. The filtered material was transferred on a tray and dried in an oven at 110°C for 5 hours. Once cooled, the activated carbon material formed was ground to a fine powder using a mortar and pestle. The powder was sieved through sieved through 300 µm and 425 µm mesh sieves. The resultant samples were stored separately in airtight containers to prevent moisture absorption and contamination.

3.2.6.3 Modifications of the Water Hyacinth-Based Biochar

The adsorbent was prepared by treatment of water hyacinth powder (WH) with both egg shell powder (EP) and phosphoric acid (PA) to form a double-activated adsorbent (EP-WH-PA). Two other adsorbents were prepared in a similar manner, except that there was no treatment with phosphoric acid, for comparative studies. One of the adsorbents comprised of water hyacinth powder and eggshell powder (EP-WH) in a ratio of 1:1 and the other comprised of only water hyacinth powder which formed water hyacinth biochar (WHB) after carbonization.

3.2.7 Characterization of the activated water hyacinth-based adsorbents

3.2.7.1 Morphological Analysis using Scanning Electron Microscopy (SEM) and Scanning Electron Microscopy with Energy Dispersive X-ray Spectroscopy (SEM-EDS)

A Zeiss Sigma 300 VP Gemin 1 (Germany) Scanning Electron microscopy coupled with energy-dispersive X-ray spectroscopy was used to obtain information on composition and morphology of the adsorbent. The prepared adsorbent powder was mounted on a sample stub using conductive carbon tape ensuring an even layer by gently tapping and removing excess powder. The stub was then loaded into the SEM chamber, secured properly, and the chamber evacuated to achieve the required vacuum. SEM parameters were set, including an accelerating voltage of 5-20 kV and a

working distance of 10 mm, and the appropriate detector was selected. The image was focused and corrected for astigmatism. This was followed by navigation of the sample while adjusting magnification to enable capture of high-quality images for analysis. Finally, the produced images were saved for further analysis and reporting. For Energy Disperse Spectroscopy analysis, elemental data was collected by scanning with the electron beam and recording the spectra. Images and EDS spectra were saved for further analysis and reporting.

3.2.7.2 Functional Group Analysis using FT-IR Spectroscopy

The Attenuated Total Reflectance (ATR) Crystal and the tip of the plunger on the FTIR Bruker Alpha II Spectrometer were cleaned with a soft tissue paper sprinkled with methanol to remove any kind of foreign material. The FTIR spectrometer was switched on and OPUS software was launched to establish communication between the FTIR machine and the monitor. 10 mg of the activated adsorbent was weighed using a Mettler Toledo meter and placed on the centre of the ATR crystal and the clamp arm was revolved and pressed to lock. On the monitor, "Sample scan" was clicked to scan the adsorbent and a display of the spectrum of the adsorbent showing the chemical group composition of the material was displayed.

The same procedure was repeated for the activated adsorbent after adsorption of heavy metals whereby; the activated water hyacinth residue after adsorption and filtration was further oven dried at 120 ^{o}C overnight to remove moisture completely. 0.5 g of the dried metal-loaded adsorbent was ground into powder using a mortar and pestle. 10 mg of the resultant powder was analysed using FTIR Bruker Alpha II Spectrometer. The displayed spectrum was compared with that of the activated water hyacinth-based adsorbent before adsorption.

3.2.8. Adsorption Experiments

3.2.8.1. Batch Adsorption Studies

For batch adsorption studies, 100 mL samples of each of the prepared working solutions were placed in separate 500mL beakers and 0.5 g of the activated adsorbent (EP-WH-PA) was added. The mixtures were sonicated for 5 minutes and allowed a pre-determined adsorption time.

Control experiments were conducted using unmodified biochar (WHB) and eggshell activated water hyacinth biochar (EP-WH) for comparison.

The adsorption parameters studied included; nature of the adsorbent, particle size, pH, contact time, mass of the adsorbent, and particle size on heavy metal adsorption.

3.2.8.1.1 Effect of adsorbent type

To 100 mL of each of the prepared working solutions placed in separate 500mL beakers, 0.5 g of EP-WH-PH (300 µm) powder was added, the mixtures sonicated for 5 minutes and allowed an adsorption time of 2 hours. The mixtures were filtered and the concentration of the filtrates determined using AAS. The obtained concentrations were used to determine the absorption efficiencies of the EP-WH-PA adsorbent for each of the selected metal ions. The above procedure was repeated using EP-WH and WHB powdered adsorbents respectively. The effect of adsorbent type was further assessed based on the porosity, surface area and functional groups of the adsorbent based on the results obtained from SEM and SEM-EDS. The adsorbent with the best adsorption physico-chemical characteristics and the highest adsorption efficiency was used for the subsequent studies.

3.2.8.1.2 The effect of particle size of the adsorbent on heavy metal removal

In five 500 mL beakers, 0.5 g of ground-activated water hyacinth with 300 µm particle size was added. 100 mL of metal ions from ready-made working solutions was added to each beaker. The corresponding mixtures were constantly sonicated for 5 minutes before being let to stand for 2 hours to enable for adsorption to take place. The mixtures were then filtered by gravity filtration. AAS was employed to determine the concentrations (C_2) of specific heavy metal ions in the filtrate. The procedure was repeated using ground water hyacinth with particle size 425 µm. The ratio of the amount of adsorbent required for adsorption expressed in milligrammes to the amount of adsorbate absorbed in mg was used to calculate the water hyacinth's efficiency of adsorption (q_e). The effect of pH, contact time, and adsorbent dosage employed the particle size that corresponded to the maximum adsorption efficiency.

3.2.8.1.3 The effect of pH of the adsorbent on heavy metal removal

To five 500 mL beakers each containing 0.5 g of activated water hyacinth with an average particle size (300µm), 100mL of aqueous solutions (pre-made working solutions) were added respectively. 0.1 M NaOH or 0.1 M H_2SO_4 were used to adjust the pH of the mixture, and a benchtop OHAUS Aquasearcher pH metre was used to measure the pH. The pH values were set at 3, 4, 5, 6 and 7 for the study. The mixtures were sonicated for 5 minutes before being let to stand for 2 hours to enable for adsorption to take place. The mixture was gravity-filtered and AAS was used to determine the concentrations (C_2) of particular heavy metal ions in the filtrate.

3.2.8.1.4 Effect of contact time on heavy metal removal

In 500 mL beakers (10), 0.5 g of ground water hyacinth was added. 100 mL of metal ion, produced in working solutions, with a pH set at the optimum values obtained from the results for the effect of pH (4 for Pb, Cr and Cu and 5 for Zn and Cd) were added to each beaker. Adsorption was given

a set amount of time (10, 20, 30, 40, 50, 60, 70, 80, 90, 100, 110 and 120) minutes respectively. After the mixtures were filtered, an atomic absorption spectrometer was used to measure the concentrations (C_2) of particular heavy metal ions in the filtrate. The water hyacinth's adsorption efficiency (q) was computed.

3.2.8.1.5 The effect of the mass of the adsorbent on heavy metal removal

In ten 500 mL beakers, 0.25 g of activated water hyacinth that was 300 μm was added. 100 mL of prepared metal ion was put to each beaker. The mixtures were allowed a contact time of 20 minutes for lead, 40 minutes for Cr, 90 minutes for Cu, and 30 minutes for both Zn and Cd for adsorption to take place. The mixtures were then filtered. The Atomic Absorption Spectrometer was used to measure the concentrations (C_2) of particular heavy metal ions in the filtrate. With 0.75, 0.5, 1.0, 1.25, 1.75, and 2.0 g of water hyacinth powder, the above process was repeated. Calculations were made to determine the efficiency of adsorption (q) of various dosages of activated water hyacinth.

3.2.8.2. Modeling of Adsorption

To 100 mL of aqueous solutions containing a single metal ion (10 -100 ppm) was added 0.5 g of activated water hyacinth powder (300 μm) in separate 500 mL beakers at different optimum pH values obtained from the results of the effect of pH (5 for cadmium and zinc, 4 for lead, chromium and copper). The solutions were sonicated for 5 minutes and 2 hours were given for adsorption to take place. Every heavy metal ion studied underwent these trials at room temperature until the equilibrium was reached. The mixtures were filtered, and an Atomic Absorption spectrometer was used to measure the concentrations (C_2) of heavy metal ions in the filtrate.

3.2.8.2.1 Adsorption equilibrium experiments (Adsorption isotherm models)

To characterize the reaction process, the experiment's data was fitted in Langmuir and Freundlich isotherms. The equilibrium adsorption capacity, q_e (mg/g) for activated water hyacinth was

calculated using Equation 3.6 and the linear form of Langmuir isotherm that was used is shown in Equation 2.3

$$\frac{1}{q_e} = \left(\frac{1}{q_{mb}}\right) \times \frac{1}{C_e} + \frac{1}{q_m} \quad \text{(Equation 3.1)}$$

Where;

C_o is the initial equilibrium concentration of the heavy metal in (mg/L),

C_e is the final equilibrium concentration of the heavy metal in (mg/L),

v (L) is volume of the sample,

w (g) is the mass of the adsorbent used,

Qe is equilibrium adsorption capacity measured in mg/g,

C_e is the equilibrium concentration of adsorbed heavy metal ion measured in mg/L,

q_m is the highest concentration of the heavy metal ion per unit weight of water hyacinth measured in mg/g,

b is Langmuir constant measured in l/mg.

1/qe was plotted against $1/C_e$. The qm and b values were determined graphically. The linear form of the Freundlich isotherm equation which was used in the study is shown in Equation

$$\log q_e = {}^{1}/_{n} \log C_e + \log K_f \quad \text{(Equation 3.2)}$$

Where;

q_e (mg/g) - Amount of solute adsorbed per unit weight of the adsorbent

Ce (mg/L) - the amount of unadsorbed heavy metal ions in the solution

K_f - Constant indicating adsorption capacity

n- Adsorption intensity.

$\log q_e$ Was plotted against $\log C_e$ and the gradient of 1/n and intercept of $\log K_f$ was be used in comparing the correlation coefficient.

3.2.8.2.2 Kinetic Models of heavy metal adsorption on activated water hyacinth biochar

To 100 mL of single metal aqueous solutions at various concentrations was added 0.5 g of activated water hyacinth whose particle size is 300 μm was added in separate 500 mL beakers. The pH of the solutions in the beakers was adjusted by adding 0.1 M H_2SO_4 and 0.1 M NaOH. The mixtures were continually sonicated for 5 minutes and allowed to settle for 2 hours to enable adsorption to take place and then filtered. AAS was used to determine the concentrations (C_2) of particular heavy metal ions in the filtrate. The measured concentrations (Co and C_2) were used to calculate the adsorption efficiency. The data obtained was used to draw a plot that helped to determine the reaction order which described the adsorption of the heavy metal on water hyacinth biomaterial. Pseudo-first-order and pseudo-second-order was applied.

The linear pseudo-first-order equation is;

$$\log(q_e - q_t) = \log(q_e) - \frac{K_1}{2.303} t \qquad \text{(Equation 3.8)}$$

The linear pseudo-second-order equation is;

$$\frac{t}{q_t} = \frac{1}{k_e q_e^2} \frac{t}{q_e} \qquad \text{(Equation 3.9)}$$

where;

q_e (mg g^{-1}) is the amount of heavy metal adsorbed on water hyacinth at equilibrium,

K_1 (Min^{-1}) is the rate constant of adsorption for pseudo-first-order,

q_t (mg g^{-1})- amount of heavy metal adsorbed on water hyacinth at time t,

K_2 (g $mg^{-1}min^{-1}$) - rate constant of adsorption for pseudo-second-order.

3.2.9 Heavy metal analysis using Atomic Absorption Spectroscopy (AAS)

3.2.9.1 Sample Preparation for AAS Analysis

For preparation of stock solutions, Cadmium sulphate ($3CdSO_4.8H_20$), copper (II) sulphate ($CuSO_4.5H_2O$), Chromium nitrate ($Cr\ (NO_3)_3.\ 9H_2O$), lead (II) nitrate ($Pb\ (NO_3)_2$), and Zinc (II) sulphate ($Zn\ (NO_3)_2.\ 6H_2O$) salts were used. The quantity of salt to be dissolved in a litre of distilled water to create an aqueous solution with a concentration of 1000 ppm (1000mg/L) were determined using the formula in the following equation 3.5

$$m = \frac{Mw}{Aw} \times \frac{100}{P} \times \frac{V}{1000} \qquad \text{(Equation 3.5)}$$

Where: m is the soluble salt's mass (in grammes). MW is its molecular weight. Aw is the element of interest's atomic mass. V is the volume of the stock solution to be prepared (in litres). P is percentage purity.

The mass of each salt was determined (Table 3.1), weighed and put into separate 1000 mL volumetric flasks. 100 mL of distilled water was added and the mixture sonicated to dissolve. Once the salts had completely dissolved, 30 mL of 1M HNO_3 was added and the solutions swirled. This was followed by the addition of distilled water to bring the solutions up to the mark. The stock solutions were serially diluted with distilled water to create the working standard solutions.

Table 3.1: Amount of salt weighed to prepare Stock solution

Metal	Salt of metal	Purity (%)	MW (g)	Amount weighed (g)
Cd	$3CdSO_4.8H_2O$	98 %	769. 56	6. 9857
Cr	$Cr\ (NO_3)_3.\ 9H_2O$	98 %	400. 21	7. 8534
Pb	$Pb\ (NO_3)_2$	98 %	331. 2	1. 6311
Zn	$Zn\ (NO_3)_2.\ 6H_2O$	96 %	297. 48	4. 7403
Cu	$CuSO_4.5H_2O$	98.5%	249. 68	3. 9893

3.2.9.2 Digestion of wastewater samples

Using concentrated analytical grade nitric acid, water samples were digested in triplicates for metal analysis, following the methodology by Zhang (2024) with some slight modification. To 15.0 mL of concentrated nitric acid was added to 250 mL of each of the wastewater samples in 500mL flasks and sonicated for 15 minutes. To remove turbidity, the samples were filtered through a 0.42 µm filter paper placed onto a filter funnel. The filtrate (100 mL) was transferred into a beaker followed by 5.0 mL of acquaregia. An equal amount of acquaregia was added to another beaker with 100mL distilled water to create a blank. The samples were heated on a hot plate in a fuming hood until the volume was decreased to 20 mL. Following digestion, the samples were left to stand for 30 minutes to cool and the odors to diminish. The samples were poured into 100 mL volumetric flasks respectively and then diluted up to the mark. This was followed by filtration after which the concentration of the heavy metals in the samples was determined using a Shimadzu Electro Thermal Graphite Furnace Atomic Absorption Spectrometer (GF-AAS, Model AA-6300 Japan).

3.2.9.3 AAS Analysis

Working standard solutions of known and increasing concentrations for each analyte element of interest were used for calibration to ascertain the instrument signal response to concentration fluctuations. The AAS was then turned on and configured to work by the operational guidelines. Pb, Cd, Cu, Zn and Cr concentrations were measured in the solution in triplicate, and the blank concentration was adjusted. Additionally, standard solutions of the corresponding metals were made at five different concentrations, and their absorbance was measured.

The metal concentrations in the sample analyte were calculated using a calibration curve that was created for each metal by fitting the measured absorbance values into the equation of the curve ($y = mx + c$), where x represents concentration, y represents absorbance, and m represents gradient. Some of the samples were diluted based on the concentration values discovered to confirm that the concentration falls within the tolerances of the standards. Heavy metals were determined at wavelengths (λ) 283.3, 228.8, 324.7, 213.9 and 357.9 nm for Pb, Cd, Cu, Zn and Cr respectively.

3.2.10 Data Analysis

3.2.10.1 Adsorption Capacity and Adsorption Efficiency Calculations

Based on the ratio of the concentration of metal ion to the amount of adsorbate adsorbed in mg, the adsorption efficiency (q) of water hyacinth powder (300 µm) was computed.

The equation illustrates the adsorption efficiency formula:

$$q = \frac{C_0 - C_1}{C_0} \times 100 \qquad \text{(Equation 3.6)}$$

Where;

q- Adsorption efficiency,

C_o - initial concentration of the selected heavy metals

C_1- final concentration of the selected heavy metals in waste-water.

The difference between the initial concentration of a single metal in aqueous solution, C_0, and the equilibrium concentration, C_1, were used to compute the adsorption capacity, qe, using the following formula:

$$q_e = \frac{(C_0 - C_1)V}{W} \quad \text{(Equation 3.7)}$$

Where: V is the volume of aqueous solution (L) and W is the mass of the adsorbent (g).

3.2.10.3 Statistical Analysis

Microsoft excel was used for data analysis and presentation. The heavy metal concentrations and other selected physico-chemical parameters of the water samples were compared with the national and international set standards (NEMA, WHO and EU). One-way ANOVA test was used to compare the mean concentrations of the selected heavy metals in the waste water samples to determine whether they differ significantly.

CHAPTER FOUR

RESULTS AND DISCUSSION

4.1 Determination of physicochemical parameters of wastewater

The selected physicochemical parameters (Temperature, pH, Turbidity, Electrical conductivity, Total Dissolved Solids, Turbidity, Dissolved Oxygen, chlorides and Total Hardness) were determined and the results presented in Table 4.1. It should be noted that the adsorption of heavy metals from wastewater is significantly influenced by various physicochemical parameters. For example; pH affects the solubility of metals and the ionization state of adsorbents (Huang *et al*., 2019). Temperature also plays a vital role as higher temperatures can increase the kinetic energy of metal ions, enhancing their movement towards the adsorbent surface, but can also desorb metals already adsorbed (Lashaki *et al*., 2019).

Table 4.1: Physico-chemical parameters of the collected waste water

Metal	Site	Mean ± Std. Error	Std.Dev	P value	WHO	EU
Temperature (℃)	1	33.67 ± 1.66	0.961	0.00***	20 - 26	15.0
	2	29.27 ± 0.95	0.551			
	3	29.77 ± 0.26	0.153			
pH	1	6.11 ± 2.36	1.364	0.64*	6.5 - 8.5	6.5 - 9.5
	2	6.84 ± 0.99	0.569			
	3	6.52 ± 1.03	0.592			
Turbidity (NTU)	1	440.43 ± 4.87	2.810	0.00***	2.5	4.0
	2	764.73 ± 0.82	0.473			

	3	298.53 ± 6.94	4.007			
TDS (mg/L)	1	670.30 ± 4.27	2.464	0.00***	500	1000
	2	161.93 ± 2.74	1.582			
	3	154.43 ± 17.01	9.820			
E C (μScm^{-1})	1	223.67 ± 0.78	0.451	0.00***	2500	1500
	2	324.07 ± 7.45	4.300			
	3	826.73 ± 12.23	7.060			
Dissolved Oxygen (mg/L)	1	6.90 ± 1.08	0.624	0.00***	NA	10 – 12
	2	6.47 ± 0.66	0.379			
	3	9.33 ± 0.56	0.321			
Chlorides (mg/L)	1	1592.05 ± 19.83	11.49	0.00***	250	250
	2	1608.74 ± 8.32	4.803			
	3	427.83 ± 8.50	4.908			
Total Hardness (mg/L)	1	353.20 ± 6.30	3.637	0.00***	200	1000
	2	218.00 ± 4.94	2.851			
	3	234.23 ± 6.71	3.873			

Note. *** p<0.01, ** p<0.05, *p<0.1. Analysis at 5 percent

Source: Own computation

4.1.1 Temperature

Temperature values significantly differed across all the sampling sites ($p < 0.05$) with site 1 recording the highest mean temperature value and site 2 the least. The mean temperatures for site 1, 2 and 3 were 33.67±1.66, 29.27 ± 0.95 and 29.77 ± 0.26 ^{0}C, respectively which are all beyond

the standard temperature WHO and EU value ranges indicated in Table 4.1. High-temperature values account for Industrial use of water to cool down equipment and processes. Additionally, some industrial chemical reactions are exothermic, meaning they release heat which can raise the temperature of the water used in these processes. For example, the production of active pharmaceutical ingredients (APIs) involves several exothermic reactions (Gutmann *et al*., 2015). Furthermore, high-temperature waters are used in cleaning and sterilizing equipment to meet stringent hygiene standards. Additionally, operations like distillation, crystallization, and drying are common in the pharmaceutical industry. These processes are energy-intensive and generate significant amounts of heat, which is often transferred to the wastewater (Lu *et al*., 2017).

4.1.2 pH

There was no significant variation in the mean pH values obtained for the samples obtained from the three sites. The mean pH values for sites 1, 2 and 3 were 6.11 ± 2.36, 6.84 ± 0.99 and 6.52 ± 1.03 respectively which were all slightly acidic. Nonetheless, the pH values were still within the WHO limits (6.5 – 8.5) and EU pH limits (6.5 – 9.5) for environmental discharge. The reason for the slight acidity could be traced back to organic matter from the wastewater components. When bacteria break down organic matter, they generate carbon dioxide gas, which lowers pH levels (Chidozie & Nwakanma, 2017).

4.1.3 Turbidity

The mean turbidity values differed significantly at a 5 % significance level ($p < 0.05$). Site 2 had the highest mean turbidity value (764.73 ± 0.82) NTU and site 3 had the least (298.53 ± 6.94) NTU. The mean turbidity value for site 1 was (440.43 ± 4.87) NTU. The turbidity values obtained were way above the standard limits by both WHO and EU indicated in Table 4.1. Turbidity was linked to high suspended matter levels that came from pharmaceutical, paint, and battery

wastewater components during the manufacturing process, which led to the production of high suspended matter waste water.

4.1.4 Total Dissolved Solids

The mean TDS values obtained from the three sites differed significantly at a 5% significant level ($p < 0.05$). Site 1 had the highest mean TDS value (670.30 ± 4.27) mg/L while site 3 had the least (154.43 ± 17.01) mg/L. The mean TDS value for site 2 was (161.93 ± 2.74) mg/L. The mean sample concentrations for sites 2 and 3 were within the set standards by WHO (500) mg/L and EU (1000 mg/L) while the mean TDS value of site 1 complied with the EU limit but did not meet the set standards by WHO. The high value of TDS in site 1 could be as a result of the use of inorganic chemicals in pharmaceutical industries. These include salts, acids, bases, and other chemical reagents. For instance, chloride and sulfate compounds are common contributors to TDS in pharmaceutical wastewater (Rana *et al*., 2017). Regular cleaning and maintenance of pharmaceutical production equipment also contribute to the TDS load in wastewater. The use of cleaning agents, solvents, and disinfectants can add to the dissolved solids content.

4.1.5 Electric Conductivity

The EC values for all the three sites differed significantly at a 5 % significance level ($p < 0.05$) with site 3 having the highest mean EC value (826.73 ± 12.23) μScm^{-1} followed by site 2 which had a mean value of (324.07 ± 7.45) μScm^{-1} while site 1 had the least mean EC value (223.67 ± 0.78) μScm^{-1}. The mean sample EC values from all the three sites were within the set standards by both WHO (2500) μScm^{-1} and EU (1500) μScm^{-1}. The value of EC in site 3 could be attributed to chemical additives and electrolytes such as sulfuric acid in lead-acid batteries and potassium hydroxide in alkaline batteries. These substances, when washed away with water during cleaning and processing, contribute to higher conductivity due to their high ionic nature. The presence of

heavy metal ions along with other ions such as sulfates and chlorides used in production, significantly contribute to the high electrical conductivity of the wastewater. These dissolve in water increasing its ionic strength, thus raising the conductivity levels explaining why all the three sites had some noteworthy values of conductivity (Forghani *et al*., 2023).

4.1.6 Dissolved Oxygen

There was a significant variation in the mean dissolved oxygen values ($p < 0.05$). Site had the highest mean Dissolved oxygen value (9.33 ± 0.56) mg/L while site 2 had the least mean value of dissolved oxygen (6.47 ± 0.66) mg/L. The mean value of dissolved oxygen in site 1 was (6.90 ± 1.08) mg/L. the values obtained for all the three sites were below the required limits by EU for Dissolved oxygen (10-12) mg/L. The low dissolved oxygen values could be attributed to the high temperature of the waste water samples. As the temperature rises, oxygen becomes less soluble in water. Warmer water molecules are less able to cling to oxygen molecules and travel more quickly. It is also crucial to recall that aerobic bacteria's metabolic rates rise with temperature. This indicates that at greater temperatures, they use up oxygen more quickly. As a result, not only might the amount of oxygen in the water decrease, but the oxygen that is present depletes faster (Kulkarni, 2016).

4.1.7 Chlorides

The mean concentration of chlorides differed significantly ($p < 0.05$) across the three sampling sites and all the mean values obtained were not compliant with the standard regulatory concentrations for domestic water for chlorides (250 mg/L) by both WHO and EU. The highest mean chloride concentration was recorded in site 1 (1592.05 ± 19.83) mg/L followed by site 2 which had a concentration of 1608.74 ± 8.32 mg/L while site 3 had the least (427.83 ± 8.50) mg/L. High concentrations of chlorides in pharmaceutical industry wastewater are mainly due to the

widespread use of chloride-containing compounds like hydrochloric acid, methylene chloride trichloromethylpropanol, chloroform and sodium chloride in various manufacturing processes, including drug synthesis, purification, and cleaning procedures (Gadipelly *et al*., 2014). For instance, hydrochloric acid is used in synthesizing active pharmaceutical ingredients (APIs), while sodium chloride serves as a reagent and in buffer solutions (Caron *et al*., 2006; Rahimi *et al*., 2023).

4.1.8 Total Hardness

The mean concentrations of total hardness differed significantly across all three sampling sites at a 5 % significance level ($p < 0.05$) with site 1 having the highest mean concentration of total hardness (353.20 ± 6.30) mg/L and site 2 the lowest (218.00 ± 4.94) mg/L. The mean concentration of water hyacinth in site 3 was 234.23 ± 6.71 mg/L. The obtained values deviated slightly from the regulatory standard value by WHO of 200 mg/L but complied with the EU regulatory value of 1000 mg/L. The presence of total hardness in the three sites could be due to the extensive use of chemicals, solvents, and minerals containing calcium and magnesium ions in the manufacturing processes. For instance, the paint industry utilizes pigments and fillers, such as calcium carbonate, which increase hardness levels (Alvarez & Paulis, 2017). Stearates of magnesium and calcium are used as lubricants in tablet manufacturing by the pharmaceutical industry to ensure smooth tablet formation and prevent ingredients from sticking to the equipment (Li & Wu, 2014). Additionally, battery manufacturing industries use magnesium salts, such as magnesium chloride, serve as electrolytes, providing high energy density and efficiency in batteries (Shah *et al*., 2021).

4.2 Concentration of Heavy metals in wastewater

An Atomic Absorption Spectrometer was used to determine the absorbance of the samples. The results are presented in Table 4.2

Table 4.2: Heavy metal concentration (ppm) in wastewater

Metal (ppm)	Site	Mean ± Std. Error	Std.Dev	P value	NEMA	WHO	EU
Cadmium	1	7.45 ± 0.02	0.010	0.00***	0.005	0.005	0.005
	2	40.18 ± 0.17	0.100				
	3	77.13 ± 0.23	0.130				
Chromium	1	8.21 ± 0.12	0.070	0.00***	NA	0.050	0.050
	2	13.07 ± 0.19	0.111				
	3	0.54 ± 0.04	0.021				
Lead	1	4.75 ± 0.03	0.015	0.00***	0.050	0.010	0.100
	2	72.03 ± 0.10	0.057				
	3	93.54 ± 0.07	0.042				
Zinc	1	63.02 ± 0.03	0.015	0.00***	5.000	5.000	NA
	2	84.62 ± 0.27	0.156				
	3	0.91 ± 0.07	0.038				
Copper	1	8.73 ± 0.08	0.046	0.00***	0.100	2.000	2.000
	2	54.03 ± 0.18	0.104				
	3	0.64 ± 0.08	0.047				

NA: Not Applicable

Note. *** p<0.01, ** p<0.05, *p<0.1. Analysis at 5 percent

Source: Own computation

4.2.1 Cadmium

The concentration of cadmium ions varied significantly ($p < 0.5$) across all the wastewater samples collected from the three sites. Site 3 had the highest mean concentration of cadmium ions (77.13 ± 0.23) ppm while site 1 had the least concentration of cadmium ions (7.45 ± 0.02) ppm. The concentration of cadmium ions in site 2 was 40.18 ± 0.17 ppm. The high concentration of cadmium ions in Site 3 may be related to the battery manufacturing process that uses cadmium oxide as a conductor (Munene, 2019). Another source of high cadmium levels may be attributed to the continuous manufacture of Ni-Cd batteries. As a result of a successful combination of feasibility studies and achieved sustainable electrical characteristics, alkaline nickel-cadmium (Ni-Cd) batteries are widely used as autonomous sources of industrial and household current (power banks) and therefore hold a significant market share among industrial secondary sources of current (Blumbergs *et al*., 2021). The cadmium in site 2 may be attributed to the use of cadmium-containing compounds as pigments in the manufacture of paints. For example, the yellow paint manufacturing process uses cadmium sulfide as a pigment (Ogilo *et al*., 2017; Singare *et al*., 2011). The values obtained for cadmium in all the samples were above the set limit of 0.005 ppm by NEMA, WHO and USEPA.

4.2.2 Chromium

The mean chromium concentration values obtained had a significant difference across the samples collected from the three sites with site 2 having the highest mean concentration of chromium ions (13.07 ± 0.19) ppm and site 3 having the least mean concentration of chromium ions (0.54 ± 0.04) ppm. Site 1 had a mean chromium concentration of (8.21 ± 0.12) ppm. A high mean value of chromium ions in site 2 could be as a result of the usage of Cr_2O_3 and $Cr_2O_3.H_2O$ as a colorant in chrome green paints (Sabty-Daily *et al*., 2005).

4.2.3 Zinc

The mean concentration of zinc differed significantly across the three samples. Site 2 had the highest concentration of zinc ions (84.62 ± 0.27) ppm followed by site 1 which had a concentration of 63.02 ± 0.03 ppm while site 3 had the lowest concentration of zinc ions (0.91 ± 0.07) ppm. The presence of a high concentration of zinc ions in site 2 may be attributed to the usage of ZnO and $ZnCrO_4$ as pigments in the production of white and yellow paints respectively (Osmond, 2012). For site 1, the presence of zinc ions could be due to the use of zinc in various pharmaceutical formulations including cold remedies such as zinc lonzenzes and skin creams where zinc oxide is added (Gupta *et al*., 2014). The use of zinc in the manufacture of dietary supplements might have also contributed as part of the raw material may end up in the wastewater (Ośko *et al*., 2023; Shi *et al*., 2024). The mean concentrations of zinc ions in the wastewater samples collected from site 1 and site 2 were higher than the regulatory standard value (5.000 ppm) set by NEMA and WHO while the samples from site 3 were within the set limits.

4.2.4 Lead

There was a significant variation of lead ions in all the three samples at a 5% significant level ($p < 0.05$) as presented in Table 4.2. Site 3 had the highest mean concentrations of lead ions (93.54 ± 0.07) ppm while site 1 had the least (4.75 ± 0.03) ppm. The concentration of lead ions in site 2 was 72.03 ± 0.10 ppm. The high concentration of lead ions in waste water from site 3 may be attributed to the use of lead metal and lead oxide as electrodes during battery manufacturing (Saaidia *et al*., 2017). The presence of lead ions in site 2 may be attributed to the use of $Pb(CO_3)_2$ and $PbCrO_4$ to give the paints a fresh look and color, respectively (Ayinla *et al*., 2024; Gonzalez *et al*., 2023). The significant usage of lead driers and inorganic lead pigment during manufacture was also linked to the high content of lead in site 2 (Puthran & Patil, 2023).

4.2.5 Copper

The concentration of copper ions across the three sites differed significantly at a 5 % significant level ($p < 0.05$). Site 2 had the highest concentration of copper ions (54.03 ± 0.18) ppm followed by site 1 which had a concentration of 8.73 ± 0.08 ppm while, site 3 had the lowest concentration of copper ions (0.64 ± 0.08) ppm. The presence of a high concentration of copper ions in site 2 was a result of Copper-based pigments like copper phthalocyanine (CuPc) and copper oxides commonly used in paints for their vibrant colors (Wigger *et al*., 2018). Copper-based preservatives such as copper naphthenate are also added to paints to prevent microbial growth (Janssens *et al*., 2016). The copper in wastewater samples from site 1 could be as a result of application of copper acetate in some topical creams and ointments for its antimicrobial properties. Salts of copper such as copper carbonate and copper nitrate are also often used in pharmaceutical formulations (Badea *et al*., 2020). Additionally, Copper is employed in certain organic synthesis reactions in the pharmaceutical industry, such as the Ullmann reaction (Fui *et al*., 2020).

4.3 Characterization of the adsorbent

4.3.1 SEM characterization of the prepared adsorbent

The surface morphology and fundamental physical properties of the prepared double-activated activated water hyacinth adsorbent treated with both eggshell powder and phosphoric acid (Ca-WH-PA) were examined by a Sigma 300 VP, Gemin 1 Scanning Electron Microscope and compared with unactivated water hyacinth biochar (WHB) and egg shell treated water hyacinth biochar (EP-WH) as shown in the figures below.

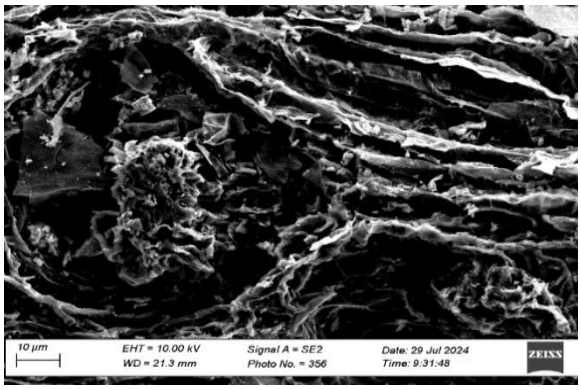

Figure 4.2: SEM Characterization results (10 µm) for WHB.

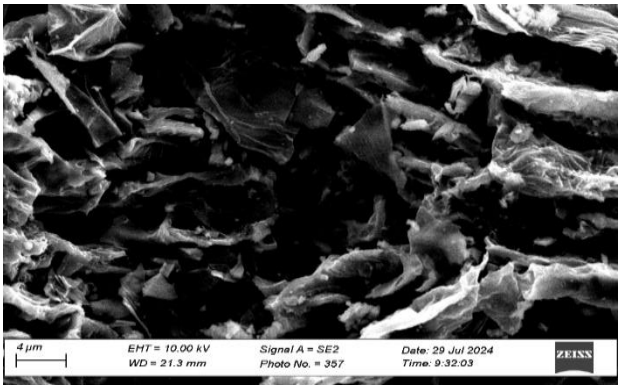

Figure 4.3: SEM Characterization results (4 µm) for WHB.

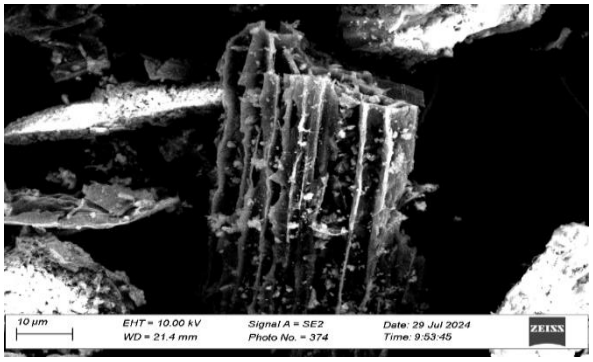

Figure 4.4: SEM Characterization results (10 µm) for EP-WH.

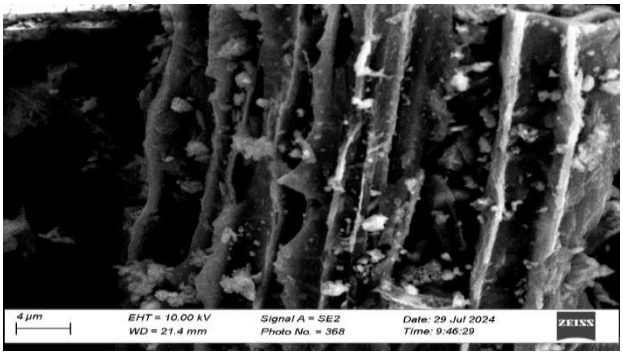

Figure 4.5: SEM Characterization results (4 µm) for biochar EP-WH.

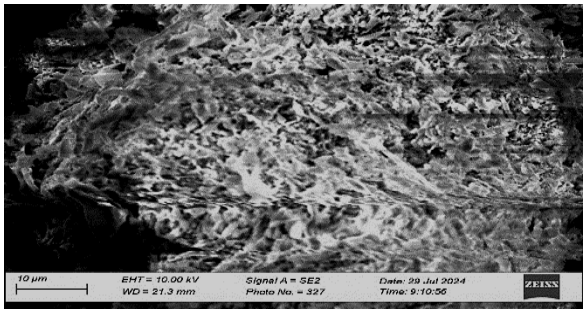

Figure 4.6: SEM Characterization (10 µm) results for EP-WH-PA.

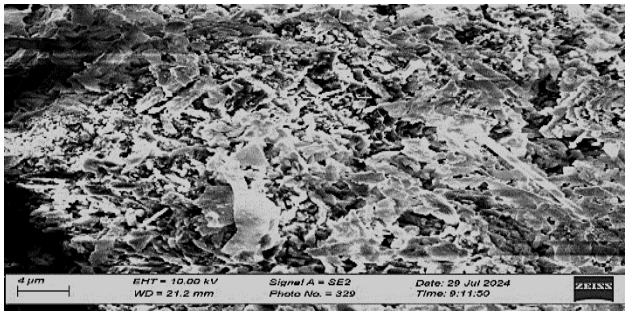

Figure 4.7: SEM Characterization (4 µm) results for EP-WH-PA.

The highly porous morphology in all three circumstances is the source of the extremely uneven and rough surface stature (Hagemann *et al*., 2018). Sponge-like pore structures were formed on

the surface of EP-WH during activation and calcification. The eggshell powder contains calcium carbonate ($CaCO_3$) particles and because of their larger atomic number, these particles frequently show as bright spots which are evident in Figure 4.4 and Figure 4.5 (Chen *et al*., 2016). In EP-WH-PA, the adsorbent surface developed pore patterns resembling honeycombs after additional activation with phosphoric acid. The evaporation of the acid during carbonization left the area previously occupied by the acidic reagent, resulting in the many pores of various sizes and shapes that were seen (González-García, 2018). Phosphoric acid-activated biochar was shown to have enhanced porosity and novel pore structures, which suggest increased surface area and pore volume. The first step in treatment of the adsorbent with phosphoric acid is the depolymerization of cellulose, which is followed by the dehydration of biopolymers, the formation of aromatic rings, and, finally, the elimination of phosphate clusters leaving a porous structure (Deliyanni, 2019; Li *et al*., 2015).

4.3.2 SEM-EDS characterization results of the synthesized adsorbents

EDS spectra and elemental composition of the prepared water hyacinth-based adsorbents are presented in figures 4.8, 4.9 and 4.10 with their respective tables:

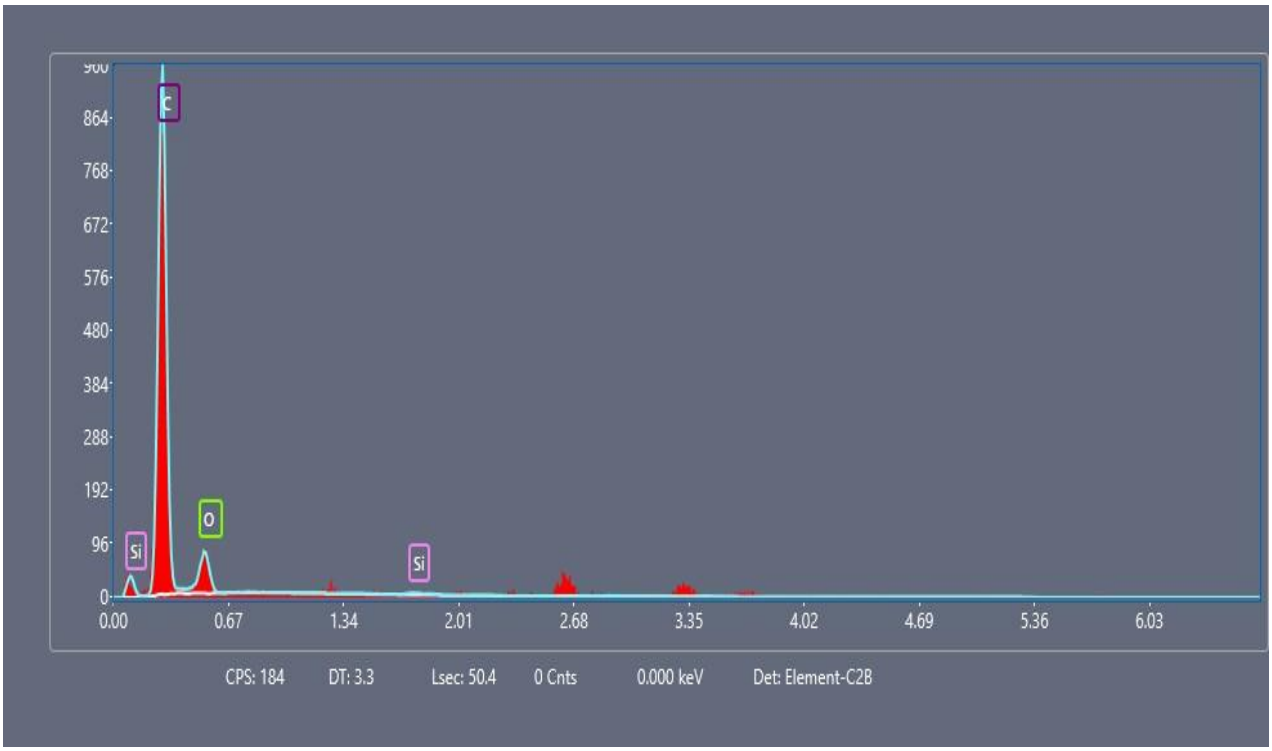

Figure 4.8: EDS Results for unactivated water hyacinth biochar (WHB).

Table 4.3: Elemental composition of unactivated water hyacinth biochar

Element	Line	Weight %	Atomic %	Error %	Net Int.	R	A	F
C K	K	92.82	94.56	7.39	111.59	0.9476	0.5985	1.0000
O K	K	7.04	5.38	24.44	7.28	0.9556	0.2298	1.0000
Si K	K	0.14	0.06	76.63	0.51	0.9724	0.9278	1.0055

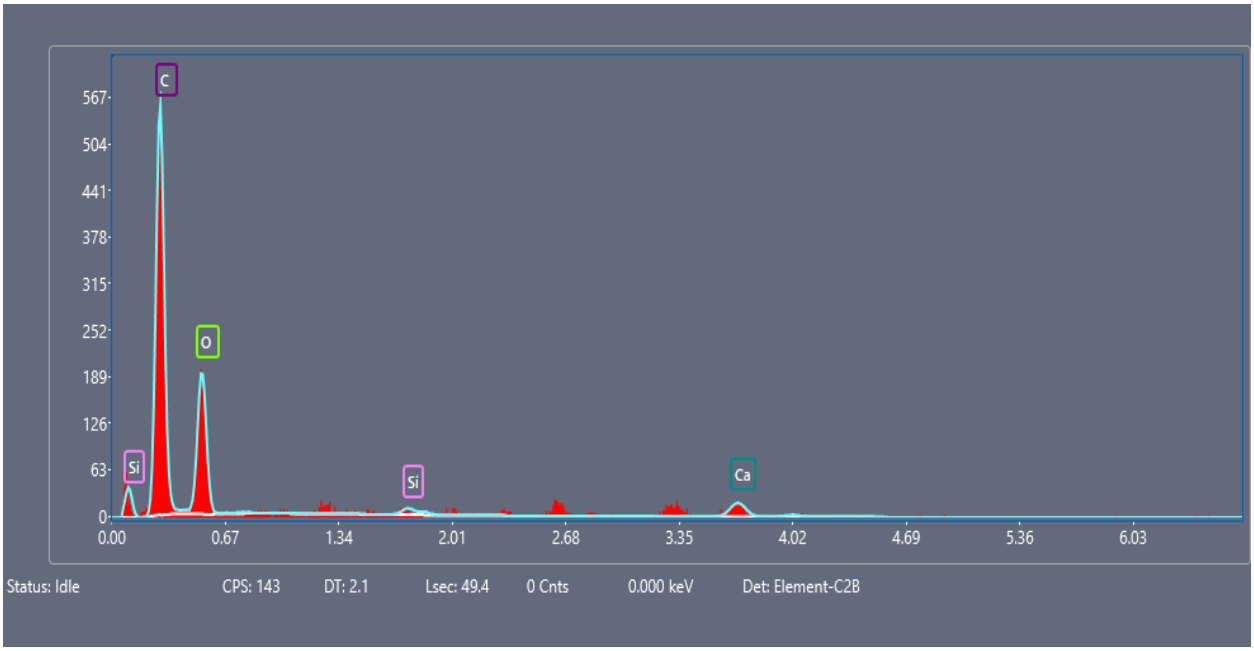

Figure 4.9: EDS Results for eggshell-treated activated water hyacinth biochar (EP-WH).

Table 4.4: Elemental composition of eggshell-treated activated water hyacinth biochar

Element	Line	Weight %	Atomic %	Error %	Net Int.	R	A	F
C K	K	70.59	78.10	8.62	61.78	0.9395	0.5241	1.0000
O K	K	24.21	20.11	13.61	23.85	0.9486	0.2630	1.0000
Si K	K	0.48	0.23	44.52	1.43	0.9675	0.9088	1.0076
Ca K	K	4.72	1.56	19.69	4.17	0.9819	0.9916	1.0243

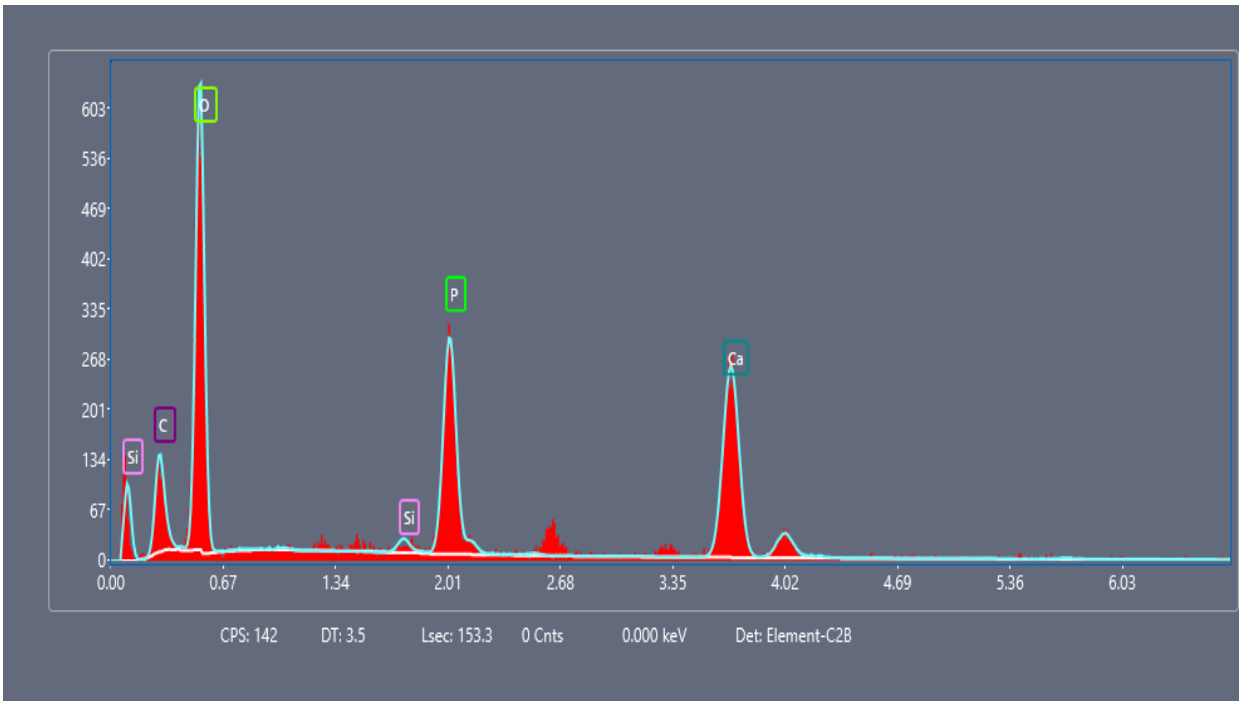

Figure 4.10: EDS Results for double activated water hyacinth biochar (EP-WH-PA).

Table 4.5: Elemental composition of activated water hyacinth biochar

Element	Line	Weight %	Atomic %	Error %	Net Int.	R	A	F
C K	K	12.86	21.96	16.57	3.78	0.8965	0.2599	1.0000
O K	K	40.93	52.45	11.16	26.85	0.9099	0.2578	1.0000
Si K	K	0.51	0.37	32.38	1.01	0.9391	0.8673	1.0206
P K	K	12.17	8.06	5.69	17.78	0.9433	0.9093	1.0174
Ca K	K	33.53	17.15	5.72	19.72	0.9632	0.9766	1.0108

The EDS spectra and obtained elemental composition of the adsorbent prepared from a mixture of water hyacinth and eggshell powder using phosphoric acid activating agent and controls involving unactivated water hyacinth and eggshell powder treated water hyacinth shown in Figures 4.8, 4.9 and 4.10 and Tables 4.3, 4.4 and 4.5. Elements: C, O, Si, P and Ca were found to be present in the final activated carbon adsorbent. This signified successful incorporation of both calcium and phosphorous groups into the adsorbent (Saeb *et al*., 2017; Zhang *et al*., 2020). The highest

percentage of carbon was found in the unactivated sample. This could be attributed to the fact that the incorporation of calcium carbonate from eggshell powder and phosphate groups from phosphoric acid treatment added significant amounts of non-carbon elements thus reducing the relative carbon content (Tran *et al*., 2018).

4.3.3 FTIR characterization of the adsorbent

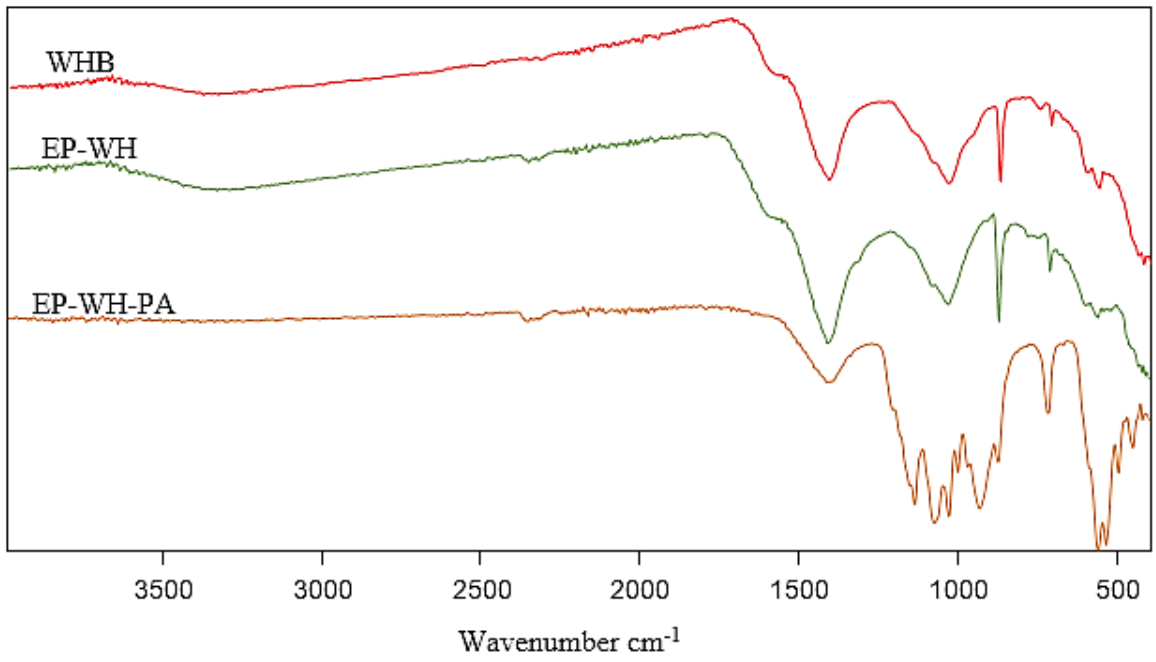

Figure 4.11: FTIR Spectra of WHB, EP-WH and EP-WH-PA.

In the spectrum of unactivated water hyacinth biochar (WHB), the broad peak at around 3200 - 3600 cm^{-1} (Appendix 10.1) can be attributed to the OH stretching vibration mode of the hydroxyl functional groups due to the presence of cellulose and lignin (Liang *et al*., 2011). There was no peak at around 2900 cm^{-1} that is often found in raw water hyacinth corresponding to aliphatic hydrocarbons which reflects the decomposition of aliphatic hydrocarbons due to pyrolysis. The peak at 1423.0775 cm^{-1} in the FTIR spectrum of water hyacinth biochar is indicative of the (C=C)

stretching vibrations of aromatic carbon-carbon bonds, which are commonly found in biochars due to the formation of stable aromatic structures during pyrolysis (Wang *et al*., 2011). The peak at 1038.2964 cm^{-1} could be attributed to phenolic C-O and O-H stretching, indicating alcohols, ethers, or esters, common in cellulose and hemicellulose. It could also correspond to the Si-O-Si stretching vibrations due to the presence of silica-derived compounds in the inorganic content within the biochar matrix. The peaks at 871.9395 cm^{-1} and 565.9958 cm^{-1} in the FTIR spectrum of water hyacinth biochar are typically associated with Si-O-Si bending vibrations, which are characteristic of silicate minerals derived from the inorganic silica present in plant tissues (Currie & Perry, 2007). At 713.2312 $cm^{-1,}$, the peak is indicative of the out-of-plane bending vibrations of C-H bonds in aromatic rings common in biochar due to the thermal decomposition of lignocellulosic materials during pyrolysis.

In the eggshell-treated water hyacinth biochar (EP-WH) the broad peak around 3200-3600 cm^{-1} (Appendix 10.2) was reduced causing a reduction in O-H stretching**.** This indicated dehydration and loss of hydroxyl groups due to pyrolysis (Ronsse *et al*., 2013). There was shifting in all the peaks except the one at a wavelength 871.9395 cm^{-1} which is Si-O-Si stretch. However the intensity of this peak increased due to the addition of silicate material from eggshell powder (Mahato *et al*., 2024) . The shifting in the C=C stretching of the peak at 1413.0775 cm^{-1} to 1414.9896 cm^{-1} indicated an increase in aromatic C=C Stretching of Ca-WH. Furthermore, the peaks around 1000-1300 cm^{-1} shifted indicating changes in oxygenated functional groups due to thermal degradation and interaction with eggshell powder. The peak at 713.2312 cm^{-1} in unactivated water hyacinth shifted to 709.4070 cm^{-1} in Ca-WH and also increased in intensity indicating an increase in C-H bonds in aromatic rings. The peak at a wavelength of 565.9958 cm^{-1} also experienced shifting to a new wavelength of 565.4351 cm^{-1} and new peaks were created

around the same position. The creation of new peaks indicates the creation of Ca-O bonds. This suggested the successful incorporation of Ca from eggshell powder into the biochar matrix.

The FTIR spectrum of phosphoric acid activated-calcium doped water hyacinth biochar (EP-WH-PA) showed further reduction in the broad O-H stretching peak around 3200-3600 cm^{-1} (Appendix 10.3), indicating complete dehydration. New peaks were created around 936.9526 cm^{-1} to 1143.4646 cm^{-1}, indicating P-O stretching vibrations from phosphates introduced during activation with phosphoric acid. The peak at 871.9395 cm^{-1} disappeared due to interaction with phosphoric acid with the Metal-O bond at this position. There was an increase in the intensity of the peak at 565.4351 cm^{-1} and the creation of new peaks below this wavelength to around 449.35 cm^{-1}. These peaks observed are typically associated with both the Ca-O stretching vibrations and P-O bending vibrations. In the Ca-O context, the peaks indicate the presence of $CaCO_3$ from the eggshell powder within the biochar structure (Nakamoto, 2009). The appearance of P-O bending vibrations in this region are indicative of the successful activation of the biochar with phosphoric acid, integrating phosphate groups into the structure (Smith, 2018). The obtained FTIR results reveal carbon-containing functional groups which were consistent with the EDS results obtained.

4.3.4 FTIR spectrum of the adsorbent after adsorption of metal ions

The FTIR spectra of the adsorbent after adsorption of selected metal ions were compared against reference spectrum (c) of the adsorbent before adsorption of the ions to understand the interaction between the functional groups of the adsorbent with the metal ions.

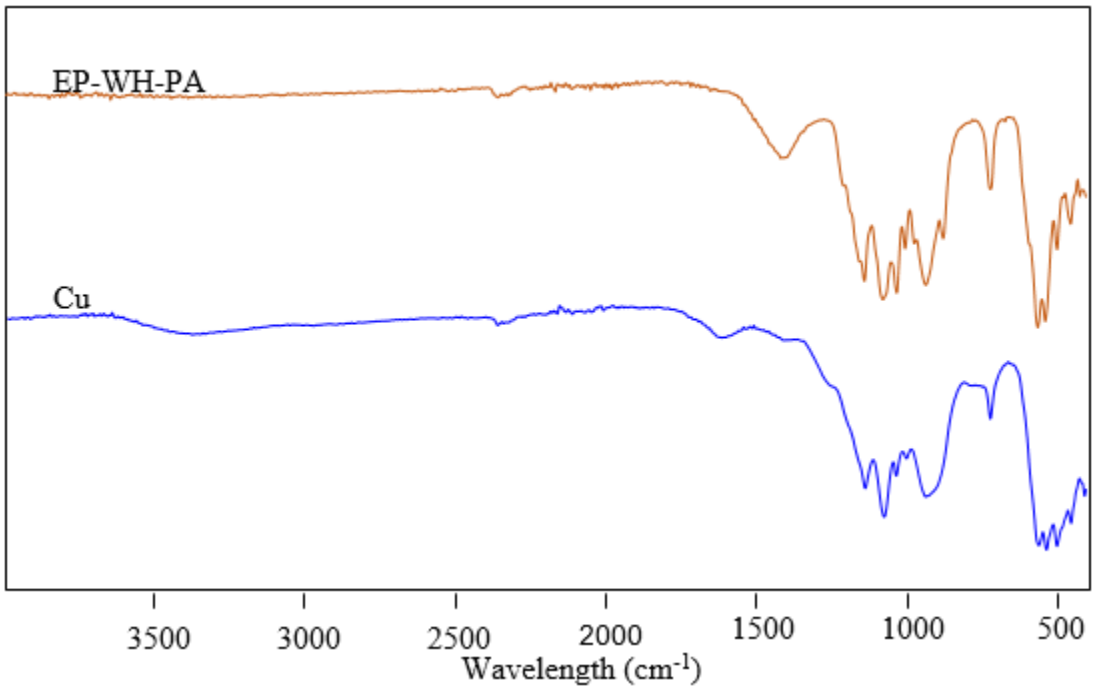

Figure 4.12: FTIR Spectrum of the activated adsorbent before and after adsorption of Cu^{2+}.

Loading of the activated adsorbent with Cu^{2+} caused the disappearance of the peak at 1414.9896 cm^{-1}. There was reduction in intensity of the peak at around 565.4351 cm^{-1} indicating interactions of phosphate groups with Cu (II) ions and 480 cm^{-1} reflecting interactions between calcium sites and Cu (II) ions. The observed changes confirmed the successful adsorption of Cu (II) ions onto the biochar. The loading of the adsorbent with heavy metal ions, in general, led to shifts in the peaks and a reduction in intensity of the peak at 1414.9896 cm^{-1} (Appendix 10.4) due to the interaction of aromatic structures in the biochar with heavy metals.

4.4 Adsorption efficiency and adsorption capacity of activated water hyacinth powder

Equation 3.6 was used to determine the quantity of heavy metals adsorbed (adsorption efficiency) on powdered water hyacinth, and Equation 3.7 was used to determine the adsorption capacity (q) and the results are provided in Table 4.6 below.

Table 4.6: Adsorption efficiency and adsorption capacity of water hyacinth powder

Sites	Heavy metal (ppm)	Adsorption Efficiency (%)		Adsorption Capacity (mg/g)	
		Waste water	Aqueous solution	Waste water	Aqueous solution
Site 1	Cadmium (7.45)	85.8	96.8	1.29	1.46
	Chromium (8.21)	82.9	94.0	1.36	1.54
	Lead (4.75)	100.0	100.0	0.95	0.95
	Zinc (63.02)	69.2	77.1	8.72	9.71
	Copper (8.73)	81.7	90.1	1.43	1.57
Site 2	Cadmium (40.18)	77.5	83.6	6.23	6.72
	Chromium (13.07)	80.3	92.9	2.10	2.43
	Lead (72.03)	71.7	76.4	10.33	11.0
	Zinc (84.62)	62.2	71.5	10.52	12.10
	Copper (54.03)	77.6	81.4	8.39	8.79
Site 3	Cadmium (77.13)	73.9	76.4	11.41	11.78
	Chromium (0.54)	100.0	100.0	0.11	0.11
	Lead (93.54)	60.4	64.9	11.3	12.14
	Zinc (0.91)	100.0	100.0	0.18	0.18
	Copper (0.64)	100	100	0.13	0.13

The percentage of metal ions adsorbed by water hyacinth varied according to concentrations and media, as shown in Table 4.6. In wastewater from all three sites, the percentage of metal ions adsorbed was low at high metal concentrations, but the percent of metal ions adsorbed was high at

low concentrations. The level of competition for an adsorption site increases with a high percent of metal ion concentration and decreases with a low concentration (Medellin *et al*., 2017).

In addition to this, for a given concentration, the percentage of absorbed metal on water hyacinth was higher in an aqueous solution than in wastewater. According to Park *et al*. (2016), there may be external competition from other metal ions in the wastewater for adsorption sites, which could explain the low adsorption efficiency from the wastewater. Since there was just one type of metal ion available in the aqueous solution, there was no outside competition for the adsorption sites.

The results of the study demonstrated that water hyacinth could efficiently adsorb heavy metals from wastewater that was contaminated with heavy metals; as a result, heavy metals from wastewater could be eliminated by using water hyacinth powder.

4.5 Factors influencing the adsorption of heavy metals

The effects of adsorbent type, particle size, pH, contact time and adsorbent dose on heavy metal adsorption by activated water hyacinth from industrial wastewater were investigated and the results are presented as below.

4.5.1 Effect of adsorbent type

The results for the effect of adsorbent type (Appendix 2) showed that EP-WH-PA had a more adsorption efficiency for heavy metals than WHB. The EP-WH also had an adsorption efficiency higher than WHB but lower than EP-WH-PA. This showed that double-activation with eggshell powder and phosphoric acid increased the adsorption efficiency of the adsorbent which could be attributed to the addition of more functional groups from both the eggshell and the acid (Saeb *et al*., 2017; Zhang *et al*., 2020). Additionally, water hyacinth biochar treated with egg shell powder (Figure 4.4) had an increased surface area in comparison to water hyacinth biochar (Figure 4.2)

making the former a better adsorbent. By treating water hyacinth with eggshell powder before pyrolysis, calcium oxide (CaO) was formed due to the thermal decomposition of $CaCO_3$ at high temperatures (Hart & Onyeaka, 2020). This treatment increases the alkalinity and introduces calcium-containing functional groups on the surface of the biochar. Furthermore, the introduction of calcium compounds promotes greater porosity and surface area, creating more active sites for adsorption (Mitrogiannis *et al*., 2017). This makes a better adsorbent than water hyacinth biochar. Pyrolyzed eggshell and biochar material from sugarcane bagasse was investigated as adsorbent for phosphate removal by (Liao *et al*., 2022), and it exhibited higher phosphate adsorption capacity than biochar alone (Liu *et al*., 2019).

Nonetheless, the best adsorbent was the one where double activation was done (EP-WH-PA) by treatment with both eggshell powder and phosphoric acid (Figure 4.6). The combination of eggshell powder and phosphoric acid activation further enhances the biochar's properties by increasing surface area and creating additional functional groups. Phosphoric acid activation increases the porosity of the biochar, leading to more accessible adsorption sites. (Sarker *et al*., 2023). Synergistic effects of calcium and phosphate groups enhance both the adsorption rate and capacity. This is because increased surface area and porosity provide more sites for heavy metal capture (Zeng *et al*., 2021). Therefore, EP-WH-PA would show superior adsorption compared to WHB and EP-WH. This adsorbent was considered for the subsequent optimization studies.

4.5.2 Effect of adsorbent particle size

The effect of particle size of the activated water hyacinth-based adsorbent on the removal of cadmium, lead, zinc, copper, and chromium ions was studied using two different particle sizes (300 µm and 425 µm), and results are illustrated in Appendix 3.

4.5.2.1 Effect of particle size on the adsorption of cadmium ions.

Cadmium concentrations of 7.54 ppm, 40.18 ppm and 77.13 ppm were used for particle size studies and the data obtained in Appendix 3 was used to construct Figure 4.13.

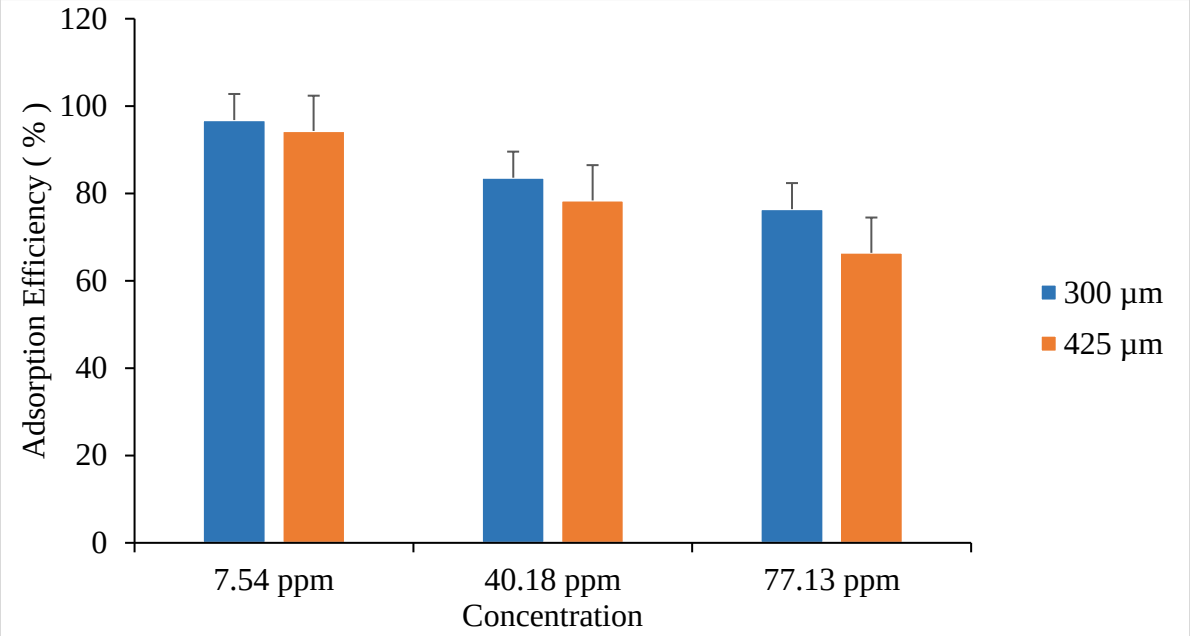

Figure 4.13: Effect of particle size on the adsorption of cadmium ions.

The highest adsorption was noted for the lowest particle size. This was probably due to the larger surface area, which provided more sorption sites for metal ions (Volesky, 2007). Adsorption is improved when the adsorbent's particle size decreases because it increases surface area. This trend was observed for the heavy metals lead, zinc, copper, and chromium, as illustrated graphically in Appendices 2a, 2b, 2c, and 2d respectively.

For low heavy metal concentrations (0.91 ppm zinc, 0.64 ppm copper, 0.54 ppm copper and 4.75 ppm lead), an adsorption efficiency of 100 was obtained on the treatment of the prepared working solutions with the activated water hyacinth adsorbent of 300 µm particle size. This indicated that

activated water hyacinth can adsorb heavy metal ions completely from solutions of a low concentration.

In the ensuing studies, a particle size of less than 300 µm was employed since it was discovered to provide the maximum adsorption rate.

4.5.3 Effect of pH on adsorption

The concentration of heavy metal ions in the wastewater solution is influenced by the pH value of the solution, which makes it a crucial component for adsorption. The adsorbent's affinity for the target metal ions is influenced by the charge distribution on its surface as well as the chemical state of the active groups (i.e., degree of protonation) on these surfaces. Appendix 4 shows the pH results for the selected heavy metals.

4.5.3.1 Effect of pH on adsorption of Cd^{2+} ions by activated water hyacinth

The effect of the pH of the solution on the biosorption of Cd^{2+} ions was examined by calculating the percentage adsorption from 100 mL metal solutions at various pH values (range from 3.0 to 7.0) and the results displayed in Figure 4.14 below.

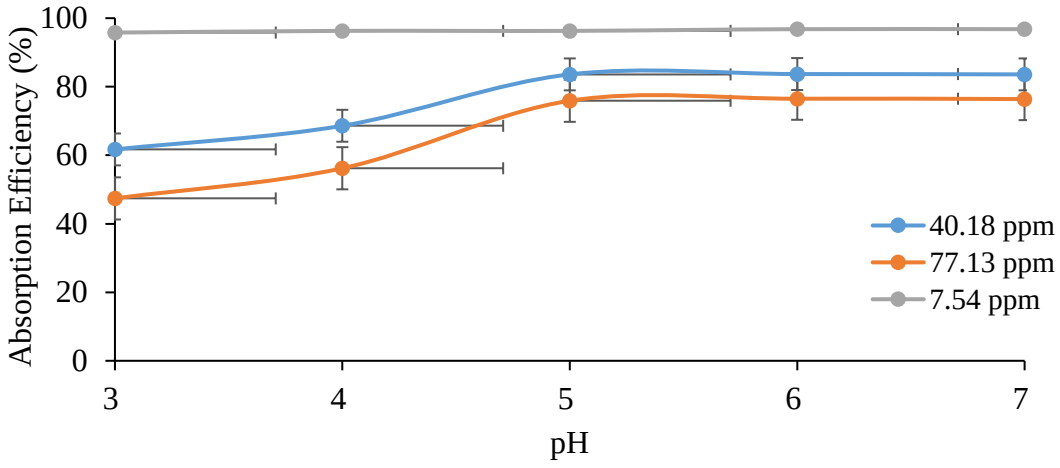

Figure 4.14: Effect of pH on adsorption of cadmium ions by activated water hyacinth-based adsorbent.

The adsorption efficiency rose for Cd^{2+} ion concentrations of 77.13 ppm and 40.18 ppm as pH rose from 3 to 5. At pH 3 to 4, there was a gradual rise in the quantity of cadmium ions adsorbed, nevertheless. The competition between cadmium and hydrogen ions for the exchange sites on the outer surface of the adsorbent could provide an explanation for this. When the pH rises, more metal ions adsorb because the H^+ ions compete with the metal ions for adsorption sites on the adsorbent at a lower pH (Taty-Costodes *et al*., 2003). At pH values of 4 to 5, the adsorption of Cd rose quickly. Less competition may have existed because the concentration of hydrogen ions, which were preventing adsorption at lower pH, was reduced. In other words, a higher pH is predicted to raise the surface charge of biomass and allow for the maximum amount of positively charged cation adsorption. At pH 5, optimal adsorption was noted. Above pH 5, the gradual increase may have resulted from metal ion saturation at the majority of the adsorption sites. The investigation revealed that a pH of 5 was ideal for the adsorption of cadmium ions.

Appendices 3a, 3b, 3c, and 3d provide a graphic representation of the effects of pH on the adsorption of lead, zinc, chromium, and copper. Lead, chromium, and copper adsorbed best at a pH of 4, while zinc and cadmium adsorbed best at a pH of 5. Zinc and cadmium exhibited a similar tendency, however lead, copper, and chromium heavy metals displayed distinct trends in the pH range of 6-7. That is, lead, copper, and chromium adsorption effectiveness began to decrease above pH 6. This could be due to the precipitation of $Pb(OH)_2$, $Cu(OH)_2$ and $Cr(OH)_3$ respectively which are insoluble hydroxides. At these high pH values, the metal cations are eliminated by precipitation rather than through adsorption processes. Similar results were reported by Kumar *et al*. (2006) and Semerjian (2010).

4.5.4 Effect of contact time on adsorption

4.5.4.1 Effect of contact time on adsorption of cadmium ions

According to the study results (Appendix 5), the extent of cadmium ions absorbed by activated water hyacinth increased with the length of contact time as shown in Figure 4.15.

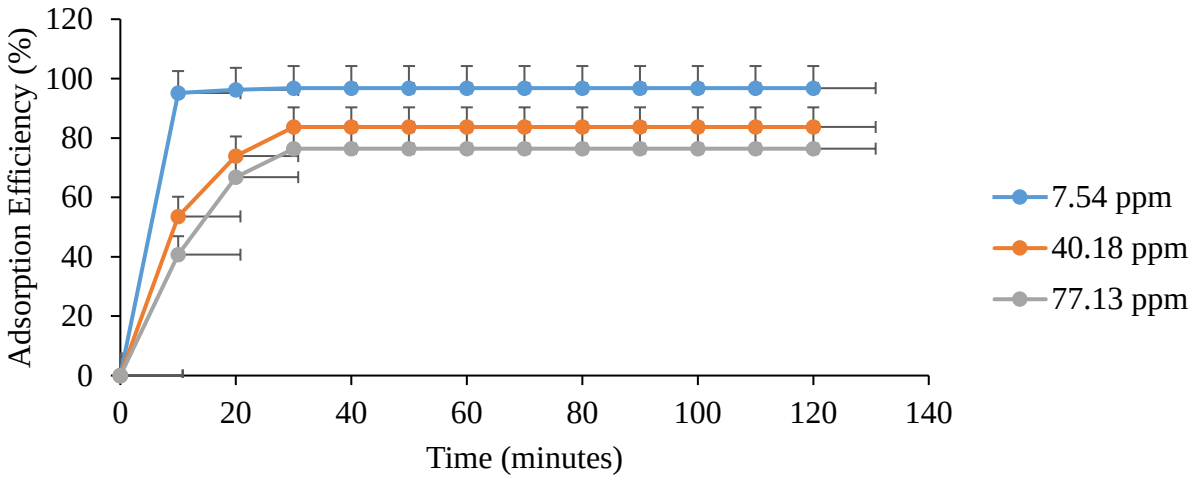

Figure 4.15: The effect of contact time on adsorption of cadmium ions by activated water hyacinth-based adsorbent.

Three separate initial concentrations of aqueous cadmium (7.54, 40.18, and 77.13 ppm) are shown in the figure 4.15. The percentage of cadmium ions adsorbed increased quickly in the first ten minutes, at low cadmium ion concentrations (7.54 ppm). From ten minutes to 120 minutes, the percentage of cadmium ions at low concentration of 7.54 ppm adsorbed remained at 96.8%. This might be the result of decreased competition for the adsorption sites due to decreasing cadmium ion concentrations. It also demonstrated the extremely high efficiency with which water hyacinth could adsorb cadmium ions from wastewater solutions with low concentrations. The equilibrium took some time to develop at cadmium ion concentrations of 40.18 ppm and 77.13 ppm. This was a result of competition for the adsorption sites at high concentrations. Saturation of the adsorption sites resulted in reduced adsorption efficiency for each metal at higher initial concentrations. In

other words, binding sites become almost saturated as the concentration rises, able to only accept a percentage of the available metal ions in search of binding sites.

4.5.5 Effect of mass of the adsorbent on adsorption of cadmium ions

The dosage of the adsorbent is a crucial factor that affects adsorption and, consequently, the expense of utilizing the adsorbent for commercial applications. The effect of mass of the adsorbent on adsorption of cadmium ions from the solutions was studied using adsorbent dosages in the range of 0.25 to 2.0 g. Figure 4.16 presents the acquired results.

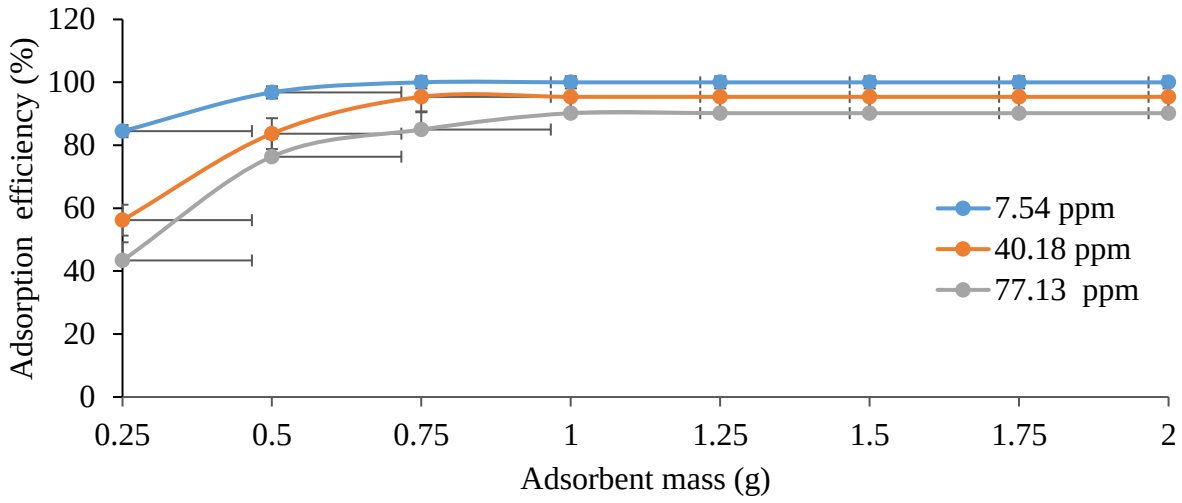

Figure 4.16: Effect of adsorbent mass on adsorption of cadmium ions by activated water hyacinth-based adsorbent.

According to the study results, the percentage of metal ions adsorbed on the activated adsorbent increased as the adsorbent dosage was increased. After 120 minutes of exposure, the highest removal percentage was 43.4%, which corresponded to a concentration of 77.13 ppm of cadmium ions, while the lowest removal percentage was 100% for a concentration of 7.54 ppm. According to Figure 4.16, the percentage of adsorption increases as the bulk of the biosorbent increases because there are more potential adsorption binding sites. A mass of 0.75 g was adequate to adsorb

all the ions present in 100 mL of 7.54 ppm of Cd ions. Optimum adsorption for cadmium concentration 40.18 ppm (90.2%) and 77.13 ppm (95.4%) was reached at an adsorbent mass of 0.75 g and 1.0 g of the activated water hyacinth-based adsorbent respectively.

The 100 % adsorption for cadmium ions obtained for 7.54 ppm solution was because cadmium ions contained in the solutions were entirely adsorbed by 0.75 g of the adsorbent and hence the curve formed a plateau at adsorption efficiency 100% on the corresponding adsorbent mass. The optimum adsorption for lead was at 1.25 g while that of zinc, copper and chromium was 1.0 g. Appendices 6a, 6b, 6c and 6d show graphic representations of the effects of adsorbent mass on the adsorption of lead, zinc, copper and chromium respectively.

4.6 Adsorption Equilibrium isotherms

Equilibrium sorption isotherms, which are defined by specific constants expressing the surface characteristics and affinity of the biosorbent for various contaminants, can be used to characterize a biosorbent's sorption capacity (Dursun *et al*., 2005). In this study, Freundlich and Langmuir's isotherms were selected to fit experimental data for the amount of heavy metal adsorbed by activated water hyacinth powder.

4.6.1 Adsorption equilibrium isotherms for the adsorption of cadmium ions

The data (Appendix 7a) from the studies was fitted to both Langmuir and Freundlich isotherms to give plots shown in Figures 4.17 and 4.18.

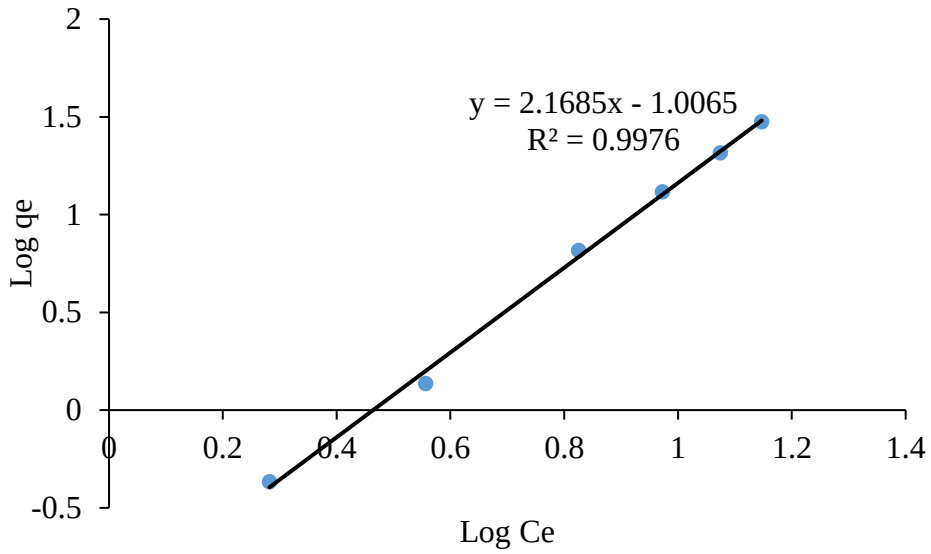

Figure 4.17: Linear Freundlich plot for the adsorption of cadmium ions onto activated water hyacinth.

The logarithm of concentration at equilibrium (Ce) increased linearly with the logarithm of adsorption capacity at equilibrium (qe).

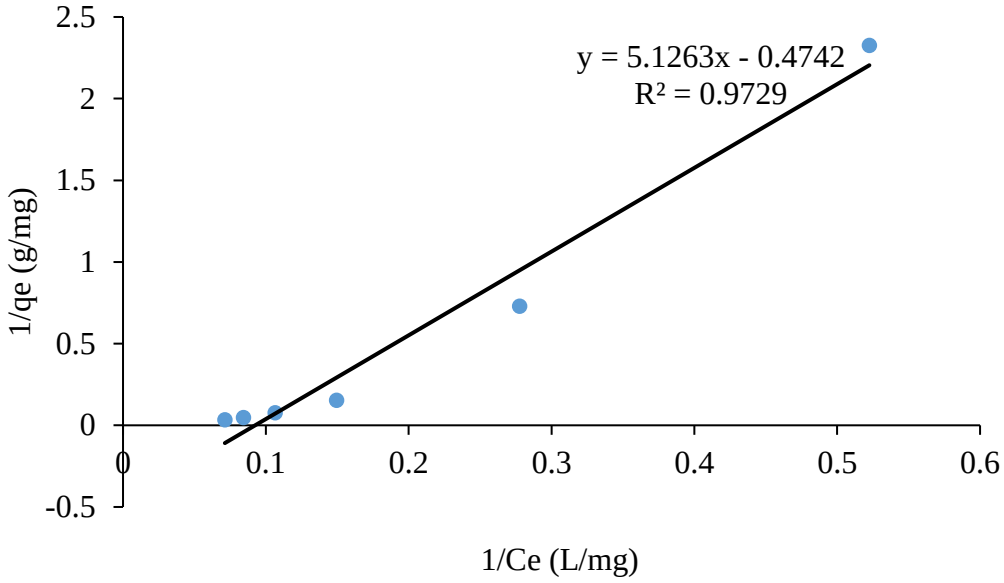

Figure 4.18: A linear Langmuir plot for the adsorption of cadmium ions onto activated water hyacinth adsorbent.

In respect to the reciprocal of concentration at equilibrium (Ce), the reciprocal of adsorption capacity at equilibrium (qe) increased linearly.

Table 4.7: Langmuir and Freundlich parameters for Cd^{2+} ions adsorption

Langmuir isotherm			Freundlich isotherm		
b(L/mg)	q_m(mg/g)	R^2	N	K_f	R^2
- 0.0925	- 2.1088	0.9729	0.4611	0.0985	0.9976

The optimal model to explain the adsorption on activated water hyacinth adsorbent was inferred using the values of R^2. Based on the R^2 values, it was discovered that the adsorption of cadmium ions onto the activated adsorbent from water hyacinth biomass was better linked with the Freundlich model than the Langmuir model. An adsorption model called the Freundlich isotherm represents multilayer adsorption, whereas the Langmuir isotherm describes monolayer adsorption. With an adsorption value of less than 1 (0.4611), the link between the adsorbent and adsorbate is weak. Thus, physisorption is suggested.

The Langmuir adsorption parameters of the experimental results showed negative intercepts, indicating that the investigated system's adsorption behavior does not conform to the Langmuir approach suppositions. Similar results were obtained by Kiurskic et al. (2012) in their study about the adsorption feasibility in the Cr^{3+} ions removal from waste printing developers.

4.6.2 Adsorption isotherms for the adsorption of lead ions

Both Langmuir and Freundlich isotherms were fitted to the study data (Appendix 7b), with the resulting Figures 4.19 and 4.20 displaying the observed differences.

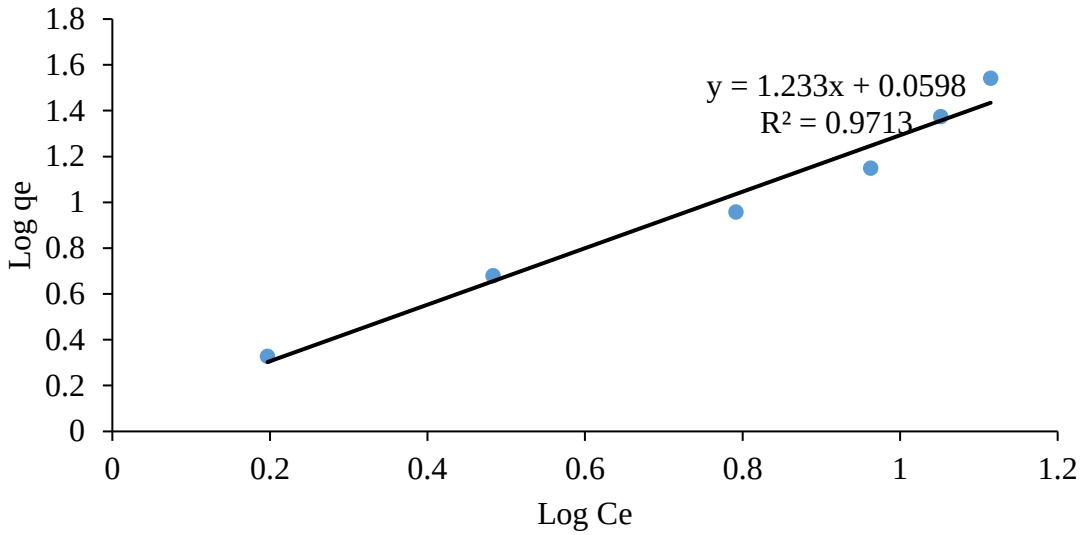

Figure 4.19: A linear Freundlich plot for the adsorption of lead ions onto activated water hyacinth adsorbent.

In respect to the logarithm of concentration at equilibrium (Ce), the logarithm of adsorption capacity at equilibrium (qe) increased linearly.

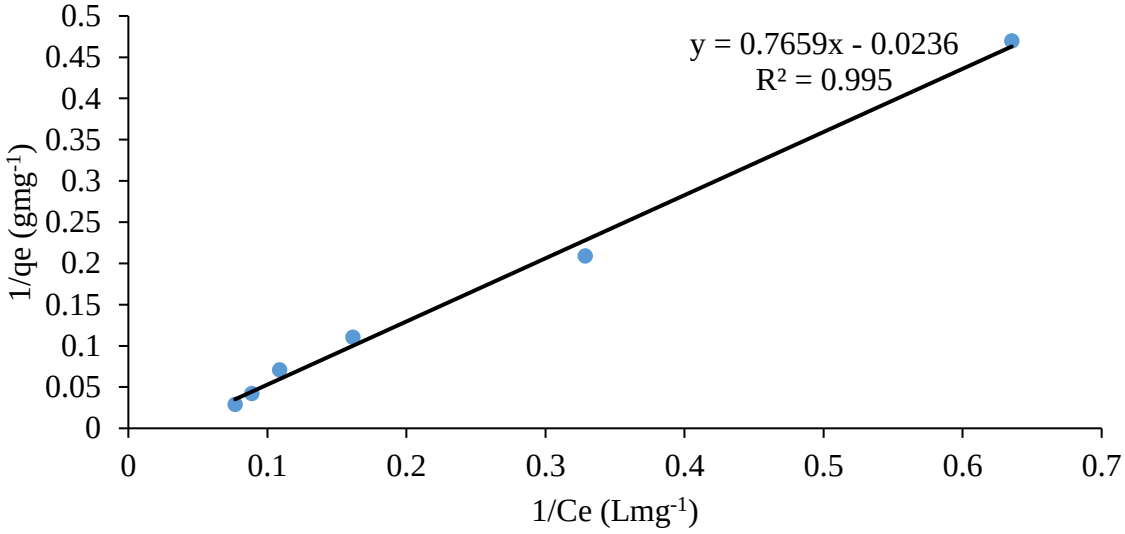

Figure 4.20: A linear Langmuir plot for the adsorption of lead ions onto activated water hyacinth adsorbent.

In relation to the reciprocal of concentration at equilibrium (Ce), the reciprocal of adsorption capacity at equilibrium (qe) increased linearly.

Table 4.8: Langmuir and Freundlich parameters for Pb^{2+} ions adsorption

Langmuir isotherm			Freundlich isotherm		
b(L/mg)	q_m(mg/g)	R^2	n	K_f	R^2
- 0.0308	- 42.3729	0.995	0.8110	0.9471	0.9713

The linear plots of 1/Qe versus 1/Ce suggested the applicability of the Langmuir isotherms (Figure 4.20). However, when Values of q_m and b were determined from slope and intercepts of the plots and presented in Table 4.8, the experimental data of Langmuir adsorption parameters gave negative values due to the negative intercept. This suggested that the adsorption behavior of the tested system does not follow the assumption of the Langmuir approach.

The Freundlich isotherm was also employed and the effects of powdered water hyacinth biochar on lead ion adsorption correlated well with the Freundlich isotherm model which implies multilayer adsorption on the binding sites of the activated biochar.

4.6.3 Adsorption isotherms for the adsorption of zinc ions

The data obtained (Appendix 7c) was displayed as Figures 4.21 and 4.22.

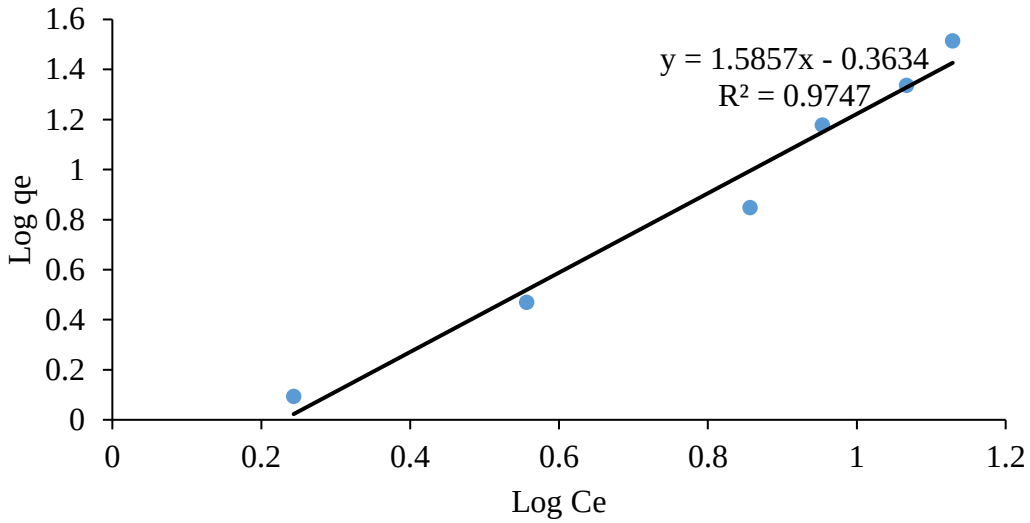

Figure 4.21: A linear Freundlich plot for the adsorption of zinc ions onto activated water hyacinth adsorbent.

In respect to the logarithm of concentration at equilibrium (Ce), the logarithm of adsorption capacity at equilibrium (qe) increased linearly.

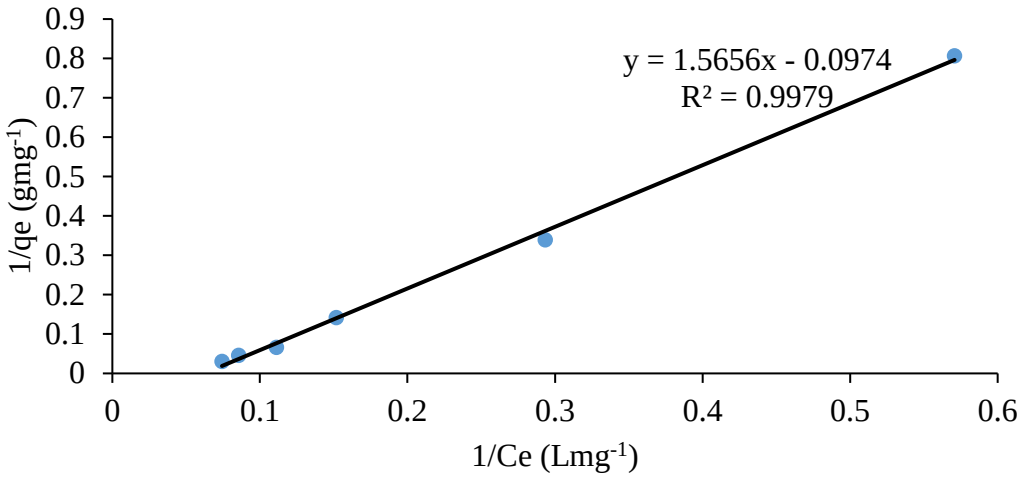

Figure 4.22: A linear Langmuir plot for the adsorption of zinc ions onto activated water hyacinth adsorbent.

The reciprocal of adsorption capacity at equilibrium (qe) increased linearly in relation to the reciprocal of concentration at equilibrium (Ce).

Table 4.9: Langmuir and Freundlich parameters for Zn^{2+} ions adsorption

Langmuir isotherm			Freundlich isotherm		
b(L/mg)	q_m(mg/g)	R^2	n	K_f	R^2
- 0.0622	- 10.2669	0.9979	0.6306	0.4331	0.9747

In the Langmuir isotherm adsorption model of zinc ions by activated water hyacinth powder. A linear plot of 1/qe versus 1/Ce suggested the applicability of Langmuir isotherms. However, the negative intercept showed that the adsorption behaviour of zinc ions did not follow Langmuir isotherm assumptions. Fitting zinc adsorption on the regression line revealed a strong correlation (R^2 = 0.9747) with the Freundlich isotherm model. Therefore, through multilayer adsorption, the metal ions were adsorbed onto the activated water hyacinth adsorbent at the binding sites.

4.6.4 Adsorption isotherms for the adsorption of copper ions

Figures 4.23 and 4.24 show the outcomes of fitting the data from the studies (Appendix 7.d) to both Langmuir and Freundlich isotherms.

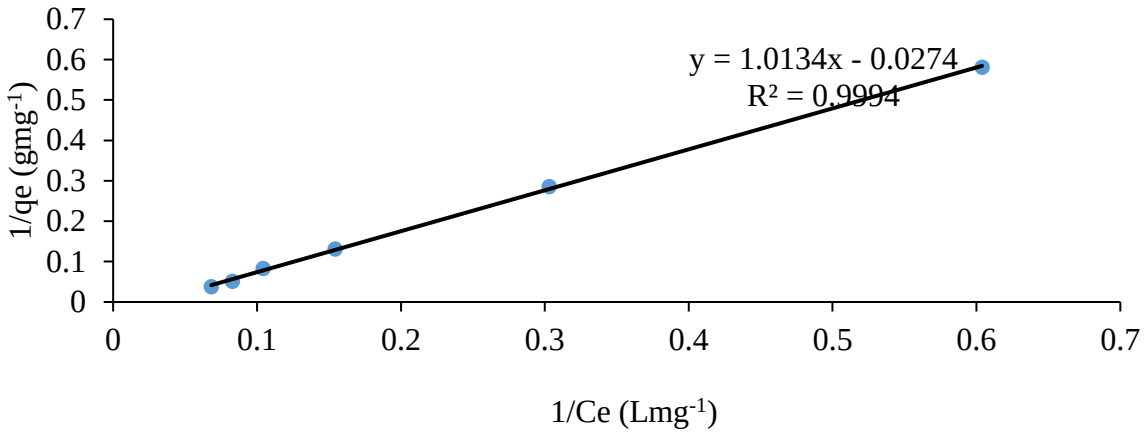

Figure 4.23: A linear Freundlich plot for the adsorption of copper ions onto activated water hyacinth adsorbent.

In respect to the logarithm of concentration at equilibrium (Ce), the logarithm of adsorption capacity at equilibrium (qe) increased linearly.

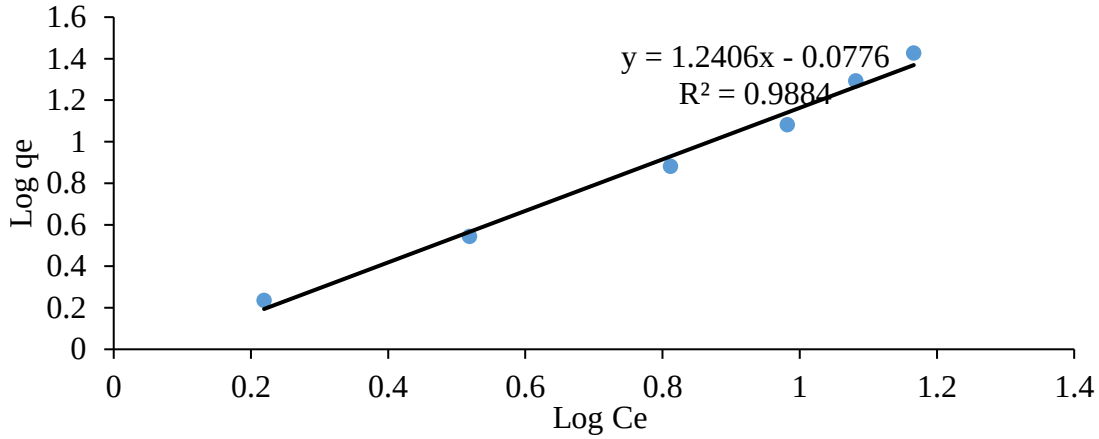

Figure 4.24: A linear Langmuir plot for the adsorption of copper ions onto activated water hyacinth adsorbent.

The reciprocal of adsorption capacity at equilibrium (qe) increased linearly in relation to the reciprocal of concentration at equilibrium (Ce)

Table 4.10: Langmuir and Freundlich parameters for Cu^{2+} ions adsorption

Langmuir isotherm			Freundlich isotherm		
b(L/mg)	q_m(mg/g)	R^2	N	K_f	R^2
- 0.0270	- 36.4964	0.9994	0.8061	0.8364	0.9884

The use of water hyacinth activated adsorbent on the adsorption of copper ions correlated well with the Freundlich model with an R^2 value of 0.9884. The Langmuir adsorption isotherm model had a higher R^2 value but the negative values of b (L/mg) and q_m(mg/g) due to the negative intercept suggest that the adsorption of Cu^{2+} ions on activated water hyacinth adsorbent powder does not follow the Langmuir approach assumptions.

4.6.5 Adsorption isotherms for the adsorption of chromium ions

The data obtained (Appendix 7.e) from the studies was then fitted into both Langmuir and Freundlich isotherms. The isotherms are given in Figures 4.25 and 4.26.

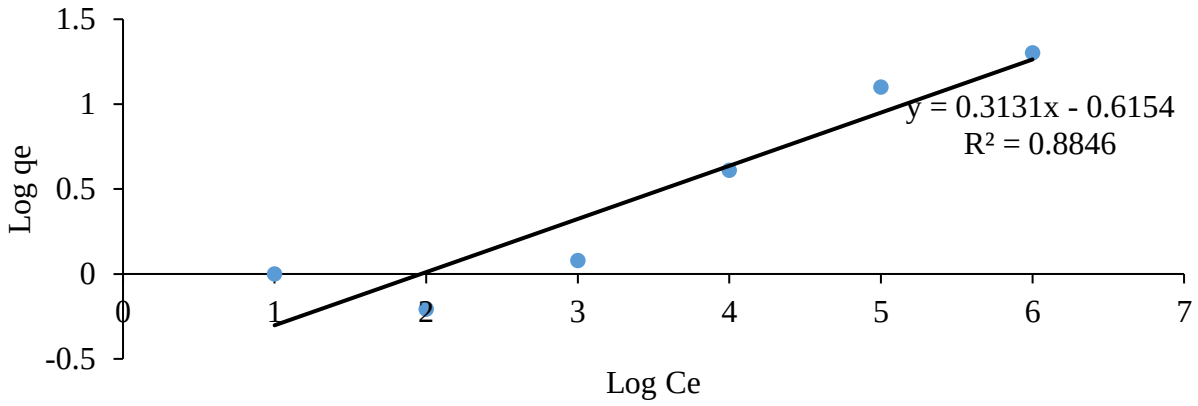

Figure 4.25: A linear Freundlich plot for the adsorption of chromium ions onto activated water hyacinth adsorbent.

In respect to the logarithm of concentration at equilibrium (Ce), the logarithm of adsorption capacity at equilibrium (qe) increased linearly.

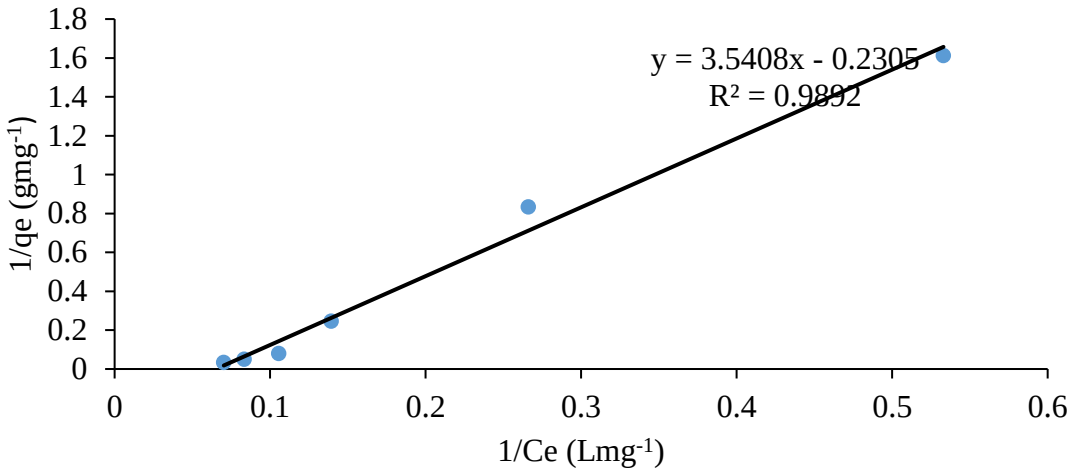

Figure 4.26: A linear Langmuir plot for the adsorption of chromium ions onto activated water hyacinth adsorbent.

In respect to the reciprocal of concentration at equilibrium (Ce), the reciprocal of adsorption capacity at equilibrium (qe) increased linearly.

Table 4.11: Langmuir and Freundlich parameters for Cr^{3+} ions adsorption

Langmuir isotherm			Freundlich isotherm		
b(L/mg)	q_m(mg/g)	R^2	N	K_f	R^2
- 0.0651	- 4.3384	0.9892	3.1939	4.1248	0.8846

The Langmuir adsorption isotherm model had a higher R^2 value (R^2 = 0.9892) compared to the Freundlich isotherm but the negative values of b (L/mg) and q_m(mg/g) suggest that the adsorption of Cr^{3+} ions on activated water hyacinth adsorbent powder does not follow the Langmuir approach assumptions. With water hyacinth powder, chromium adsorption can thus be explained by the Freundlich Isotherm. Kiurskic *et al*. (2012) observed similar findings on the adsorption of chromium ions.

Generally, the negative intercept on the Langmuir adsorption isotherm indicates chemisorption, as the adsorption process favored the Freundlich adsorption model, which involves the adsorbent and adsorbate forming chemical bonds. Chemisorption can occur even at very low gas phase pressures. In such instances, a portion of the surface may already be covered by adsorbate molecules, resulting in a non-zero fractional coverage (θ) even at zero gas phase pressure.

4.7 Kinetic studies

The pseudo-first-order and pseudo-second-order kinetic models were used to examine the adsorption data's kinetics.

4.7.1 Kinetic studies for the adsorption of cadmium ions

Figures 4.27 and 4.28 display the results of the data from Appendix 9a against the pseudo-first and pseudo-second order models.

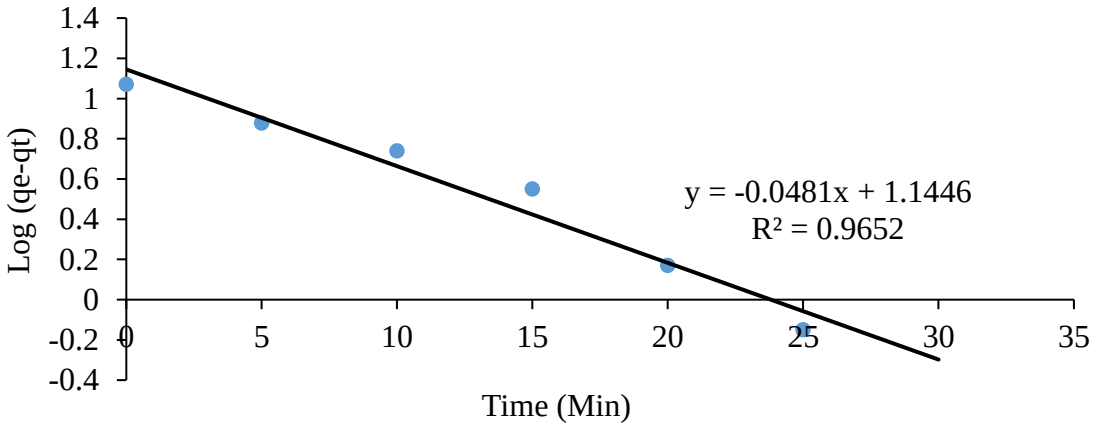

Figure 4.27: Pseudo-first-order for the adsorption of 77.13 ppm cadmium ions onto water hyacinth powder.

Log (qe-qt), the logarithmic difference between the adsorption capacity at equilibrium and at a specific time, decreased linearly with increasing adsorption duration.

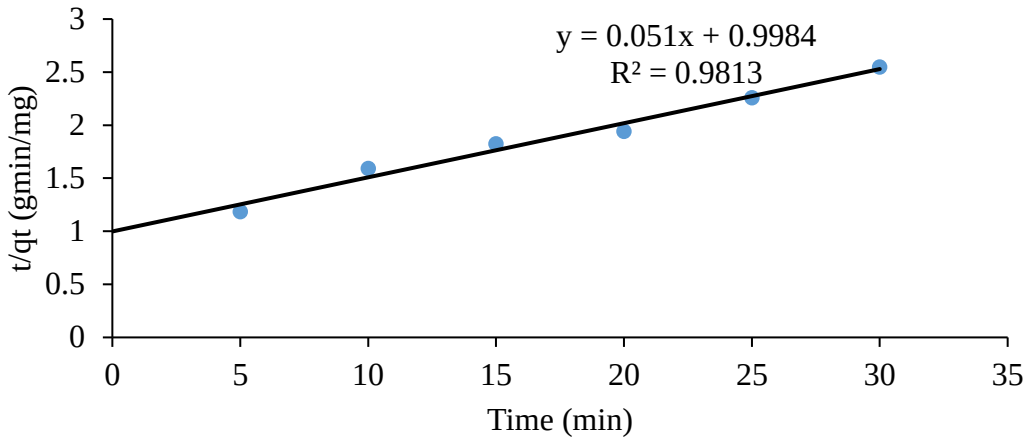

Figure 4.28: Pseudo-second-order for the adsorption of 77.13 ppm cadmium ions onto activated water hyacinth powder.

The adsorption time rose linearly in the quotient of t /qt. The pseudo-second-order plot (R^2 = 0.9813) has a higher correlation coefficient than the pseudo-first-order plot (R^2 = 0.9652), according to the aforementioned data. This suggests that chemisorption was the rate-limiting phase. Therefore, the pseudo-second-order process fits the adsorption of Cd^{2+}.

Appendix 9 presents the graphic calculations of the pseudo-first order and pseudo-second order parameters for the adsorption from the following solutions: 93.54 ppm lead ion solution, 63.01 ppm zinc ion solution, 54.03 ppm copper ion solution, and 13.07 ppm chromium ion solution. The outcomes are displayed below in Table 4.12.

Table 4.12: The Pseudo first-order and Pseudo second-order kinetic parameters of adsorption of cadmium, lead, zinc, copper and chromium ions on activated water hyacinth-based adsorbent.

	Pseudo first-order kinetics Parameters			Pseudo second-order kinetics Parameters		
Metal ions	$K_1(min^{-1})$	$q_e(mgg^{-1})$	R^2	$K_2(gmg^{-1}min^{-1})$	$q_e(mgg^{-1})$	R^2
Cd^{2+} ions	0.1108	13.9508	0.9652	0.0026	19.6078	0.9813
Pb^{2+} ions	0.2084	13.9508	0.9652	0.0042	20.202	08777
Zn^{2+} ions	0.1147	8.533	0.941	0.0317	12.8041	0.9998
Cu^{2+} ions	0.2142	9.7477	0.9883	0.0117	12.1655	0.9735
Cr^{3+} ions	0.1177	1.6588	0.9297	0.1767	2.5543	0.9998

It was observed that the R^2 values for the pseudo-second-order in the adsorption of cadmium (R^2 = 0.9813), zinc (R^2 = 0.9998) and chromium ions (R^2 = 0.9998) were higher than that of pseudo first-order for the respective metal ions. This implied that the kinetics of adsorption of cadmium, zinc and chromium ions on activated water hyacinth adsorbent powder were better expressed by the pseudo second order model. Therefore, the rate-limiting step for the adsorption of these metals was chemisorption. For metals, lead and copper, it was observed that the R^2 value for the pseudo-first order (R^2 = 0.9652) and (R^2 = 0.9883) corresponding to two respective metals was higher than that of pseudo second order. Therefore, the adsorption kinetics of lead and copper on activated water hyacinth adsorbent powder were better expressed by the pseudo first order model. This implies that their rate limiting step is physisorption.

CHAPTER FIVE

CONCLUSIONS AND RECOMMENDATIONS

5.1 Conclusions

From the results of the study, it can be concluded that; activated water hyacinth-based adsorbents can be used for the removal of heavy metals in wastewater. For low heavy metal concentrations, an adsorption efficiency as high as 100% was achieved by activated water hyacinth-based adsorbents. A synergistically activated water hyacinth-based adsorbent (EP-WH-PA) had a higher adsorption efficiency compared to both the adsorbent activated with a single activating agent (WH-PA) and the unactivated water hyacinth-based adsorbent (WHB). The mean heavy metal concentrations were in the range of 7.45-77.13 ppm for cadmium, 0.54-13.07 ppm for chromium, 4.75-93.54 ppm for lead, 0.91-84.62 ppm for zinc and 0.64-54.03 ppm for copper. The removal of heavy metal ions in wastewater is affected by the adsorbent type, particle size of the adsorbent, pH, contact time and mass of the adsorbent. Activated water hyacinth-based adsorbents have a higher adsorption efficiency than unactivated ones. The optimal adsorption of metal ions was at a pH range of 4 to 5. Adsorption occurred through multilayer coverage, as indicated by the experimental data which fitted well to the Freundlich isotherm. It is possible, nevertheless, for homogenous adsorption to occur. The studied heavy metals were found to exceed the maximum recommended limits by both national and international bodies (NEMA, WHO, EU, USEPA) and therefore industrial waste water should be treated before discharge into the environment. By utilizing water hyacinth which is a renewable resource to remove heavy metals from wastewater, this approach will help Uganda to meet Sustainable Development Goals (SDGs) particularly goal number 06 regarding clean water and sanitation by improving water quality and goal 07 of ensuring access to affordable and sustainable energy and promoting responsible resource management. The

utilization of water hyacinth for removal of heavy metals in wastewaters also aligns with Uganda's National Development Plan (NDP) IV goals focused on sustainable development and economic growth by providing a cost-effective and sustainable solution for wastewater treatment.

5.2 Recommendations

1. To retrieve both the adsorbents and the adsorbate, detailed regeneration experiments with pollutants-laden adsorbents are need to be made. This will increase the economic viability of the process.
2. It is necessary to evaluate the feasibility of using the inexpensive adsorbent in systems with several components. This would have a major effect on the potential of the adsorbent for commercial use in industrial systems. This application will assist the nation in achieving its Vision 2030 objectives related to environmental preservation for the benefit of future generations.
3. Studies should be made to ascertain whether the heavy metal concentration of the portable water of the streams that flow from and/or through the Nakawa Industrial area are within the acceptable regulatory limits by national and international regulatory bodies to ensure that the consuming population is not subject to heavy metal intoxication.
4. Research needs to be done to optimize and characterize the activated carbon material. This will entail measuring the material's specific surface area, ash content, volatile matter content, and pore size and volume. To maximize adsorption capacity and boost adsorbent efficiency for the removal of organic and metallic pollutants from effluents, it is important to investigate alternative activation techniques.

REFERENCES

Abba, A., & Sankarannair, S. (2024). Global impact of water hyacinth (Eichhornia Crassipes) on rural communities and mitigation strategies: a systematic review. *Environmental Science and Pollution Research*, *31*(31), 43616–43632.

Abdelkreem, M. (2013). Adsorption of phenol from industrial wastewater using olive mill waste. *APCBEE Procedia*, *5*, 349–357.

Aboulroos, S., Helal, M. I., & Kamel, M. (2006). Remediation of Pb and Cd polluted soils using in situ immobilization and phytoextraction techniques. *Soil and Sediment Contamination*, *15*(2), 199–215. https://doi.org/10.1080/15320380500506362

Acevedo, B., & Barriocanal, C. (2015). *Texture and surface chemistry of activated carbons obtained from tyre wastes*.

Afroze, S., Sen, T. K., Ang, M., & Nishioka, H. (2016). Adsorption of methylene blue dye from aqueous solution by novel biomass Eucalyptus sheathiana bark: equilibrium, kinetics, thermodynamics and mechanism. *Desalination and Water Treatment*, *57*(13), 5858–5878. https://doi.org/10.1080/19443994.2015.1004115

Ahmad, S. Z. N., Wan Salleh, W. N., Ismail, A. F., Yusof, N., Mohd Yusop, M. Z., & Aziz, F. (2020). Adsorptive removal of heavy metal ions using graphene-based nanomaterials: Toxicity, roles of functional groups and mechanisms. *Chemosphere*, *248*, 126008. https://doi.org/10.1016/j.chemosphere.2020.126008

Akinbile, C. O., & Yusoff, M. S. (2012). Assessing water hyacinth (Eichhornia crassopes) and lettuce (Pistia stratiotes) effectiveness in aquaculture wastewater treatment. *International Journal of Phytoremediation*, *14*(3), 201–211.

Al-Rub, F. A. A., El-Naas, M. H., Ashour, I., & Al-Marzouqi, M. (2006). Biosorption of copper on Chlorella vulgaris from single, binary and ternary metal aqueous solutions. *Process Biochemistry*, *41*(2), 457–464. https://doi.org/10.1016/j.procbio.2005.07.018

Al-Tohamy, R., Ali, S. S., Li, F., Okasha, K. M., Mahmoud, Y. A.-G., Elsamahy, T., Jiao, H., Fu, Y., & Sun, J. (2022). A critical review on the treatment of dye-containing wastewater: Ecotoxicological and health concerns of textile dyes and possible remediation approaches for environmental safety. *Ecotoxicology and Environmental Safety*, *231*, 113160.

Ali, H., & Khan, E. (2018). What are heavy metals? Long-standing controversy over the scientific use of the term 'heavy metals'–proposal of a comprehensive definition. *Toxicological and Environmental Chemistry*, *100*(1), 6–19. https://doi.org/10.1080/02772248.2017.1413652

Alslaibi, T. M., Abustan, I., Ahmad, M. A., & Foul, A. A. (2013). Cadmium removal from aqueous solution using microwaved olive stone activated carbon. *Journal of Environmental Chemical Engineering*, *1*(3), 589–599. https://doi.org/10.1016/j.jece.2013.06.028

Alvarez, V., & Paulis, M. (2017). Effect of acrylic binder type and calcium carbonate filler amount on the properties of paint-like blends. *Progress in Organic Coatings*, *112*(July), 210–218. https://doi.org/10.1016/j.porgcoat.2017.07.023

Aravindhan, R., Rao, J. R., & Nair, B. U. (2009). Application of a chemically modified green macro alga as a biosorbent for phenol removal. *Journal of Environmental Management*, *90*(5), 1877–1883. https://doi.org/10.1016/j.jenvman.2008.12.005

Augustynowicz, J., Grosicki, M., Hanus-Fajerska, E., Lekka, M., Waloszek, A., & Kołoczek, H. (2010). Chromium(VI) bioremediation by aquatic macrophyte Callitriche cophocarpa Sendtn. *Chemosphere*, *79*(11), 1077–1083. https://doi.org/10.1016/j.chemosphere.2010.03.019

Aurich, A., Hofmann, J., Oltrogge, R., Wecks, M., Gläser, R., Blömer, L., Mauersberger, S., Müller, R. A., Sicker, D., & Giannis, A. (2017). Improved Isolation of Microbiologically Produced (2R,3S)-Isocitric Acid by Adsorption on Activated Carbon and Recovery with Methanol. *Organic Process Research and Development*, *21*(6), 866–870. https://doi.org/10.1021/acs.oprd.7b00090

Ayinla, K. I., Baba, A. A., Tripathy, B. C., & Dwari, R. K. (2024). Production of Industrial-Grade Monoclinic Lead Chromate (PbCrO4) from Indigenous Chromite ore for Paint Pigment Utilization. *Journal of Nepal Chemical Society*, *44*(2), 101–109.

Badea, M., Uivarosi, V., & Olar, R. (2020). Improvement in the pharmacological profile of copper biological active complexes by their incorporation into organic or inorganic matrix. *Molecules*, *25*(24), 5830.

Bapat, S. A., & Jaspal, D. K. (2020). Surface-modified water hyacinth (Eichhornia crassipes) over activated carbon for wastewater treatment: a comparative account. *South African Journal of Chemistry*, *73*(1), 70–80.

Barakat, M. A. (2011). New trends in removing heavy metals from industrial wastewater. In *Arabian Journal of Chemistry* (Vol. 4, Issue 4, pp. 361–377). https://doi.org/10.1016/j.arabjc.2010.07.019

Barrera-Díaz, C., Canizares, P., Fernández, F. J., Natividad, R., & Rodrigo, M. A. (2014). Electrochemical advanced oxidation processes: an overview of the current applications to actual industrial effluents. *Journal of the Mexican Chemical Society*, *58*(3), 256–275.

Bashir, I., Lone, F. A., Bhat, R. A., Mir, S. A., Dar, Z. A., & Dar, S. A. (2020). Concerns and threats of contamination on aquatic ecosystems. *Bioremediation and Biotechnology:*

Sustainable Approaches to Pollution Degradation, 1–26.

Bazrafshan, E., Amirian, P., Mahvi, A. H., & Ansari-Moghaddam, A. (2016). Application of adsorption process for phenolic compounds removal from aqueous environments: a systematic review. *Global NEST Journal*, *18*(1), 146–163.

Bazrafshan, E., Mohammadi, L., Ansari-Moghaddam, A., & Mahvi, A. H. (2015). Heavy metals removal from aqueous environments by electrocoagulation process–a systematic review. *Journal of Environmental Health Science and Engineering*, *13*, 1–16.

Benalia, M. C., Youcef, L., Bouaziz, M. G., Achour, S., & Menasra, H. (2022). Removal of heavy metals from industrial wastewater by chemical precipitation: mechanisms and sludge characterization. *Arabian Journal for Science and Engineering*, *47*(5), 5587–5599.

Bernard, E., Jimoh, A., & Odigure, J. (2013). Heavy metals removal from industrial wastewater by activated carbon prepared from coconut shell. *Res J Chem Sci*, *2231*, 606X.

Biswas, S., Bal, M., Behera, S. K., Sen, T. K., & Meikap, B. C. (2019). Process optimization study of Zn2+ adsorption on biochar-alginate composite adsorbent by response surface methodology (RSM). *Water*, *11*(2), 325.

Blumbergs, E., Serga, V., Platacis, E., Maiorov, M., & Shishkin, A. (2021). Cadmium recovery from spent ni-cd batteries: A brief review. *Metals*, *11*(11), 1–14. https://doi.org/10.3390/met11111714

Caron, S., Dugger, R. W., Ruggeri, S. G., Ragan, J. A., & Brown Ripin, D. H. (2006). Large-scale oxidations in the pharmaceutical industry. *Chemical Reviews*, *106*(7), 2943–2989. https://doi.org/10.1021/cr040679f

Changmai, M., Banerjee, P., Nahar, K., & Purkait, M. K. (2018). A novel adsorbent from carrot, tomato and polyethylene terephthalate waste as a potential adsorbent for Co (II) from aqueous solution: Kinetic and equilibrium studies. *Journal of Environmental Chemical Engineering*, *6*(1), 246–257. https://doi.org/10.1016/j.jece.2017.12.009

Chen, S., Li, H., Liu, L., Liang, J., & Liu, C. (2016). The laser direct deposition iron-based alloy coating with high wear resistance. *6th International Conference on Mechatronics, Materials, Biotechnology and Environment (ICMMBE 2016)*, 259–263.

Chen, X.-L., Li, F., Xie, X. J., Li, Z., & Chen, L. (2019). Nanoscale zero-valent iron and chitosan functionalized Eichhornia crassipes biochar for efficient hexavalent chromium removal. *International Journal of Environmental Research and Public Health*, *16*(17), 3046.

Chidozie, K., & Nwakanma, C. (2017). Assessment of Saclux Paint Industrial Effluents on Nkoho River in Abia State, Nigeria. *Journal of Ecosystem & Ecography*, *07*(02). https://doi.org/10.4172/2157-7625.1000240

Chisti, H. (2018). *Heavy metal sequestration from contaminated water : A review*. *2508*(2), 2345–2355.

Crini, G., Lichtfouse, E., Wilson, L. D., & Morin-Crini, N. (2019). Conventional and non-conventional adsorbents for wastewater treatment. *Environmental Chemistry Letters*, *17*, 195–213.

Currie, H. A., & Perry, C. C. (2007). Silica in plants: Biological, biochemical and chemical studies. *Annals of Botany*, *100*(7), 1383–1389. https://doi.org/10.1093/aob/mcm247

Cychosz, K. A., Guillet-Nicolas, R., García-Martínez, J., & Thommes, M. (2017). Recent advances

in the textural characterization of hierarchically structured nanoporous materials. *Chemical Society Reviews*, *46*(2), 389–414.

Da Silva Correia, I. K., Santos, P. F., Santana, C. S., Neris, J. B., Luzardo, F. H. M., & Velasco, F. G. (2018). Application of coconut shell, banana peel, spent coffee grounds, eucalyptus bark, piassava (Attalea funifera) and water hyacinth (Eichornia crassipes) in the adsorption of Pb2+ and Ni2+ ions in water. *Journal of Environmental Chemical Engineering*, *6*(2), 2319–2334. https://doi.org/10.1016/j.jece.2018.03.033

Danish, M., Ahmad, T., Nadhari, W., Ahmad, M., Khanday, W. A., Ziyang, L., & Pin, Z. (2018). Optimization of banana trunk-activated carbon production for methylene blue-contaminated water treatment. *Applied Water Science*, *8*, 1–11.

de Carvalho Costa, L. R., de Moraes Ribeiro, L., Hidalgo, G. E. N., & Féris, L. A. (2022). Evaluation of efficiency and capacity of thermal, chemical and ultrasonic regeneration of tetracycline exhausted activated carbon. *Environmental Technology*, *43*(6), 907–917.

Deliyanni, E. A. (2019). Low-cost activated carbon from rice wastes in liquid-phase adsorption. In *Interface Science and Technology* (Vol. 30, pp. 101–123). Elsevier.

Deng, Y., Huang, S., Laird, D. A., Wang, X., & Meng, Z. (2019). Adsorption behaviour and mechanisms of cadmium and nickel on rice straw biochars in single- and binary-metal systems. *Chemosphere*, *218*, 308–318. https://doi.org/10.1016/j.chemosphere.2018.11.081

Deshpande, J., Joshi, M., & Giri, P. (2013). Zinc: The trace element of major importance in human nutrition and health. *International Journal of Medical Science and Public Health*, *2*(1), 1. https://doi.org/10.5455/ijmsph.2013.2.1-6

Dinari, M., Soltani, R., & Mohammadnezhad, G. (2017). Kinetics and thermodynamic study on novel modified–mesoporous silica MCM-41/polymer matrix nanocomposites: effective adsorbents for trace CrVI removal. *Journal of Chemical & Engineering Data*, *62*(8), 2316–2329.

Donkadokula, N. Y., Kola, A. K., Naz, I., & Saroj, D. (2020). A review on advanced physico-chemical and biological textile dye wastewater treatment techniques. *Reviews in Environmental Science and Bio/Technology*, *19*, 543–560.

Duan, C., Ma, T., Wang, J., & Zhou, Y. (2020). Removal of heavy metals from aqueous solution using carbon-based adsorbents: A review. *Journal of Water Process Engineering*, *37*(130), 101339. https://doi.org/10.1016/j.jwpe.2020.101339

Dursun, G., Çiçek, H., & Dursun, A. Y. (2005). Adsorption of phenol from aqueous solution by using carbonised beet pulp. *Journal of Hazardous Materials*, *125*(1–3), 175–182. https://doi.org/10.1016/j.jhazmat.2005.05.023

El-Bery, H. M., Saleh, M., El-Gendy, R. A., Saleh, M. R., & Thabet, S. M. (2022). High adsorption capacity of phenol and methylene blue using activated carbon derived from lignocellulosic agriculture wastes. *Scientific Reports*, *12*(1), 5499.

Faheem, Bao, J., Zheng, H., Tufail, H., Irshad, S., & Du, J. (2018). Adsorption-assisted decontamination of Hg(ii) from aqueous solution by multi-functionalized corncob-derived biochar. *RSC Advances*, *8*(67), 38425–38435. https://doi.org/10.1039/c8ra06622a

Fahmi, A. H., Samsuri, A. W., Jol, H., & Singh, D. (2018). Physical modification of biochar to expose the inner pores and their functional groups to enhance lead adsorption. *RSC Advances*, *8*(67), 38270–38280. https://doi.org/10.1039/c8ra06867d

Fahmi Khairol, N., Sapawe, N., & Danish, M. (2019). Effective Photocatalytic Removal of Different Dye Stuffs Using ZnO/CuO-Incorporated onto Eggshell Templating. *Materials Today: Proceedings*, *19*, 1255–1260. https://doi.org/10.1016/j.matpr.2019.11.130

Febrianto, J., Kosasih, A. N., Sunarso, J., Ju, Y. H., Indraswati, N., & Ismadji, S. (2009). Equilibrium and kinetic studies in adsorption of heavy metals using biosorbent: A summary of recent studies. *Journal of Hazardous Materials*, *162*(2–3), 616–645. https://doi.org/10.1016/j.jhazmat.2008.06.042

Feng, Y., Yang, L., Liu, J., & Logan, B. E. (2016). Electrochemical technologies for wastewater treatment and resource reclamation. *Environmental Science: Water Research & Technology*, *2*(5), 800–831.

Foo, K. Y., & Hameed, B. H. (2010). Insights into the modeling of adsorption isotherm systems. *Chemical Engineering Journal*, *156*(1), 2–10. https://doi.org/10.1016/j.cej.2009.09.013

Forghani Tehrani, G., Rubinos, D. A., Rahimi-Nia, A., Bagherian, G., & Goudarzi, N. (2023). Lead(II) removal from aqueous solutions and battery industry wastewater by sorption using seawater-neutralized red mud. *International Journal of Environmental Science and Technology*, *20*(4), 3713–3732. https://doi.org/10.1007/s13762-023-04801-3

Fu, F., & Wang, Q. (2011). Removal of heavy metal ions from wastewaters: A review. *Journal of Environmental Management*, *92*(3), 407–418. https://doi.org/10.1016/j.jenvman.2010.11.011

Fuhrimann, S., Stalder, M., Winkler, M. S., Niwagaba, C. B., Babu, M., Masaba, G., Kabatereine, N. B., Halage, A. A., Schneeberger, P. H. H., & Utzinger, J. (2015). Microbial and chemical contamination of water, sediment and soil in the Nakivubo wetland area in Kampala, Uganda. *Environmental Monitoring and Assessment*, *187*, 1–15.

Fui, C. J., Sarjadi, M. S., Sarkar, S. M., & Rahman, M. L. (2020). Recent advancement of ullmann condensation coupling reaction in the formation of aryl-oxygen (CO) bonding by copper-mediated catalyst. *Catalysts*, *10*(10), 1103.

Gadipelly, C., Pérez-González, A., Yadav, G. D., Ortiz, I., Ibáñez, R., Rathod, V. K., & Marathe, K. V. (2014). Pharmaceutical industry wastewater: Review of the technologies for water treatment and reuse. *Industrial and Engineering Chemistry Research*, *53*(29), 11571–11592. https://doi.org/10.1021/ie501210j

Gaete Olivares, H., Moyano Lagos, N., Jara Gutierrez, C., Carrasco Kittelsen, R., Lobos Valenzuela, G., & Hidalgo Lillo, M. E. (2016). Assessment oxidative stress biomarkers and metal bioaccumulation in macroalgae from coastal areas with mining activities in Chile. *Environmental Monitoring and Assessment*, *188*(1), 1–11. https://doi.org/10.1007/s10661-015-5021-5

Gallardo, B., & Aldridge, D. C. (2018). Inter-basin water transfers and the expansion of aquatic invasive species. *Water Research*, *143*, 282–291.

Garai, P., Banerjee, P., Mondal, P., & Saha, N. C. (2021). Effect of heavy metals on fishes: Toxicity and bioaccumulation. *J Clin Toxicol. S*, *18*.

Garba, Z. N., Ugbaga, N. I., & Abdullahi, A. K. (2016). Evaluation of optimum adsorption conditions for Ni (II) and Cd (II) removal from aqueous solution by modified plantain peels (MPP). *Beni-Suef University Journal of Basic and Applied Sciences*, *5*(2), 170–179. https://doi.org/10.1016/j.bjbas.2016.03.001

Ghaedi, M., Najibi, A., Hossainian, H., Shokrollahi, A., & Soylak, M. (2012). Kinetic and equilibrium study of Alizarin Red S removal by activated carbon. *Toxicological and*

Environmental Chemistry, *94*(1), 40–48. https://doi.org/10.1080/02772248.2011.636043

Ghaedi, M., Ramazani, S., & Roosta, M. (2011). Gold nanoparticle loaded activated carbon as novel adsorbent for the removal of Congo red. *Indian Journal of Science and Technology*, *4*(10), 1208–1217.

Gong, X., Huang, D., Liu, Y., Peng, Z., Zeng, G., Xu, P., Cheng, M., Wang, R., & Wan, J. (2018). Remediation of contaminated soils by biotechnology with nanomaterials: bio-behavior, applications, and perspectives. *Critical Reviews in Biotechnology*, *38*(3), 455–468. https://doi.org/10.1080/07388551.2017.1368446

González-García, P. (2018). Activated carbon from lignocellulosics precursors: A review of the synthesis methods, characterization techniques and applications. *Renewable and Sustainable Energy Reviews*, *82*(August 2017), 1393–1414. https://doi.org/10.1016/j.rser.2017.04.117

Gonzalez, V., Gourier, D., Wallez, G., Calligaro, T., Artesani, A., Rosi, F., Romani, A., Grazia, C., Miliani, C., & Monico, L. (2023). *Luminescent Inorganic Pigments Used in Ancient and Modern Times*. Springer.

Gopinathan, P. (2023). Human Health Risks due to Exposure to Water Pollution: A Review. *Water*, *15*(14).

Govind, P., & Madhuri, S. (2014). Heavy metals causing toxicity in humans, animals and environment. *Research Journal of Animal, Veterinary and Fishery Sciences*, *2*(2), 17–23.

Gu, S., Kang, X., Wang, L., Lichtfouse, E., & Wang, C. (2019). Clay mineral adsorbents for heavy metal removal from wastewater: a review. *Environmental Chemistry Letters*, *17*(2), 629–654. https://doi.org/10.1007/s10311-018-0813-9

Güereña, D., Neufeldt, H., Berazneva, J., & Duby, S. (2015). Water hyacinth control in Lake Victoria: Transforming an ecological catastrophe into economic, social, and environmental benefits. *Sustainable Production and Consumption*, *3*, 59–69.

Guerra, F. D., Attia, M. F., Whitehead, D. C., & Alexis, F. (2018). Nanotechnology for environmental remediation: materials and applications. *Molecules*, *23*(7), 1760.

Guna, V., Ilangovan, M., Anantha Prasad, M. G., & Reddy, N. (2017). Water hyacinth: a unique source for sustainable materials and products. *ACS Sustainable Chemistry & Engineering*, *5*(6), 4478–4490.

Guo, E. L., & Katta, R. (2017). Diet and hair loss: effects of nutrient deficiency and supplement use. *Dermatology Practical & Conceptual*, 1–10. https://doi.org/10.5826/dpc.0701a01

Gupta, M., Mahajan, V. K., Mehta, K. S., & Chauhan, P. S. (2014). Zinc therapy in dermatology: A review. *Dermatology Research and Practice*, *2014*. https://doi.org/10.1155/2014/709152

Gupta, V. K., & Ali, I. (2004). Removal of lead and chromium from wastewater using bagasse fly ash - A sugar industry waste. *Journal of Colloid and Interface Science*, *271*(2), 321–328. https://doi.org/10.1016/j.jcis.2003.11.007

Guragain, Y. N., De Coninck, J., Husson, F., Durand, A., & Rakshit, S. K. (2011). Comparison of some new pretreatment methods for second generation bioethanol production from wheat straw and water hyacinth. *Bioresource Technology*, *102*(6), 4416–4424.

Gutmann, B., Cantillo, D., & Kappe, C. O. (2015). Continuous-flow technology - A tool for the safe manufacturing of active pharmaceutical ingredients. *Angewandte Chemie - International Edition*, *54*(23), 6688–6728. https://doi.org/10.1002/anie.201409318

Hagemann, N., Spokas, K., Schmidt, H.-P., Kägi, R., Böhler, M. A., & Bucheli, T. D. (2018). Activated carbon, biochar and charcoal: linkages and synergies across pyrogenic carbon's ABC s. *Water*, *10*(2), 182.

Haleem, A., Shafiq, A., Chen, S.-Q., & Nazar, M. (2023). A comprehensive review on adsorption, photocatalytic and chemical degradation of dyes and nitro-compounds over different kinds of porous and composite materials. *Molecules*, *28*(3), 1081.

Hart, A., & Onyeaka, H. (2020). Eggshell and seashells biomaterials sorbent for carbon dioxide capture. *Carbon Capture*, *83*.

Havel, J. E., Kovalenko, K. E., Thomaz, S. M., Amalfitano, S., & Kats, L. B. (2015). Aquatic invasive species: challenges for the future. *Hydrobiologia*, *750*, 147–170.

Hayati, B., Maleki, A., Najafi, F., Daraei, H., Gharibi, F., & McKay, G. (2017). Super high removal capacities of heavy metals (Pb2+ and Cu2+) using CNT dendrimer. *Journal of Hazardous Materials*, *336*, 146–157. https://doi.org/10.1016/j.jhazmat.2017.02.059

Helaluddin, A. B. M., Khalid, R. S., Alaama, M., & Abbas, S. A. (2016). Main analytical techniques used for elemental analysis in various matrices. *Tropical Journal of Pharmaceutical Research*, *15*(2), 427–434. https://doi.org/10.4314/tjpr.v15i2.29

Hossain, M. E., Ritt, C. L., Almeelbi, T. B., & Bezbaruah, A. N. (2018). Biopolymer Beads for Aqueous Phosphate Removal: Possible Applications in Eutrophic Lakes. *Journal of Environmental Engineering*, *144*(5), 1–10. https://doi.org/10.1061/(asce)ee.1943-7870.0001347

Huang, Q., Song, S., Chen, Z., Hu, B., Chen, J., & Wang, X. (2019). Biochar-based materials and

their applications in removal of organic contaminants from wastewater: state-of-the-art review. *Biochar*, *1*(1), 45–73. https://doi.org/10.1007/s42773-019-00006-5

Huang, Y., Li, S., Chen, J., Zhang, X., & Chen, Y. (2014). Adsorption of Pb (II) on mesoporous activated carbons fabricated from water hyacinth using H3PO4 activation: adsorption capacity, kinetic and isotherm studies. *Applied Surface Science*, *293*, 160–168.

Inyang, M. I., Gao, B., Yao, Y., Xue, Y., Zimmerman, A., Mosa, A., Pullammanappallil, P., Ok, Y. S., & Cao, X. (2016). A review of biochar as a low-cost adsorbent for aqueous heavy metal removal. *Critical Reviews in Environmental Science and Technology*, *46*(4), 406–433.

Jaishankar, M., Tseten, T., Anbalagan, N., Mathew, B. B., & Beeregowda, K. N. (2014). Toxicity, mechanism and health effects of some heavy metals. *Interdisciplinary Toxicology*, *7*(2), 60–72. https://doi.org/10.2478/intox-2014-0009

Janssens, K., Van der Snickt, G., Vanmeert, F., Legrand, S., Nuyts, G., Alfeld, M., Monico, L., Anaf, W., De Nolf, W., Vermeulen, M., Verbeeck, J., & De Wael, K. (2016). Non-Invasive and Non-Destructive Examination of Artistic Pigments, Paints, and Paintings by Means of X-Ray Methods. *Topics in Current Chemistry*, *374*(6). https://doi.org/10.1007/s41061-016-0079-2

Kansara, N., Bhati, L., Narang, M., & Vaishnavi, R. (2016). *Critical Review Wastewater treatment by ion exchange method: a review of past and recent researches*.

Kant, R. (2012). Textile dyeing industry an environmental hazard. *Natural Science*, *04*(01), 22–26. https://doi.org/10.4236/ns.2012.41004

Kim, D. J., Shin, H. J., Ahn, B. K., & Lee, J. H. (2016). Competitive adsorption of thallium in

different soils as influenced by selected counter heavy metals. *Applied Biological Chemistry*, *59*(5), 695–701. https://doi.org/10.1007/s13765-016-0215-2

Kim, S. U., Owens, V. N., Kim, S. Y., & Hong, C. O. (2017). Effect of different way of bottom ash and compost application on phytoextractability of cadmium in contaminated arable soil. *Applied Biological Chemistry*, *60*(4), 353–362. https://doi.org/10.1007/s13765-017-0287-7

Kiurskic, I, I. K., & V, Č. E. (2012). *Adsorption feasibility in the Cr (total) ions removal from waste printing developer*. *14*(1), 18–23.

Koelkebeck, K. W. (2014). *What is Egg Shell Quality and How to Preserve It*.

Kulkarni, S. J. (2016). A Review on Research and Studies on Dissolved Oxygen and Its Affecting Parameters. *International Journal of Research & Review (Www.Gkpublication.In)*, *3*(8), 18. www.ijrrjournal.com

Kumar, Y. P., King, P., & Prasad, V. S. R. K. (2006). Zinc biosorption on Tectona grandis L.f. leaves biomass: Equilibrium and kinetic studies. *Chemical Engineering Journal*, *124*(1–3), 63–70. https://doi.org/10.1016/j.cej.2006.07.010

Lai, K. C., Lee, L. Y., Hiew, B. Y. Z., Thangalazhy-Gopakumar, S., & Gan, S. (2019). Environmental application of three-dimensional graphene materials as adsorbents for dyes and heavy metals: Review on ice-templating method and adsorption mechanisms. *Journal of Environmental Sciences (China)*, *79*, 174–199. https://doi.org/10.1016/j.jes.2018.11.023

Lashaki, M. J., Khiavi, S., & Sayari, A. (2019). Stability of amine-functionalized CO 2 adsorbents: a multifaceted puzzle. *Chemical Society Reviews*, *48*(12), 3320–3405.

Lee, S. Y., & Choi, H. J. (2018). Persimmon leaf bio-waste for adsorptive removal of heavy metals

from aqueous solution. *Journal of Environmental Management*, *209*, 382–392. https://doi.org/10.1016/j.jenvman.2017.12.080

Li, H., Dong, X., da Silva, E. B., de Oliveira, L. M., Chen, Y., & Ma, L. Q. (2017). Mechanisms of metal sorption by biochars: Biochar characteristics and modifications. *Chemosphere*, *178*(July), 466–478. https://doi.org/10.1016/j.chemosphere.2017.03.072

Li, J., Wang, X., Zhao, G., Chen, C., Chai, Z., Alsaedi, A., Hayat, T., & Wang, X. (2018). Metal–organic framework-based materials: superior adsorbents for the capture of toxic and radioactive metal ions. *Chemical Society Reviews*, *47*(7), 2322–2356.

Li, J., & Wu, Y. (2014). Lubricants in pharmaceutical solid dosage forms. *Lubricants*, *2*(1), 21–43. https://doi.org/10.3390/lubricants2010021

Li, X., Zhou, H., Wu, W., Wei, S., Xu, Y., & Kuang, Y. (2015). Studies of heavy metal ion adsorption on Chitosan/Sulfydryl-functionalized graphene oxide composites. *Journal of Colloid and Interface Science*, *448*, 389–397. https://doi.org/10.1016/j.jcis.2015.02.039

Li, Y., Zhang, X., Yang, R., Li, G., & Hu, C. (2015). The role of H 3 PO 4 in the preparation of activated carbon from NaOH-treated rice husk residue. *RSC Advances*, *5*(41), 32626–32636.

Liang, S., Guo, X., & Tian, Q. (2011). Adsorption of Pb2+ and Zn2+ from aqueous solutions by sulfured orange peel. *Desalination*, *275*(1–3), 212–216. https://doi.org/10.1016/j.desal.2011.03.001

Liao, Y., Chen, S., Zheng, Q., Huang, B., Zhang, J., Fu, H., & Gao, H. (2022). Removal and recovery of phosphorus from solution by bifunctional biochar. *Inorganic Chemistry Communications*, *139*, 109341.

Lim, A. P., & Aris, A. Z. (2014). A review on economically adsorbents on heavy metals removal in water and wastewater. *Reviews in Environmental Science and Bio/Technology*, *13*, 163–181.

Liu, M., Wang, Y., Chen, L., Zhang, Y., & Lin, Z. (2015). Mg (OH) 2 supported nanoscale zero valent iron enhancing the removal of Pb (II) from aqueous solution. *ACS Applied Materials & Interfaces*, *7*(15), 7961–7969.

Liu, Q., Li, Y., Chen, H., Lu, J., Yu, G., Möslang, M., & Zhou, Y. (2020). Superior adsorption capacity of functionalised straw adsorbent for dyes and heavy-metal ions. *Journal of Hazardous Materials*, *382*(130), 121040. https://doi.org/10.1016/j.jhazmat.2019.121040

Liu, X., Iocozzia, J., Wang, Y., Cui, X., Chen, Y., Zhao, S., Li, Z., & Lin, Z. (2017). Noble metal-metal oxide nanohybrids with tailored nanostructures for efficient solar energy conversion, photocatalysis and environmental remediation. *Energy and Environmental Science*, *10*(2), 402–434. https://doi.org/10.1039/c6ee02265k

Liu, X., Ma, R., Wang, X., Ma, Y., Yang, Y., Zhuang, L., Zhang, S., Jehan, R., Chen, J., & Wang, X. (2019). Graphene oxide-based materials for ef fi cient removal of heavy metal ions from aqueous solution : A review. *Environmental Pollution*, *252*, 62–73. https://doi.org/10.1016/j.envpol.2019.05.050

Liu, Z., Zhang, G., Lan, H., Liu, H., & Qu, J. (2021). Optimization of a hierarchical porous-structured reactor to mitigate mass transport limitations for efficient electrocatalytic ammonia oxidation through a three-electron-transfer pathway. *Environmental Science & Technology*, *55*(18), 12596–12606.

Lu, H., Wang, J., Wang, T., Wang, N., Bao, Y., & Hao, H. (2017). Crystallization techniques in

wastewater treatment: An overview of applications. *Chemosphere*, *173*, 474–484. https://doi.org/10.1016/j.chemosphere.2017.01.070

Lukubye, B., & Andama, M. (2017). *Physico-Chemical Quality of Selected Drinking Water Sources in Mbarara Municipality , Uganda*. 707–722. https://doi.org/10.4236/jwarp.2017.97047

LVEMP. (2005). *Lake victoria environment report - uganda water quality and ecosystems status*. *December*, 1–36.

Ma, H., Yang, J., Gao, X., Liu, Z., Liu, X., & Xu, Z. (2019). Removal of chromium (VI) from water by porous carbon derived from corn straw: Influencing factors, regeneration and mechanism. *Journal of Hazardous Materials*, *369*(October 2018), 550–560. https://doi.org/10.1016/j.jhazmat.2019.02.063

Madikizela, L. M. (2021). Removal of organic pollutants in water using water hyacinth (Eichhornia crassipes). *Journal of Environmental Management*, *295*(June), 113153. https://doi.org/10.1016/j.jenvman.2021.113153

Mahamadi, C., & Nharingo, T. (2010). Competitive adsorption of Pb2+, Cd2+ and Zn2+ ions onto Eichhornia crassipes in binary and ternary systems. *Bioresource Technology*, *101*(3), 859–864. https://doi.org/10.1016/j.biortech.2009.08.097

Mahato, P. L., Weatherby, T., Ewell, K., Jha, R., & Mishra, B. (2024). Scanning electron microscope-based evaluation of eggshell quality. *Poultry Science*, *103*(3), 103428. https://doi.org/10.1016/j.psj.2024.103428

Maher, B., Taylor, A., Batley, G., & Simpson, S. (2016). Bioaccumulation. In *Sediment quality*

assessment: a practical guide (pp. 123–156). CSIRO Publishing.

Malik, D. S., Jain, C. K., & Yadav, A. K. (2017). Removal of heavy metals from emerging cellulosic low-cost adsorbents: a review. *Applied Water Science*, *7*(5), 2113–2136. https://doi.org/10.1007/s13201-016-0401-8

Mamba, G., & Mishra, A. (2016). Advances in magnetically separable photocatalysts: smart, recyclable materials for water pollution mitigation. *Catalysts*, *6*(6), 79.

Man Mohan, K., & Gajalakshmi, S. (2024). Biosorption for Wastewater Treatment and Post-sorption Utilization of Treated Wastewater and Spent Biosorbent. In *Biological and Hybrid Wastewater Treatment Technology: Recent Developments in India* (pp. 57–90). Springer.

Manfrin, J., Gonçalves Jr, A. C., Schwantes, D., Tarley, C. R. T., Schiller, A. da P., & Klassen, G. J. (2020). Triple activation (thermal-chemical-physical) in the development of an activated carbon from tobacco: characterizations and optimal conditions for Cd2+ and Pb2+ removal from waters. *Water Practice & Technology*, *15*(4), 877–898.

Mebrahtu, G., & Zerabruk, S. (2002). *Concentration of Heavy Metals in Drinking Water from Urban Areas of the Tigray*.

Medellin-Castillo, N. A., Padilla-Ortega, E., Regules-Martínez, M. C., Leyva-Ramos, R., Ocampo-Pérez, R., & Carranza-Alvarez, C. (2017). Single and competitive adsorption of Cd (II) and Pb (II) ions from aqueous solutions onto industrial chili seeds (Capsicum annuum) waste. *Sustainable Environment Research*, *27*(2), 61–69.

Miraj, S. S., & Rao, M. (2020). Clinical toxicology of copper: source, toxidrome, mechanism of toxicity, and management. In *Metal Toxicology Handbook* (pp. 199–217). CRC Press.

Mishra, S., Bharagava, R. N., More, N., Yadav, A., Zainith, S., Mani, S., & Chowdhary, P. (2019). Heavy metal contamination: an alarming threat to environment and human health. *Environmental Biotechnology: For Sustainable Future*, 103–125.

Mitrogiannis, D., Psychoyou, M., Baziotis, I., Inglezakis, V. J., Koukouzas, N., Tsoukalas, N., Palles, D., & Kamitsos, E. (2017). *Removal of phosphate from aqueous solutions by adsorption onto Ca (OH) 2 treated natural clinoptilolite of Natural Resources Management and Agricultural Engineering , Agricultural University of Athens , 75 Iera Odos , 11855 Athens , Greece School of Eng*. 1–40.

Mohammad Jamin, W. I. (2017). *Adsorption of heavy metal using sludge activated carbon derived from sludge*.

Mohan, D., Pittman, C. U., Bricka, M., Smith, F., Yancey, B., Mohammad, J., Steele, P. H., Alexandre-Franco, M. F., Gómez-Serrano, V., & Gong, H. (2007). Sorption of arsenic, cadmium, and lead by chars produced from fast pyrolysis of wood and bark during bio-oil production. *Journal of Colloid and Interface Science*, *310*(1), 57–73. https://doi.org/10.1016/j.jcis.2007.01.020

Monowara, F., Tasmin, H., Hoque, S., & Enayet, M. (2021). *Removal of lead from aqueous solutions and wastewaters using water hyacinth (Eichhornia crassipes) roots*. *16*(2), 404–419. https://doi.org/10.2166/wpt.2021.005

Morcillo, P., Esteban, M., & Cuesta, A. (2016). Heavy metals produce toxicity, oxidative stress and apoptosis in the marine teleost fish SAF-1 cell line. *Chemosphere*, *144*, 225–233. https://doi.org/10.1016/j.chemosphere.2015.08.020

Munene, M. J. (2019). *Sequestering of selected heavy metal ions in wastewater from industrial*

area in Nairobi using water hyacinth as a low cost adsorbent.

Murithi, G., Onindo, C. O., Wambu, E. W., & Muthakia, G. K. (2014). Removal of Cadmium(II) Ions from Water by Adsorption using Water Hyacinth (Eichhornia crassipes) Biomass. *BioResources*, *9*(2), 3613–3631. https://doi.org/10.15376/biores.9.2.3613-3631

Nakamoto, K. (2009). *Infrared and Raman spectra of inorganic and coordination compounds, part B: applications in coordination, organometallic, and bioinorganic chemistry*. John Wiley & Sons.

NEA. (2019). The National Environment Act 2019. *The Uganda Gazette No. 10, Volume CXI*(2), pages 1-178.

Ngah, W. S. W., Teong, L. C., Toh, R. H., & Hanafiah, M. (2013). Comparative study on adsorption and desorption of Cu (II) ions by three types of chitosan–zeolite composites. *Chemical Engineering Journal*, *223*, 231–238.

Nollet, L. M. L. (2012). Analysis of Endocrine Disrupting Compounds in Food. In *Analysis of Endocrine Disrupting Compounds in Food*. https://doi.org/10.1002/9781118346747

Novi SB, P. W. (2018). (2018). *Scholar (19)*.

Nugent, P., Belmabkhout, Y., Burd, S. D., Cairns, A. J., Luebke, R., Forrest, K., Pham, T., Ma, S., Space, B., & Wojtas, L. (2013). Porous materials with optimal adsorption thermodynamics and kinetics for CO2 separation. *Nature*, *495*(7439), 80–84.

Obinna, I. B., & Ebere, E. C. (2019). A review: Water pollution by heavy metal and organic pollutants: Brief review of sources, effects and progress on remediation with aquatic plants. *Analytical Methods in Environmental Chemistry Journal*, *2*(03), 5–38.

Ogilo, J., Onditi, A., Salim, A., & Yusuf, A. (2017). Assessment of Levels of Heavy Metals in Paints from Interior Walls and Indoor Dust from Residential Houses in Nairobi City County, Kenya. *Chemical Science International Journal*, *21*(1), 1–7. https://doi.org/10.9734/csji/2017/37392

Ogunkunle, C. O., Odulaja, D. A., Akande, F. O., Varun, M., Vishwakarma, V., & Fatoba, P. O. (2020). Cadmium toxicity in cowpea plant: Effect of foliar intervention of nano-TiO2 on tissue Cd bioaccumulation, stress enzymes and potential dietary health risk. *Journal of Biotechnology*, *310*(January), 54–61. https://doi.org/10.1016/j.jbiotec.2020.01.009

Oliveira, T. J. J., Santiago, A. da F., Lanna, M. C. da S., Fongaro, G., Milagres, N. L., Cunha, T. R., & Corrêa, A. L. I. (2021). Rural blackwater treatment by a full-scale Brazilian Biodigester Septic Tank: microbial indicators and pathogen removal efficiency. *Environmental Science and Pollution Research*, *28*, 23235–23242.

Osasona, I., Ajayi, O. O., & Adebayo, A. O. (2014). *Equilibrium , Kinetics , and Thermodynamics of the Removal of Nickel (II) from Aqueous Solution Using Cow Hooves*. *2014*(Ii).

Ośko, J., Pierlejewska, W., & Grembecka, M. (2023). Comparison of the Potential Relative Bioaccessibility of Zinc Supplements—In Vitro Studies. *Nutrients*, *15*(12), 2813.

Otunola, B. O., & Ololade, O. O. (2020). A review on the application of clay minerals as heavy metal adsorbents for remediation purposes. *Environmental Technology and Innovation*, *18*. https://doi.org/10.1016/j.eti.2020.100692

Oumam, M., Abourriche, A., Mansouri, S., Mouiya, M., Benhammou, A., Abouliatim, Y., Hafiane, Y. El, Hannache, H., Birot, M., & Pailler, R. (2020). Comparison of chemical and physical activation processes at obtaining adsorbents from Moroccan oil shale. *Oil Shale*,

37(2), 139–157.

Pal, D. B., Tiwari, A. K., Prasad, N., Syed, A., Bahkali, A. H., Srivastava, N., Singh, R. P., & Gupta, V. K. (2023). Sustainable valorization of water hyacinth waste pollutant via pyrolysis for advance microbial fuel investigation. *Chemosphere, 314*, 137602.

Park, J. H., Ok, Y. S., Kim, S. H., Cho, J. S., Heo, J. S., Delaune, R. D., & Seo, D. C. (2016). Competitive adsorption of heavy metals onto sesame straw biochar in aqueous solutions. *Chemosphere*, *142*, 77–83. https://doi.org/10.1016/j.chemosphere.2015.05.093

Paul, W. (2011). *Impact of Industrial Effluents on Water Quality of Receiving Streams in Nakawa-Ntinda, Uganda a Dissertation Submitted in Partial Fulfillment of the Requirements for the Award of Master of Science in Environment and Natural Resources of Makerere Universit*.

Plum, L. M., Rink, L., & Hajo, H. (2010). The essential toxin: Impact of zinc on human health. *International Journal of Environmental Research and Public Health*, *7*(4), 1342–1365. https://doi.org/10.3390/ijerph7041342

Priya, E. S., & Selvan, P. S. (2017). Water hyacinth (Eichhornia crassipes)–An efficient and economic adsorbent for textile effluent treatment–A review. *Arabian Journal of Chemistry, 10*, S3548–S3558.

Puthran, D., & Patil, D. (2023). Usage of heavy metal-free compounds in surface coatings. *Journal of Coatings Technology and Research*, *20*(1), 87–112.

Qasem, N. A. A., Mohammed, R. H., & Lawal, D. U. (2021). Removal of heavy metal ions from wastewater: A comprehensive and critical review. *Npj Clean Water*, *4*(1), 1–15.

Rahimi, M., & Vadi, M. (2014). Langmuir, Freundlich and Temkin Adsorption Isotherm of

Captopril an Ace Inhibitor (or Angiotensinconverting-Enzyme Inhibitor) is a Pharmaceutical Drug used for the Treatment of Hypertension by Multi-Wall Carbon Nanotube. *Indian Journal of Fundamental and Applied Life Sciences*, *4*, 933–937. http://www.cibtech.org/sp.ed/jls/2014/04/JLS-105-S4-109-MAHDI-LANGMUIR-NANOTUBE.pdf

Rahimi, R. A., Yahaya, S. H., & Salleh, M. S. (2023). A comprehensive review of the use of Sodium Chloride (NaCl) in the development of the COVID-19 vaccine and medical applications. *Multidisciplinary Reviews*, *6*(3). https://doi.org/10.31893/multirev.2023028

Rana, R. S., Singh, P., Kandari, V., Singh, R., Dobhal, R., & Gupta, S. (2017). A review on characterization and bioremediation of pharmaceutical industries' wastewater: an Indian perspective. *Applied Water Science*, *7*(1), 1–12. https://doi.org/10.1007/s13201-014-0225-3

Rashid, R., Shafiq, I., Akhter, P., Iqbal, M. J., & Hussain, M. (2021). A state-of-the-art review on wastewater treatment techniques: the effectiveness of adsorption method. *Environmental Science and Pollution Research*, *28*, 9050–9066.

Rezania, S., Ponraj, M., Din, M. F. M., Songip, A. R., Sairan, F. M., & Chelliapan, S. (2015). The diverse applications of water hyacinth with main focus on sustainable energy and production for new era: An overview. In *Renewable and Sustainable Energy Reviews* (Vol. 41, pp. 943–954). Elsevier Ltd. https://doi.org/10.1016/j.rser.2014.09.006

Riyanto, C. A., & Prabalaras, E. (2019). The adsorption kinetics and isoterm of activated carbon from Water Hyacinth Leaves (Eichhornia crassipes) on Co (II). *Journal of Physics: Conference Series*, *1307*(1), 12002.

Ronsse, F., van Hecke, S., Dickinson, D., & Prins, W. (2013). Production and characterization of

slow pyrolysis biochar: Influence of feedstock type and pyrolysis conditions. *GCB Bioenergy*, *5*(2), 104–115. https://doi.org/10.1111/gcbb.12018

Ruan, T., Zeng, R., Yin, X.-Y., Zhang, S.-X., & Yang, Z.-H. (2016). Water hyacinth (Eichhornia crassipes) biomass as a biofuel feedstock by enzymatic hydrolysis. *BioResources*, *11*(1), 2372–2380.

Ruiz-Hitzky, E., Aranda, P., Darder, M., & Rytwo, G. (2010). Hybrid materials based on clays for environmental and biomedical applications. *Journal of Materials Chemistry*, *20*(42), 9306–9321.

Saaidia, S., Delimi, R., Benredjem, Z., & Mehellou, A. (2017). *Use of a PbO 2 electrode of a lead-acid battery for the electrochemical degradation of methylene blue*. *February*. https://doi.org/10.1080/01496395.2017.1291681

Sabir, S. (2015). Approach of cost-effective adsorbents for oil removal from oily water. *Critical Reviews in Environmental Science and Technology*, *45*(17), 1916–1945.

Sabty-Daily, R. A., Harris, P. A., Hinds, W. C., & Froines, J. R. (2005). Size distribution and speciation of chromium in paint spray aerosol at an aerospace facility. *Annals of Occupational Hygiene*, *49*(1), 47–59. https://doi.org/10.1093/annhyg/meh081

Saeb, M. R., Ghaffari, M., Rastin, H., Khonakdar, H. A., Simon, F., Najafi, F., Goodarzi, V., Puglia, D., Asl, F. H., & Formela, K. (2017). Biowaste chicken eggshell powder as a potential cure modifier for epoxy/anhydride systems: competitiveness with terpolymer-modified calcium carbonate at low loading levels. *Rsc Advances*, *7*(4), 2218–2230.

Saha, P., Shinde, O., & Sarkar, S. (2017). Phytoremediation of industrial mines wastewater using

water hyacinth. *International Journal of Phytoremediation*, *19*(1), 87–96.

Sajjadi, B., Chen, W.-Y., & Egiebor, N. O. (2019). A comprehensive review on physical activation of biochar for energy and environmental applications. *Reviews in Chemical Engineering*, *35*(6), 735–776.

Salahuddin, N., Abdelwahab, M. A., Akelah, A., & Elnagar, M. (2021). Adsorption of Congo red and crystal violet dyes onto cellulose extracted from Egyptian water hyacinth. *Natural Hazards*, *105*, 1375–1394.

Samadani Langeroodi, N., Farhadravesh, Z., & Dehno Khalaji, A. (2018). Optimization of adsorption parameters for Fe (III) ions removal from aqueous solutions by transition metal oxide nanocomposite. *Green Chemistry Letters and Reviews*, *11*(4), 404–413.

Sannino, D. (2021). Types and Classification of Nanomaterials. *Nanotechnology: Trends and Future Applications*, 15–38. https://doi.org/10.1007/978-981-15-9437-3_2

Sarker, P., Liu, X., Hata, N., Takeshita, H., Miyamura, H., & Maruo, M. (2023). Thermally modified bamboo-eggshell adsorbent for phosphate recovery and its sustainable application as fertilizer. *Environmental Research*, *231*, 115992.

Sekabira, K., Origa, H. O., Basamba, T. A., Mutumba, G., & Kakudidi, E. (2010). Heavy metal assessment and water quality values in urban stream and rain water. *International Journal of Environmental Science & Technology*, *7*, 759–770.

Semerjian, L. (2010). Equilibrium and kinetics of cadmium adsorption from aqueous solutions using untreated Pinus halepensis sawdust. *Journal of Hazardous Materials*, *173*(1–3), 236–242. https://doi.org/10.1016/j.jhazmat.2009.08.074

Sen, M., & Ghosh Dastidar, M. (2010). Review Chromium reoval using various biosorbents. In *J. Environ. Health. Sci. Eng* (Vol. 7, Issue 3).

Shah, R., Mittal, V., Matsil, E., & Rosenkranz, A. (2021). Magnesium-ion batteries for electric vehicles: Current trends and future perspectives. *Advances in Mechanical Engineering*, *13*(3), 1–9. https://doi.org/10.1177/16878140211003398

Shanker, A. K., Cervantes, C., Loza-Tavera, H., & Avudainayagam, S. (2005). Chromium toxicity in plants. *Environment International*, *31*(5), 739–753. https://doi.org/10.1016/j.envint.2005.02.003

Shi, C., Ding, H., Zan, Q., & Li, R. (2019). Spatial variation and ecological risk assessment of heavy metals in mangrove sediments across China. *Marine Pollution Bulletin*, *143*, 115–124.

Shi, Y., Hao, R., Ji, H., Gao, L., & Yang, J. (2024). Dietary zinc supplements: beneficial health effects and application in food, medicine and animals. *Journal of the Science of Food and Agriculture*, *104*(10), 5660–5674.

Siddiqua, A., Hahladakis, J. N., & Al-Attiya, W. A. K. A. (2022). An overview of the environmental pollution and health effects associated with waste landfilling and open dumping. *Environmental Science and Pollution Research*, *29*(39), 58514–58536.

Singare, P. U., Jagtap, A. G., & Lokhande, R. S. (2011). Water pollution by discharge effluents from Gove Industrial area of Maharashtra, India: Dispersion of heavy metals and their toxic effects. *International Journal of Global Environmental Issues*, *11*(1), 28–36. https://doi.org/10.1504/IJGENVI.2011.040249

Slater, A. G., & Cooper, A. I. (2015). Function-led design of new porous materials. *Science*,

348(6238), aaa8075.

Smith, B. (2018). Infrared spectral interpretation: A systematic approach. *Infrared Spectral Interpretation: A Systematic Approach*, 1–304. https://doi.org/10.1201/9780203750841

Sonmez Baghirzade, B., Zhang, Y., Reuther, J. F., Saleh, N. B., Venkatesan, A. K., & Apul, O. G. (2021). Thermal regeneration of spent granular activated carbon presents an opportunity to break the forever PFAS cycle. *Environmental Science & Technology*, *55*(9), 5608–5619.

Stehle, S., & Schulz, R. (2015). Agricultural insecticides threaten surface waters at the global scale. *Proceedings of the National Academy of Sciences*, *112*(18), 5750–5755.

Sud, D., Mahajan, G., & Kaur, M. P. (2008). Agricultural waste material as potential adsorbent for sequestering heavy metal ions from aqueous solutions - A review. In *Bioresource Technology* (Vol. 99, Issue 14, pp. 6017–6027). https://doi.org/10.1016/j.biortech.2007.11.064

Sun, Z., Lv, F., Cao, L., Liu, L., Zhang, Y., & Lu, Z. (2015). Multistimuli-responsive, moldable supramolecular hydrogels cross-linked by ultrafast complexation of metal ions and biopolymers. *Angewandte Chemie*, *127*(27), 8055–8059.

Sutherland, C. (2010). A diffusion-chemisorption kinetic model for simulating biosorption using forest macro-fungus, fomes fasciatus. *International Research Journal of Plant Science*, *1*(4), 107–117. https://doi.org/10.6084/m9.figshare.6197030.v1

Tang, Y., Yang, Q., Lu, J., Zhang, X., Suen, D., Tan, Y., Jin, L., Xiao, J., Xie, R., Rane, M., Li, X., & Cai, L. (2010). Zinc supplementation partially prevents renal pathological changes in diabetic rats. *Journal of Nutritional Biochemistry*, *21*(3), 237–246. https://doi.org/10.1016/j.jnutbio.2008.12.010

Taty-Costodes, V. C., Fauduet, H., Porte, C., & Delacroix, A. (2003). Removal of Cd(II) and Pb(II) ions, from aqueous solutions, by adsorption onto sawdust of Pinus sylvestris. *Journal of Hazardous Materials*, *105*(1–3), 121–142. https://doi.org/10.1016/j.jhazmat.2003.07.009

Tchounwou, P. B., Yedjou, C. G., Patlolla, A. K., & Sutton, D. J. (2012). Heavy metal toxicity and the environment. In *EXS* (Vol. 101, pp. 133–164). https://doi.org/10.1007/978-3-7643-8340-4_6

Teh, C. Y., Budiman, P. M., Shak, K. P. Y., & Wu, T. Y. (2016). Recent advancement of coagulation–flocculation and its application in wastewater treatment. *Industrial & Engineering Chemistry Research*, *55*(16), 4363–4389.

Torres-Perez, J., Gerente, C., & Andres, Y. (2012). Conversion of agricultural residues into activated carbons for water purification: Application to arsenate removal. *Journal of Environmental Science and Health, Part A*, *47*(8), 1173–1185.

Tran, H. N., Chao, H.-P., & You, S.-J. (2018). Activated carbons from golden shower upon different chemical activation methods: synthesis and characterizations. *Adsorption Science & Technology*, *36*(1–2), 95–113.

Tran, H. N., You, S. J., Hosseini-Bandegharaei, A., & Chao, H. P. (2017). Mistakes and inconsistencies regarding adsorption of contaminants from aqueous solutions: A critical review. *Water Research*, *120*, 88–116. https://doi.org/10.1016/j.watres.2017.04.014

Van Tran, V., Park, D., & Lee, Y.-C. (2018). Hydrogel applications for adsorption of contaminants in water and wastewater treatment. *Environmental Science and Pollution Research*, *25*, 24569–24599.

Vieira, W. T., de Farias, M. B., Spaolonzi, M. P., da Silva, M. G. C., & Vieira, M. G. A. (2020). Removal of endocrine disruptors in waters by adsorption, membrane filtration and biodegradation. A review. *Environmental Chemistry Letters*, *18*(4), 1113–1143.

Vijaya, Y., Popuri, S. R., Boddu, V. M., & Krishnaiah, A. (2008). Modified chitosan and calcium alginate biopolymer sorbents for removal of nickel (II) through adsorption. *Carbohydrate Polymers*, *72*(2), 261–271. https://doi.org/10.1016/j.carbpol.2007.08.010

Voisin, H., Bergström, L., Liu, P., & Mathew, A. P. (2017). Nanocellulose-based materials for water purification. *Nanomaterials*, *7*(3), 57.

Volesky, B. (2007). Biosorption and me. *Water Research*, *41*(18), 4017–4029. https://doi.org/10.1016/j.watres.2007.05.062

Walakira, P., & Okot-Okumu, J. (2011). Impact of industrial effluents on water quality of streams in Nakawa-Ntinda, Uganda. *Journal of Applied Sciences and Environmental Management*, *15*(2).

Wan Ngah, W. S., & Hanafiah, M. A. K. M. (2008). Removal of heavy metal ions from wastewater by chemically modified plant wastes as adsorbents: A review. *Bioresource Technology*, *99*(10), 3935–3948. https://doi.org/10.1016/j.biortech.2007.06.011

Wang, H., Liu, Y. G., Zeng, G. M., Hu, X. J., Hu, X., Li, T. T., Li, H. Y., Wang, Y. Q., & Jiang, L. H. (2014). Grafting of β-cyclodextrin to magnetic graphene oxide via ethylenediamine and application for Cr(VI) removal. *Carbohydrate Polymers*, *113*, 166–173. https://doi.org/10.1016/j.carbpol.2014.07.014

Wang, X., Liang, X., Wang, Y., Wang, X., Liu, M., Yin, D., Xia, S., Zhao, J., & Zhang, Y. (2011).

Adsorption of Copper (II) onto activated carbons from sewage sludge by microwave-induced phosphoric acid and zinc chloride activation. *Desalination*, *278*(1–3), 231–237. https://doi.org/10.1016/j.desal.2011.05.033

WHO. (2017). *Progress on drinking water, sanitation and hygiene: 2017 update and SDG baselines*.

Wigger, H., Wohlleben, W., & Nowack, B. (2018). Redefining environmental nanomaterial flows: Consequences of the regulatory nanomaterial definition on the results of environmental exposure models. *Environmental Science: Nano*, *5*(6), 1372–1385. https://doi.org/10.1039/c8en00137e

Wu, S., Yang, X., & Janiak, C. (2019). Confinement effects in zeolite-confined noble metals. *Angewandte Chemie*, *131*(36), 12468–12482.

Wuana, R. A., & Okieimen, F. E. (2011). Heavy Metals in Contaminated Soils: A Review of Sources, Chemistry, Risks and Best Available Strategies for Remediation. *ISRN Ecology*, *2011*, 1–20. https://doi.org/10.5402/2011/402647

Xu, Y., Liu, Y., Liu, S., Tan, X., Zeng, G., Zeng, W., Ding, Y., Cao, W., & Zheng, B. (2016). Enhanced adsorption of methylene blue by citric acid modification of biochar derived from water hyacinth (Eichornia crassipes). *Environmental Science and Pollution Research*, *23*, 23606–23618.

Yang, J., Hou, B., Wang, J., Tian, B., Bi, J., Wang, N., Li, X., & Huang, X. (2019). Nanomaterials for the removal of heavy metals from wastewater. *Nanomaterials*, *9*(3), 424.

Yang, X., Wan, Y., Zheng, Y., He, F., Yu, Z., Huang, J., Wang, H., Ok, Y. S., Jiang, Y., & Gao,

B. (2019). Surface functional groups of carbon-based adsorbents and their roles in the removal of heavy metals from aqueous solutions: A critical review. *Chemical Engineering Journal*, *366*(352), 608–621. https://doi.org/10.1016/j.cej.2019.02.119

Yaqoob, A. A., Parveen, T., Umar, K., & Mohamad Ibrahim, M. N. (2020). Role of nanomaterials in the treatment of wastewater: A review. *Water*, *12*(2), 495.

Zeng, H., Zeng, H., Zhang, H., Shahab, A., Zhang, K., Lu, Y., Nabi, I., Naseem, F., & Ullah, H. (2021). Efficient adsorption of Cr (VI) from aqueous environments by phosphoric acid activated eucalyptus biochar. *Journal of Cleaner Production*, *286*, 124964. https://doi.org/10.1016/j.jclepro.2020.124964

Zhan, W., Gao, L., Fu, X., Siyal, S. H., Sui, G., & Yang, X. (2018). Green Synthesis of Amino-Functionalized Carbon Nanotube-Graphene Hybrid Aerogels for High Performance Heavy Metal Ions Removal. *Applied Surface Science*. https://doi.org/10.1016/j.apsusc.2018.10.248

Zhang, B., Wu, Y., & Cha, L. (2020). Removal of methyl orange dye using activated biochar derived from pomelo peel wastes: performance, isotherm, and kinetic studies. *Journal of Dispersion Science and Technology*.

Zhang, C. (2024). *Fundamentals of environmental sampling and analysis*. John Wiley & Sons.

Zhang, C., Ma, X., Chen, X., Tian, Y., Zhou, Y., Lu, X., & Huang, T. (2020). Conversion of water hyacinth to value-added fuel via hydrothermal carbonization. *Energy*, *197*, 117193.

Zhang, F., Wang, X., Yin, D., Peng, B., Tan, C., Liu, Y., Tan, X., & Wu, S. (2015). Efficiency and mechanisms of Cd removal from aqueous solution by biochar derived from water hyacinth (Eichornia crassipes). *Journal of Environmental Management*, *153*, 68–73.

https://doi.org/10.1016/j.jenvman.2015.01.043

Zhang, H., Shen, Y., Li, M., Zhu, G., Feng, H., & Li, J. (2019). Egg shell powders-coated membrane for surfactant-stabilized crude oil-in-water emulsions efficient separation. *ACS Sustainable Chemistry & Engineering*, *7*(12), 10880–10887.

Zhang, S., Liu, H., Yin, X., Yu, J., & Ding, B. (2016). Anti-deformed polyacrylonitrile/polysulfone composite membrane with binary structures for effective air filtration. *ACS Applied Materials & Interfaces*, *8*(12), 8086–8095.

Zhang, Y., & Duan, X. (2020). Chemical precipitation of heavy metals from wastewater by using the synthetical magnesium hydroxy carbonate. *Water Science and Technology*, *81*(6), 1130–1136.

Zheng, J., Wang, Z., Ma, J., Xu, S., & Wu, Z. (2018). Development of an electrochemical ceramic membrane filtration system for efficient contaminant removal from waters. *Environmental Science & Technology*, *52*(7), 4117–4126.

Zhou, Q., Yang, N., Li, Y., Ren, B., Ding, X., Bian, H., & Yao, X. (2020). Total concentrations and sources of heavy metal pollution in global river and lake water bodies from 1972 to 2017. *Global Ecology and Conservation*, *22*, e00925.

Zhuang, H., Zhu, H., Zhang, J., Shan, S., Fang, C., Tang, H., & Xie, Q. (2020). Enhanced 2, 4, 6-trichlorophenol anaerobic degradation by Fe3O4 supported on water hyacinth biochar for triggering direct interspecies electron transfer and its use in coal gasification wastewater treatment. *Bioresource Technology*, *296*, 122306.

Zięzio, M., Charmas, B., Jedynak, K., Hawryluk, M., & Kucio, K. (2020). Preparation and

characterization of activated carbons obtained from the waste materials impregnated with phosphoric acid (V). *Applied Nanoscience*, *10*, 4703–4716.

Zotov, R., Meshcheryakov, E., Livanova, A., Minakova, T., Magaev, O., Isupova, L., & Kurzina, I. (2018). Influence of the composition, structure, and physical and chemical properties of aluminium-oxide-based sorbents on water adsorption ability. *Materials*, *11*(1), 132.

Zou, Y., Wang, X., Khan, A., Wang, P., Liu, Y., Alsaedi, A., Hayat, T., & Wang, X. (2016). Environmental Remediation and Application of Nanoscale Zero-Valent Iron and Its Composites for the Removal of Heavy Metal Ions: A Review. *Environmental Science and Technology*, *50*(14), 7290–7304. https://doi.org/10.1021/acs.est.6b01897

APPENDICES

Appendix 1: AAS Calibration Curves for the selected heavy metals

Appendix1a: Calibration curve for Cadmium

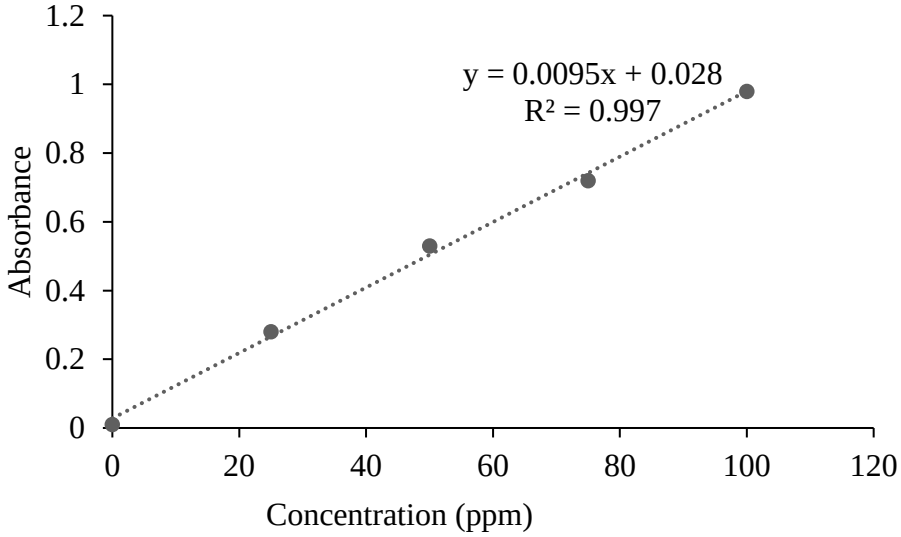

Appendix 1b: Calibration curve for Lead

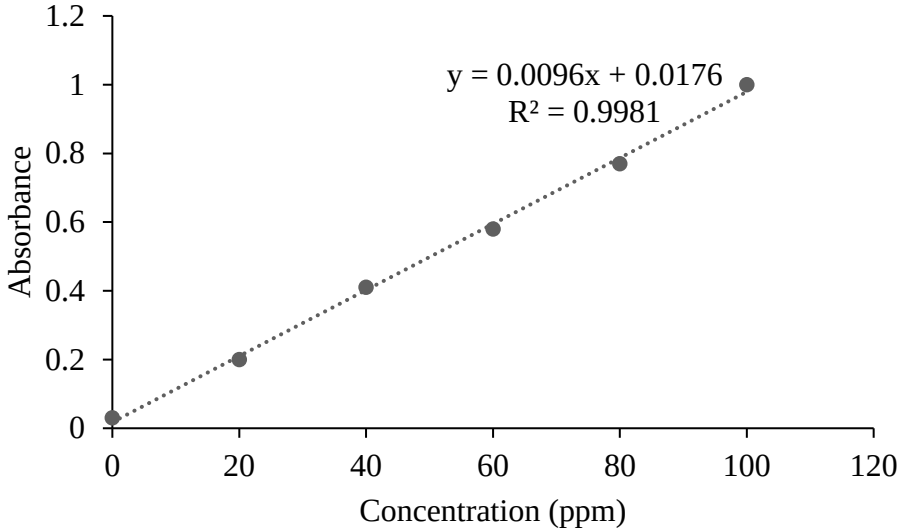

Appendix 1c: Calibration curve for Zinc

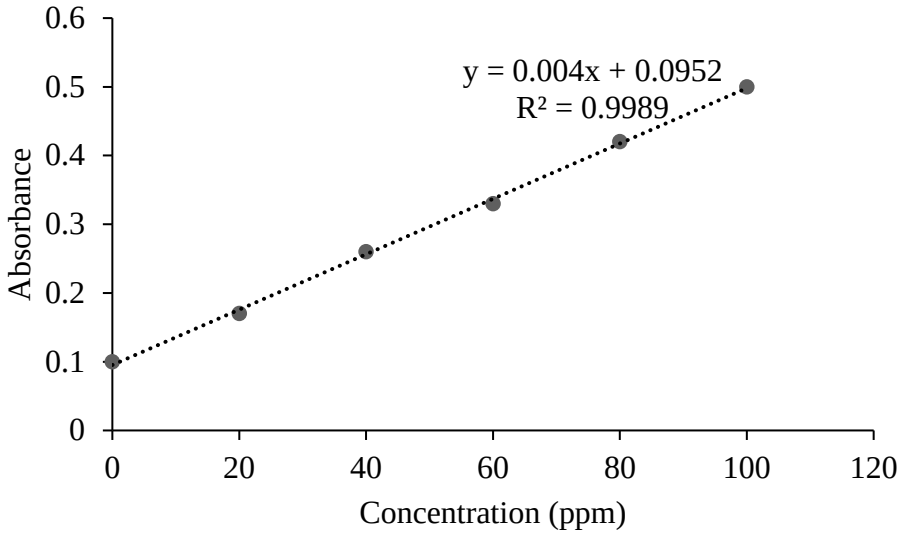

Appendix 1d: Calibration curve for copper

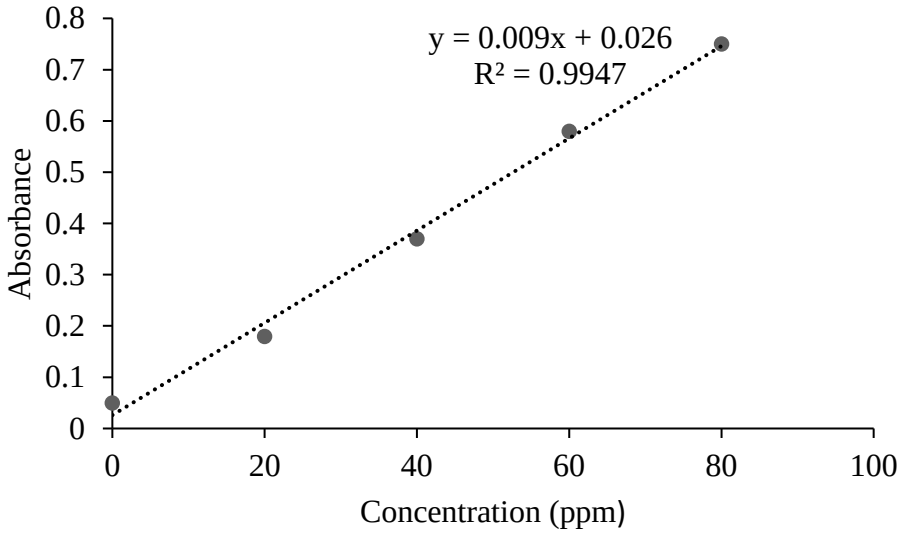

Appendix 1d: Calibration curve for Chromium

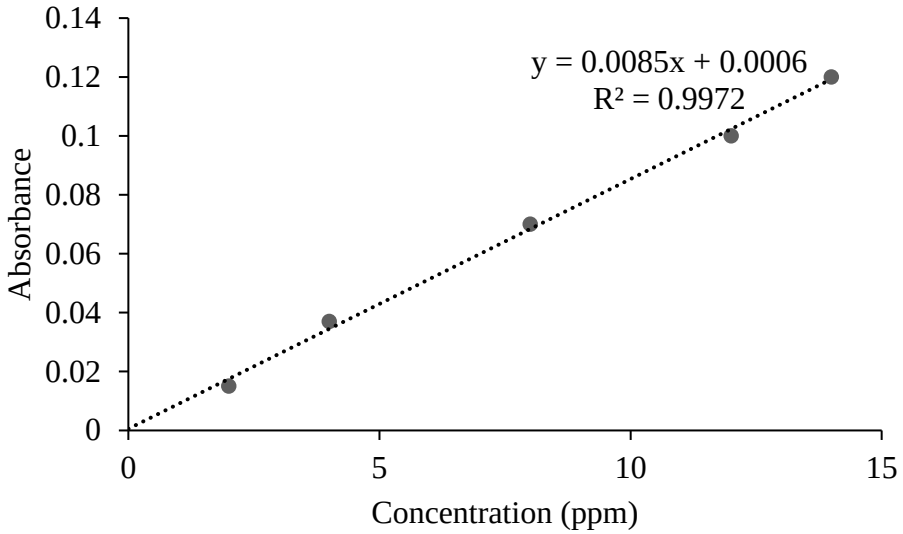

Appendix 2: Effect of adsorbent type

Site	Heavy metal		Adsorbent final concentration (C_1)			Adsorption Efficiency (%)		
		C_o	C_1 (WHB)	C_1(EP-WH)	C_1(EP-WH-PA)	WHB	EP-WH	EP-WH-PA
1	Cd	7.54	1.22	0.96	0.24	83.82	87.27	96.82
	Cr	8.21	1.47	0.72	0.49	82.10	91.23	94.03
	Pb	4.75	0	0	0	100.00	100.00	100.00
	Zn	63.01	20.02	18.92	14.45	68.23	69.97	77.07
	Cu	8.73	1.3	1.08	0.86	85.11	87.63	90.15
2	Cd	40.18	10.47	8.03	6.58	73.94	80.01	83.62
	Cr	13.07	1.97	1.16	0.93	84.93	91.12	92.88
	Pb	72.03	23.4	19.02	17.03	67.51	73.59	76.36
	Zn	84.62	27.98	26.77	24.12	66.93	68.36	71.50
	Cu	54.03	14.62	11.27	10.07	72.94	79.14	81.36
3	Cd	77.13	25.64	20.92	18.24	66.76	72.88	76.35
	Cr	0.54	0	0	0	100.00	100.00	100.00
	Pb	93.54	38.02	36.94	32.84	59.35	60.51	64.89
	Zn	0.91	0	0	0	100.00	100.00	100.00
	Cu	0.64	0	0	0	100.00	100.00	100.00

Appendix 3: Effect of adsorbent particle size on adsorption

Metal	Concentration (ppm)	Adsorption Efficiency (%)	
		300µm	425µm
Cadmium	40.18	83.6	78.4
	7.54	96.8	94.3
	77.13	76.4	66.4
Lead	93.54	64.9	51.9
	72.03	76.4	70.5
	4.75	100	96.4
Zinc	0.91	100	100
	63.01	77.1	67.9
	84.62	71.5	58.0
Copper	0.64	100	100
	8.73	90.1	85.6
	54.03	81.4	72.8
Chromium	0.54	100	100
	8.21	94.0	93.2
	13.07	92.9	90.2

Appendix 3a: Effect of adsorbent particle size on adsorption of Pb^{2+} ions

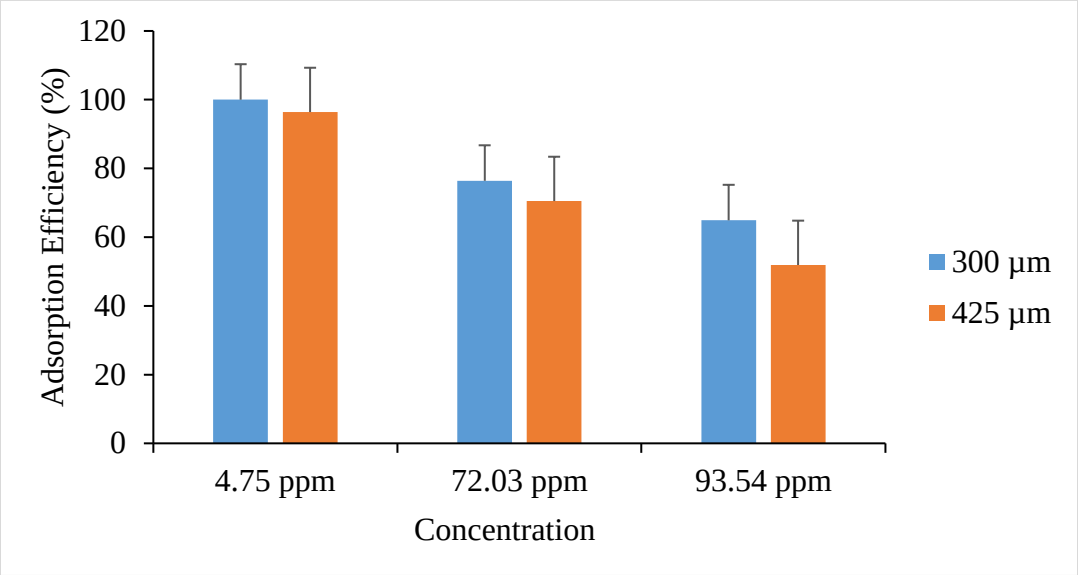

Appendix 3b: Effect of adsorbent particle size on adsorption of Zn^{2+} ions

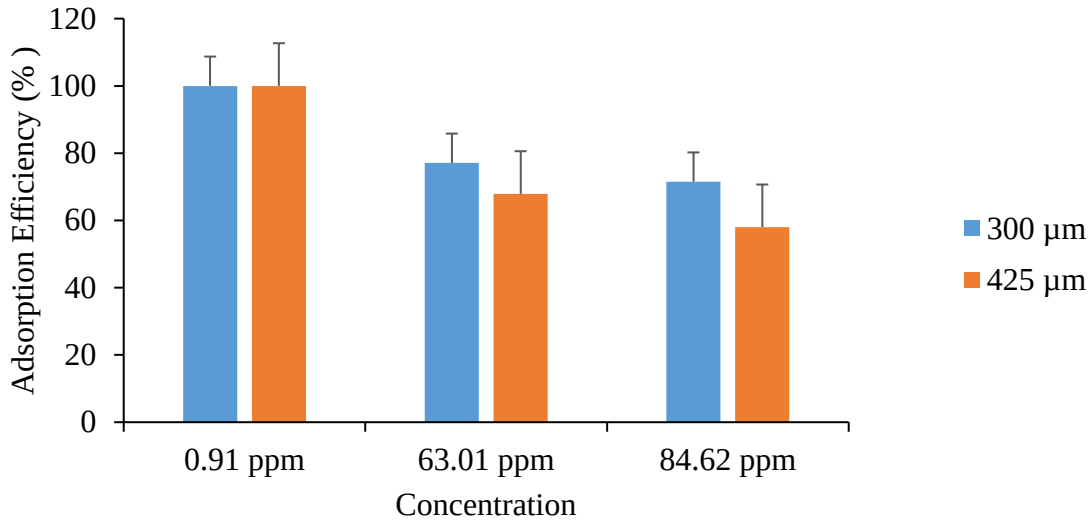

Appendix 3c: Effect of adsorbent particle size on adsorption of Cu^{2+} ions

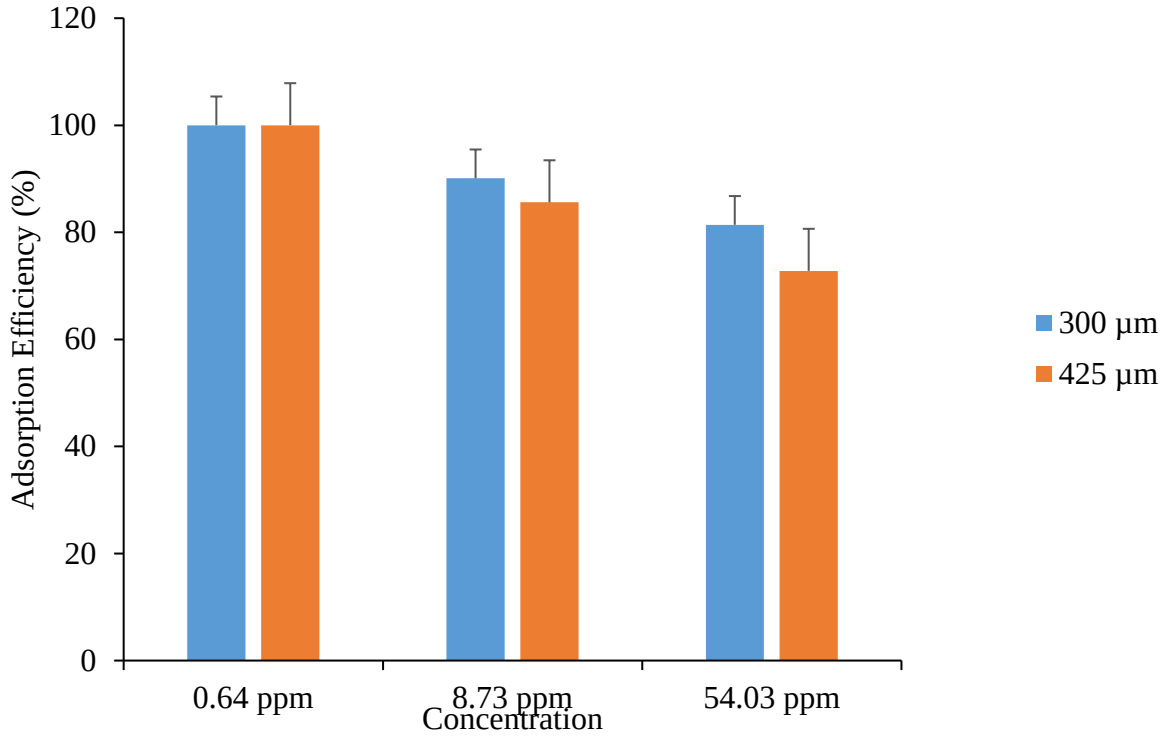

Appendix 3d: Effect of adsorbent particle size on adsorption of Cr^{3+} ions

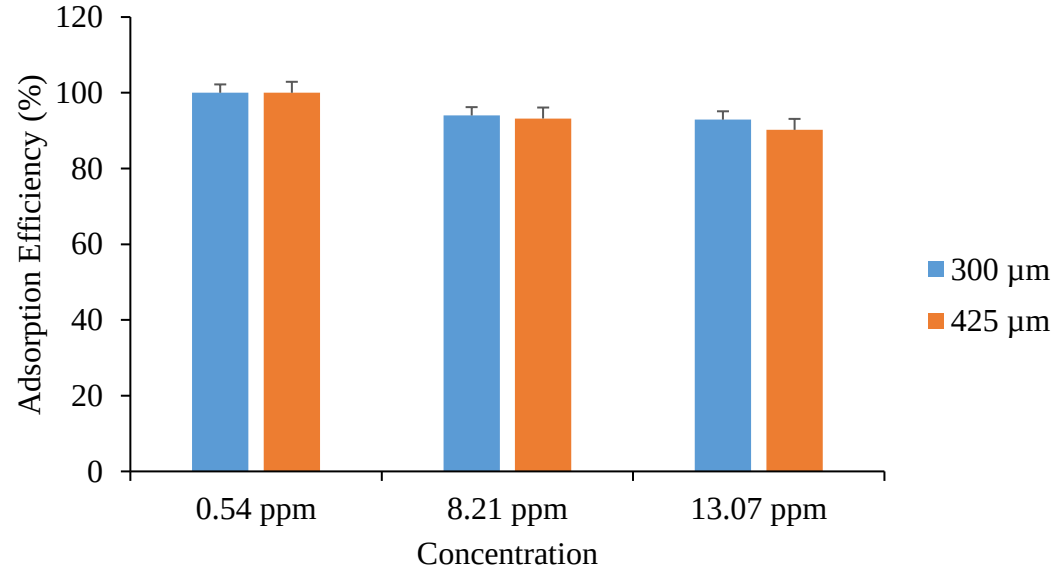

Appendix 4: Effect of pH on adsorption

Metal	Concentration (ppm)	Adsorption Efficiency (%) at a given pH				
		3	4	5	6	7
Cadmium	40.18	61.7	68.6	83.6	83.7	83.6
	7.54	95.8	96.3	96.3	96.8	96.8
	77.13	47.4	56.2	75.9	76.5	76.4
Lead	93.54	51.8	64.9	64.9	64.9	62.9
	72.03	63.8	76.4	76.4	76.4	73.7
	4.75	100	100	100	100	100
Zinc	0.91	100	100	100	100	100
	63.01	51.4	60.9	77.1	77.1	77.1
	84.62	44.8	55.1	71.5	71.5	71.5
Copper	0.64	100	100	100	100	100
	8.73	89.2	90.1	90.1	90.1	88.2
	54.03	74.6	81.4	81.4	81.4	77.3
Chromium	0.54	100	100	100	100	100
	8.21	93.1	94	94	93.9	93.7
	13.07	91.6	92.9	92.9	92.9	92.7

Appendix 4a: Effect of pH on adsorption of Pb^{2+} ions

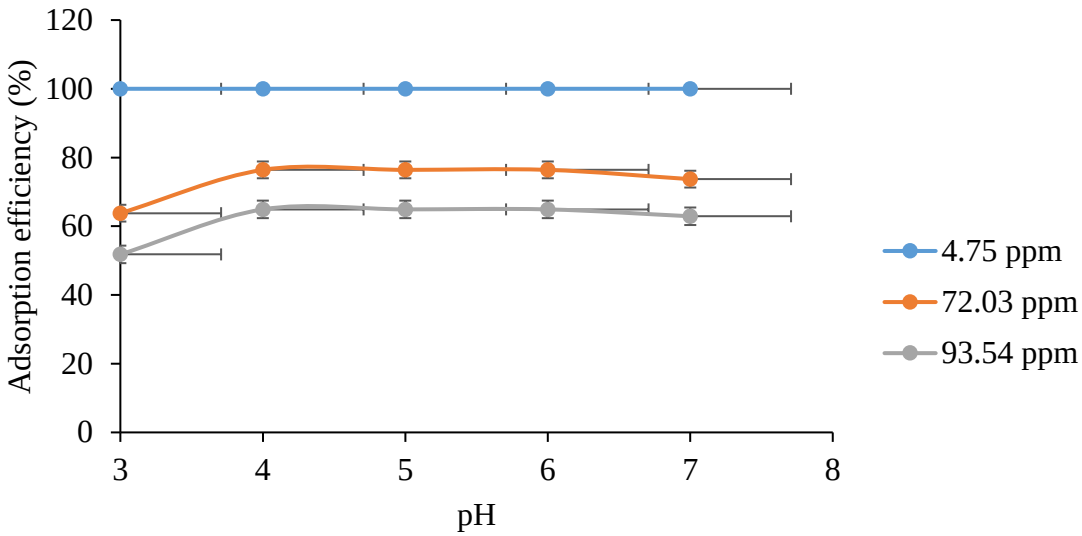

Appendix 4b: Effect of pH on adsorption of Zn^{2+} ions

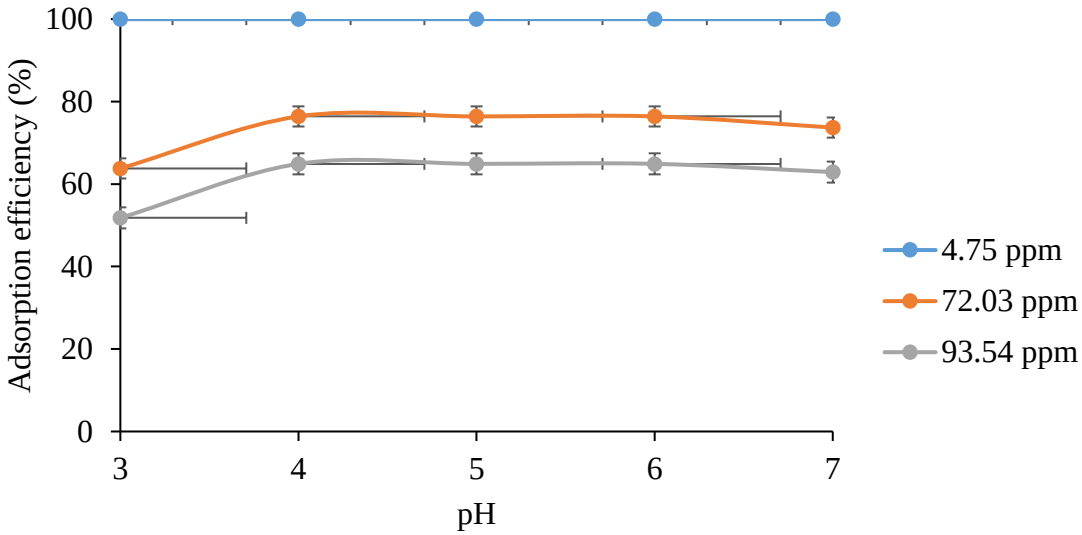

Appendix 4c: Effect of pH on adsorption of Cu^{2+} ions

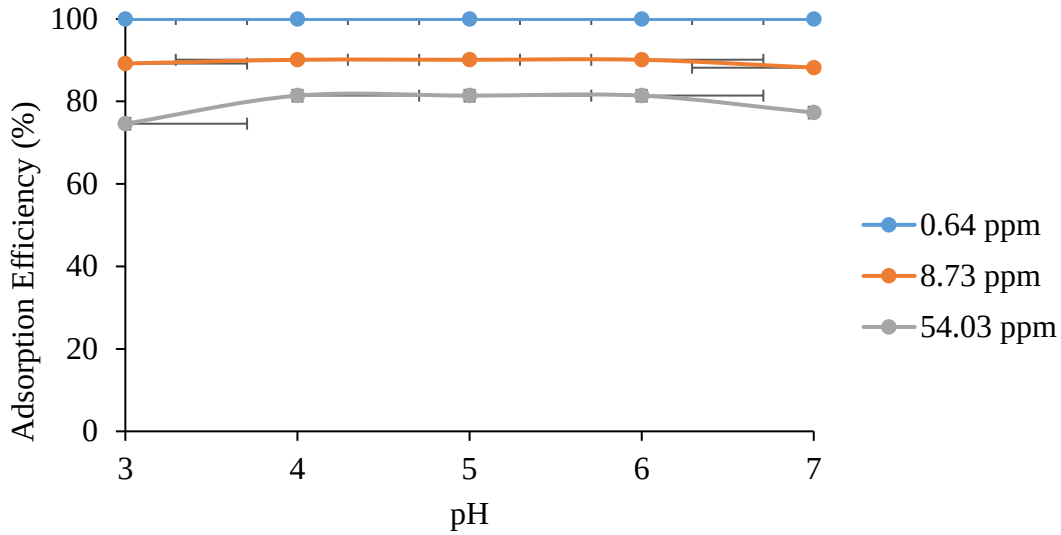

Appendix 4d: Effect of pH on adsorption of Cr^{3+} ions

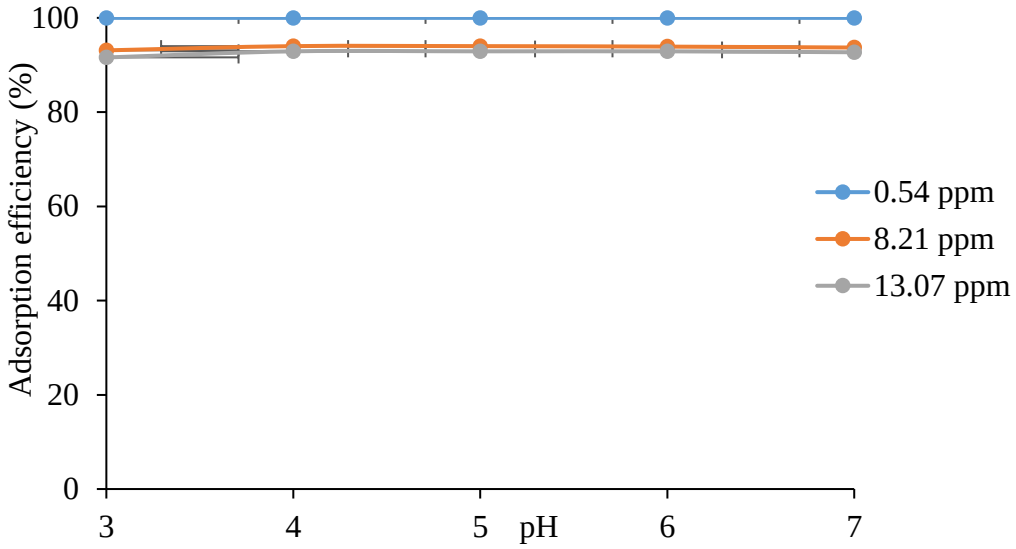

Appendix 5: Effect of contact time.

Metal	Concentration (ppm)	Adsorption Efficiency (%) at a given time												
		0	10	20	30	40	50	60	70	80	90	100	110	120
Cadmium	7.54	0	95.1	96.2	96.8	96.8	96.8	96.8	96.8	96.8	96.8	96.8	96.8	96.8
	40.18	0	53.6	73.9	83.7	83.7	83.7	83.7	83.7	83.7	83.7	83.7	83.7	83.7
	77.13	0	40.7	66.8	76.4	76.4	76.4	76.4	76.4	76.4	76.4	76.4	76.4	76.4
Lead	4.75	0	100	100	100	100	100	100	100	100	100	100	100	100
	72.03	0	76.4	76.4	76.4	76.4	76.4	76.4	76.4	76.4	76.4	76.4	76.4	76.4
	93.54	0	57.7	64.9	64.9	64.9	64.9	64.9	64.9	64.9	64.9	64.9	64.9	64.9
Zinc	0.91	0	100	100	100	100	100	100	100	100	100	100	100	100
	63.01	0	71	74.5	77.1	77.1	77.1	77.1	77.1	77.1	77.1	77.1	77.1	77.1
	84.62	0	61.1	67.3	69.54	71.5	71.5	71.5	71.5	71.5	71.5	71.5	71.5	71.5
Copper	0.64	0	100	100	100	100	100	100	100	100	100	100	100	100
	8.73	0	90.1	90.1	90.3	90.1	90.1	90.1	90.1	90.1	90.1	90.1	90.1	90.1
	54.03	0	71.9	81.4	81.4	81.4	81.4	81.4	81.4	81.4	81.4	81.4	81.4	81.4
Chromium	0.54	0	100	100	100	100	100	100	100	100	100	100	100	100
	8.21	0	89	94	94	94	94	94	94	94	94	94	94	94
	13.07	0	80.1	88.4	90.3	92.9	92.9	92.9	92.9	92.9	92.9	92.9	92.9	92.9

Appendix 5a: Effect of contact time on adsorption of Pb^{2+} ions

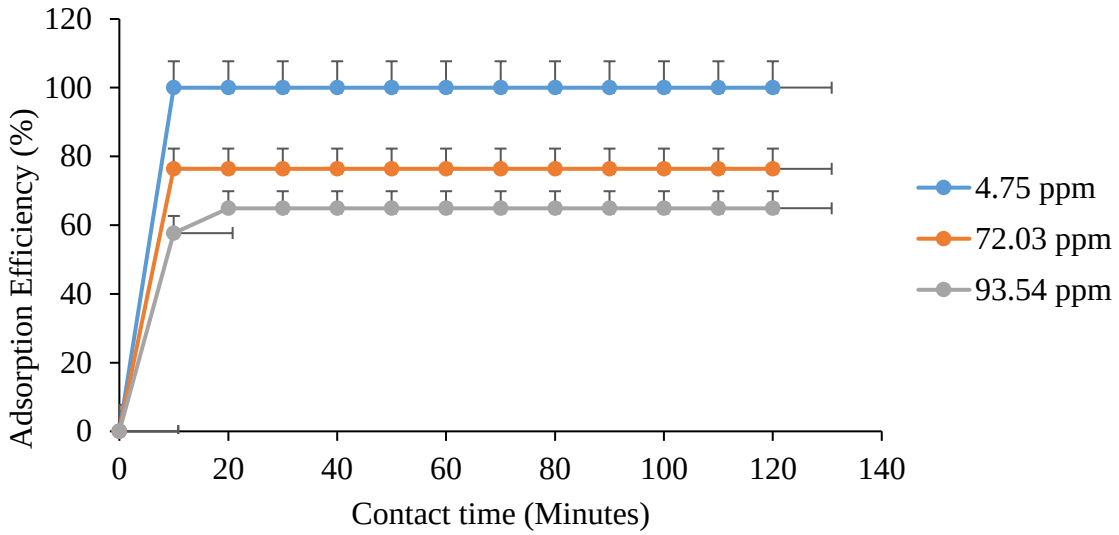

Appendix 5b: Effect of contact time on adsorption of Zn^{2+} ions

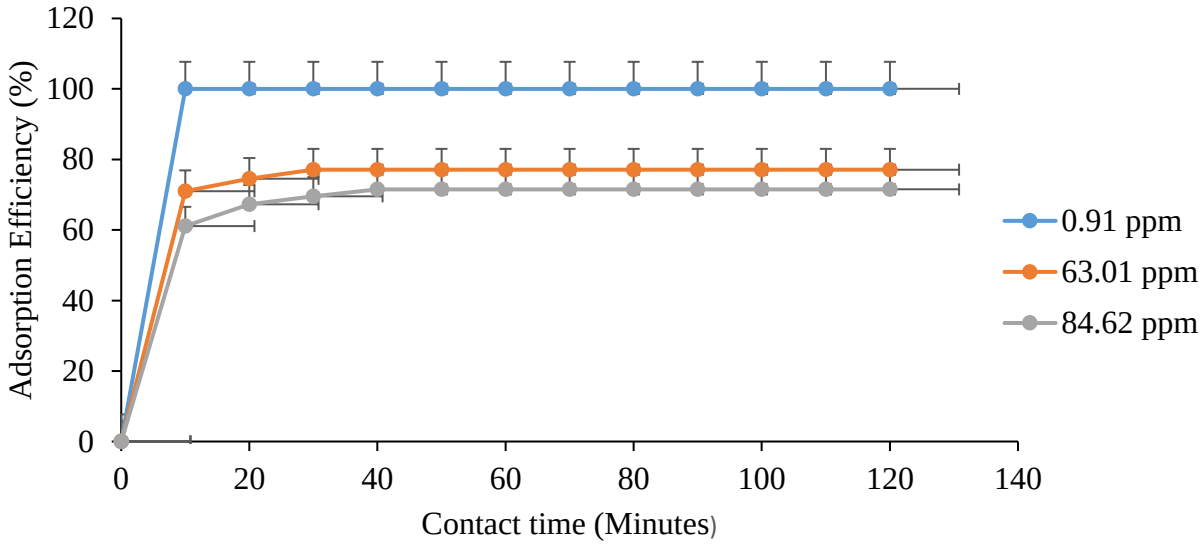

Appendix 5c: Effect of contact time on adsorption of Cu^{2+} ions

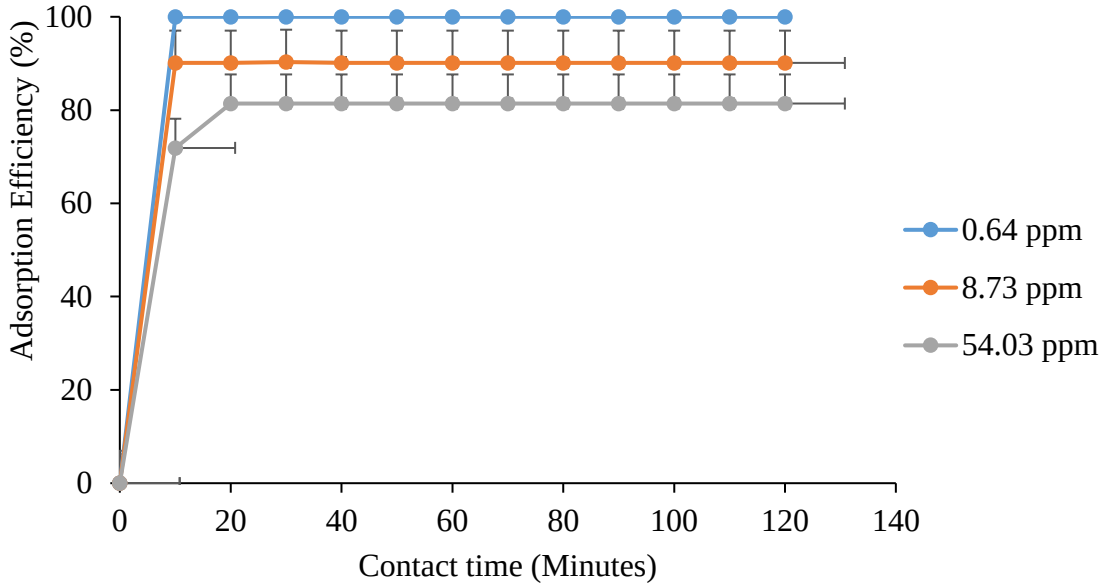

Appendix 5d: Effect of contact time on adsorption of Cr^{3+} ions

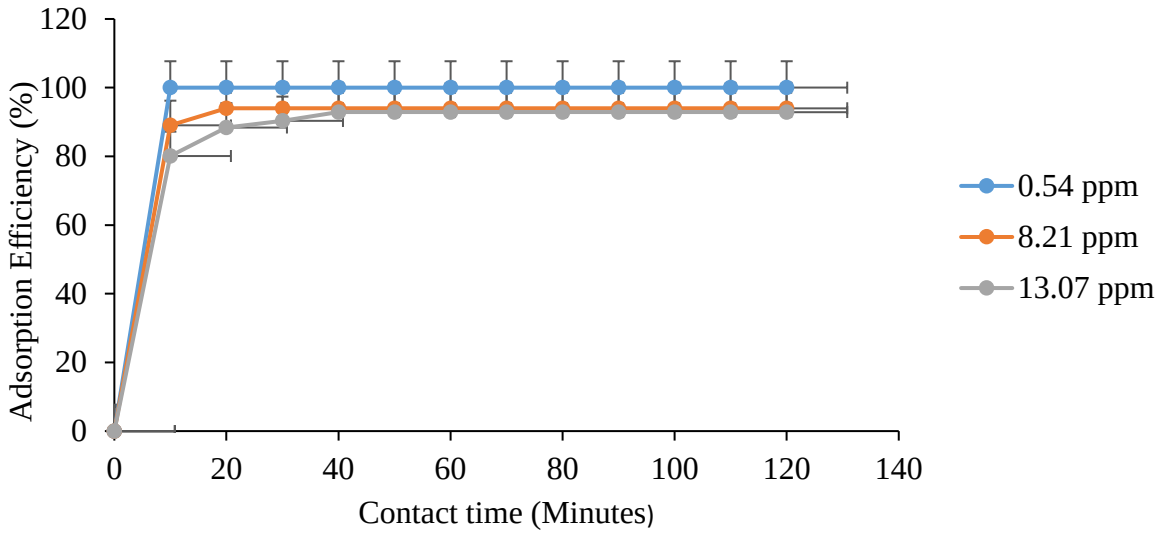

Appendix 6: Effect of adsorbent mass

Metal	Concentration (ppm)	Adsorption Efficiency (%) at a given mass (g)							
		0.25	0.5	0.75	1.0	1.25	1.5	1.75	2.0
Cadmium	7.54	84.5	96.8	100	100	100	100	100	100
	40.18	56.2	83.7	95.4	95.4	95.4	95.4	95.4	95.4
	77.13	43.4	76.4	85	90.2	90.2	90.2	90.2	90.2
Lead	4.75	100	100	100	100	100	100	100	100
	72.03	69.4	76.4	82.4	87.4	87.4	87.4	87.4	87.4
	93.54	49.6	64.9	67.8	71.3	76.8	76.8	76.8	76.8
Zinc	0.91	100	100	100	100	100	100	100	100
	63.01	70.3	77.1	85.6	92.2	92.2	92.2	92.2	92.2
	84.62	65.1	71.5	78.3	83.4	83.4	83.4	83.4	83.4

Copper	0.64	100	100	100	100	100	100	100	100
	8.73	81.6	90.5	100	100	100	100	100	100
	54.03	72.1	81.5	87.1	91.8	91.8	91.8	91.8	91.8
Chromium	0.54	100	100	100	100	100	100	100	100
	8.21	85.4	94	100	100	100	100	100	100
	13.07	80	92.9	900	100	100	100	100	100

Appendix 6a: Effect of adsorbent mass on adsorption of Pb^{2+} ions

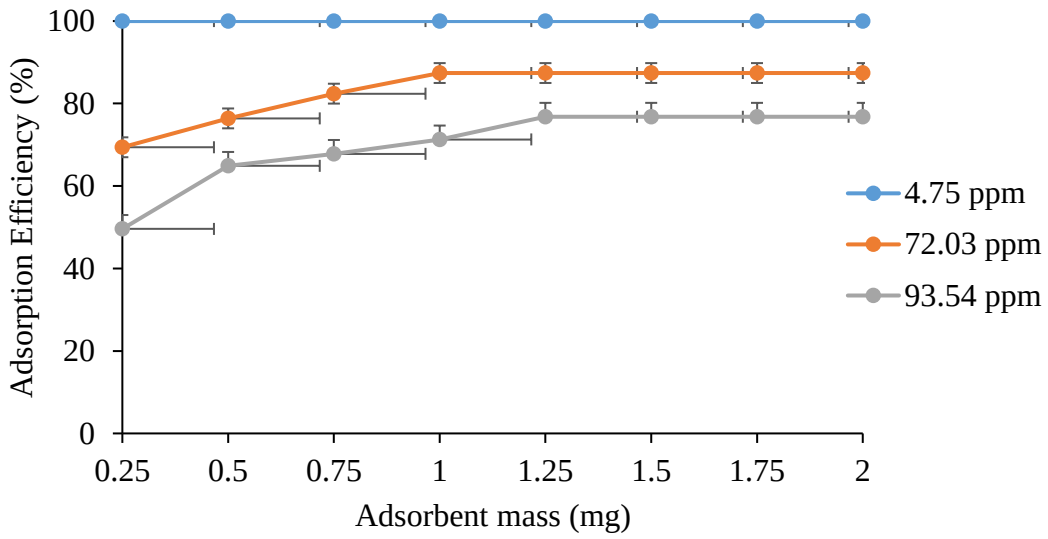

Appendix 6b: Effect of adsorbent mass on adsorption of Zn^{2+} ions

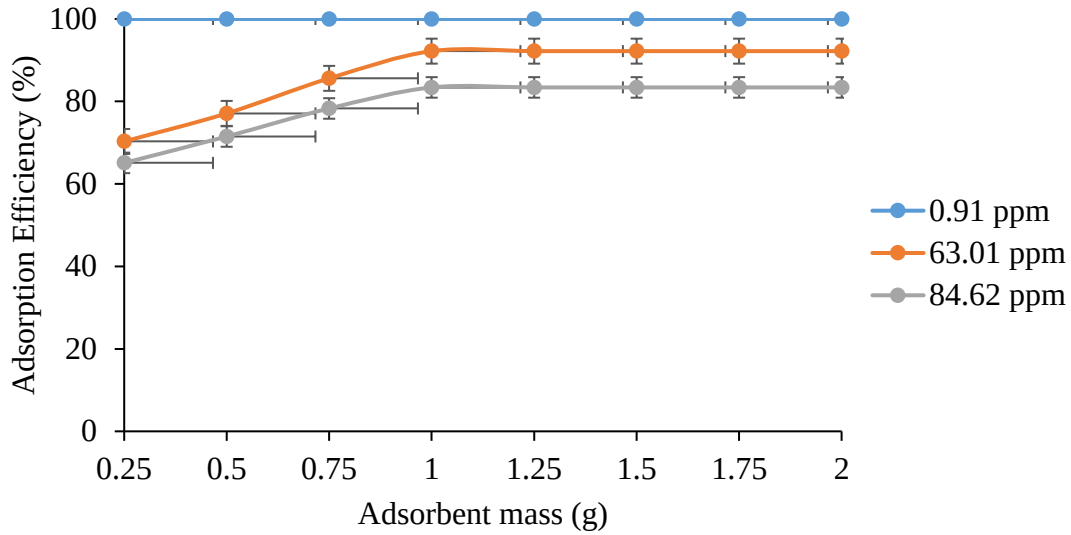

Appendix 6c: Effect of contact time on adsorption of Cu^{2+} ions

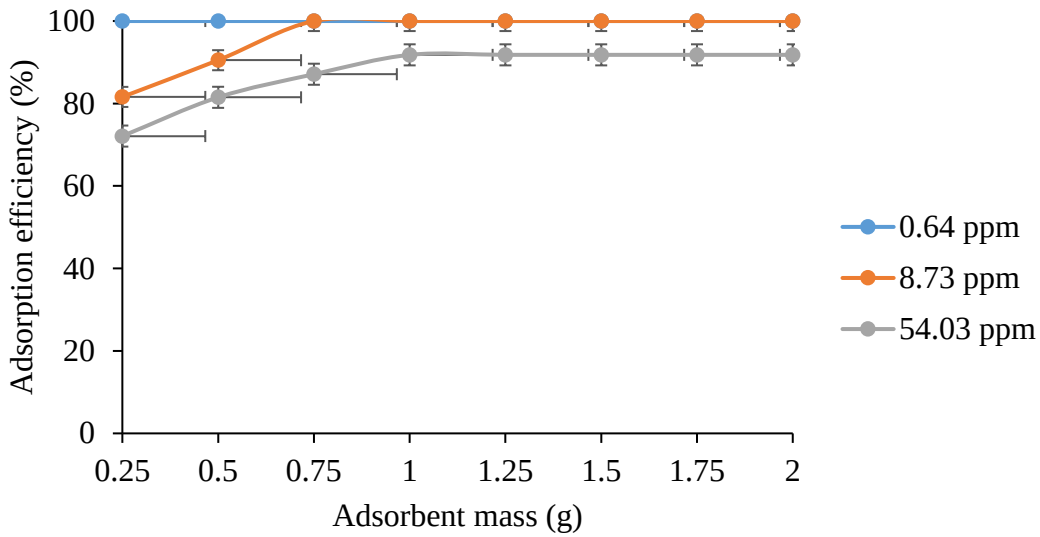

Appendix 6d: Effect of contact time on adsorption of Cr^{3+} ions

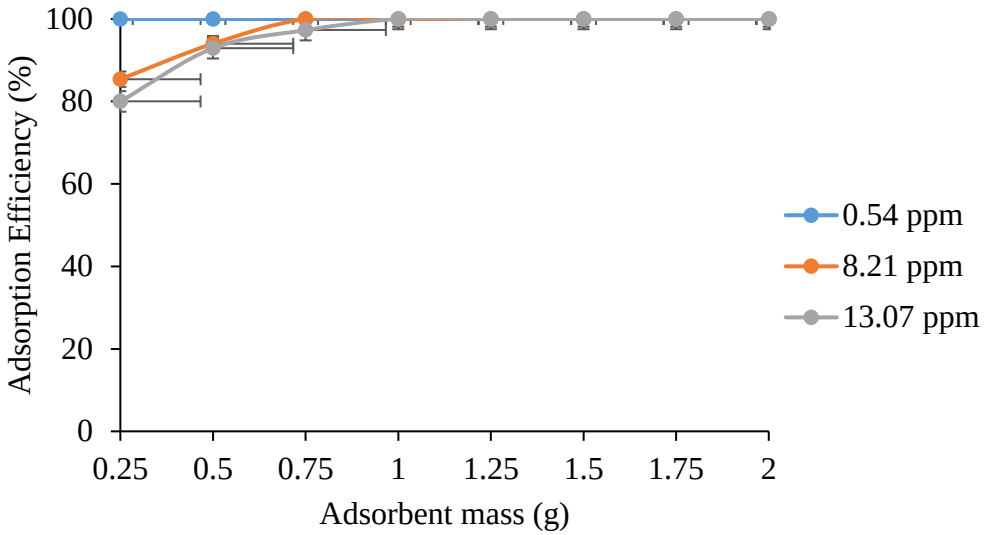

Appendix 7: Equilibrium data for cadmium, lead, zinc, copper and chromium ions

Appendix 7a: Equilibrium data for Cd^{2+} ions adsorption by activated water hyacinth-based adsorbent

C_0	C_e	$\frac{1}{C_e}$	q_e	$\frac{1}{q_e}$	$\log q_e$	$\log C_e$
10	0.43	2.3256	1.914	0.5225	0.2819	-0.3665
20	1.37	0.7299	3.602	0.2776	0.5565	0.1367
40	6.56	0.1524	6.688	0.1495	0.8253	0.8169
60	13.07	0.0765	9.386	0.1065	0.9725	1.1163
80	20.7	0.0483	11.86	0.0843	1.0741	1.3160
100	29.86	0.0334	14.028	0.0713	1.1471	1.4751

Appendix 7b: Equilibrium data for Pb^{2+} ions adsorption by activated water hyacinth-based adsorbent.

C_0	C_e	$\frac{1}{C_e}$	q_e	$\frac{1}{q_e}$	$\log q_e$	$\log C_e$
10	2.13	0.4695	1.574	0.6353	0.197	0.3284
20	4.79	0.2088	3.042	0.3287	0.4832	0.6803
40	9.06	0.1104	6.188	0.1616	0.7916	0.9571
60	14.1	0.0709	9.180	0.1089	0.9628	1.1492
80	23.7	0.0422	11.260	0.0888	1.0515	1.3747
100	34.86	0.0287	13.028	0.0768	1.1149	1.5423

Appendix 7c: Equilibrium data for Zn^{2+} ions adsorption by activated water hyacinth-based adsorbent

C_0	C_e	$\frac{1}{C_e}$	q_e	$\frac{1}{q_e}$	$\log q_e$	$\log C_e$
10	1.24	0.8065	1.752	0.5708	0.2435	0.0934
20	2.95	0.3390	3.41	0.2933	0.5565	0.4698
40	7.05	0.1418	6.59	0.1517	0.8565	0.8482
60	15.07	0.0664	8.986	0.1113	0.9536	1.1781
80	21.69	0.0461	11.662	0.0857	1.0668	1.3363
100	32.72	0.0306	13.456	0.0743	1.1289	1.5148

Appendix 7d: Equilibrium data for Cu^{2+} ions adsorption by activated water hyacinth-based adsorbent

C_0	C_e	$\frac{1}{C_e}$	q_e	$\frac{1}{q_e}$	$\log q_e$	$\log C_e$
10	1.72	0.5814	1.656	0.6039	0.2191	0.2355
20	3.5	0.2857	3.30	0.3030	0.5185	0.5441
40	7.61	0.1314	6.478	0.1544	0.8114	0.8814
60	12.07	0.0829	9.586	0.1043	0.9816	1.0817
80	19.64	0.0509	12.072	0.0828	1.0818	1.2931
100	26.7	0.0375	14.66	0.0682	1.1662	1.4265

Appendix 7e: Equilibrium data for Cr^{3+} ions adsorption by activated water hyacinth-based adsorbent

C_0	C_e	$\frac{1}{C_e}$	q_e	$\frac{1}{q_e}$	$\log q_e$	$\log C_e$
10	0.62	1.6129	1.876	0.5330	0.2732	-0.2076
20	1.2	0.8333	3.760	0.2660	0.5752	0.0792
40	4.07	0.2457	7.186	0.1392	0.8565	0.6096
60	12.61	0.0793	9.478	0.1055	0.9767	1.1007
80	19.98	0.0501	12.004	0.0833	1.0793	1.3006
100	28.79	0.0347	14.242	0.0702	1.1536	1.4592

Appendix 8: Kinetic graphs for Equilibrium data for cadmium, lead, zinc, copper and chromium ions

Appendix 8a: Pseudo first order graphs

Appendix 8a.i: Pseudo first order graphs for Cadmium ions adsorption by activated water hyacinth

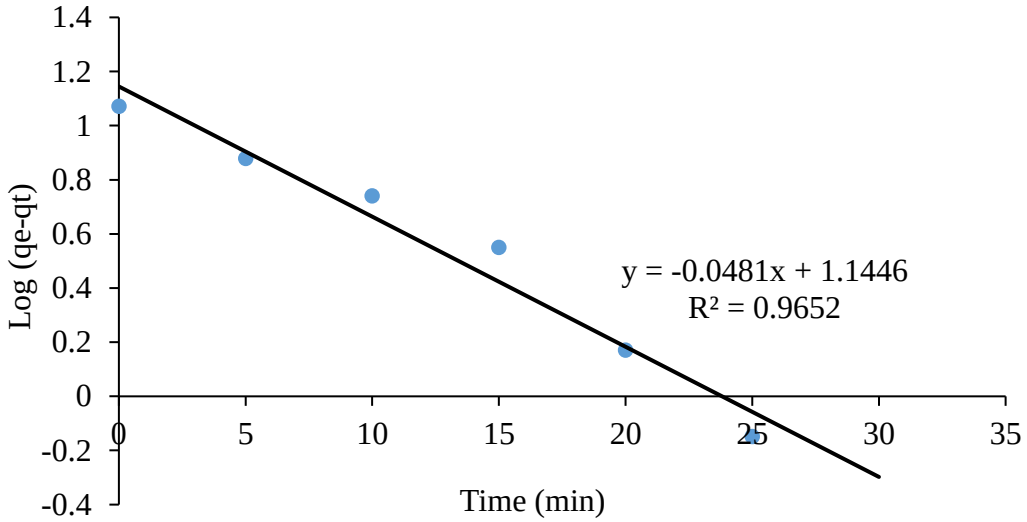

Appendix 8a.ii: Pseudo first order graph for Lead ions adsorption by activated water hyacinth

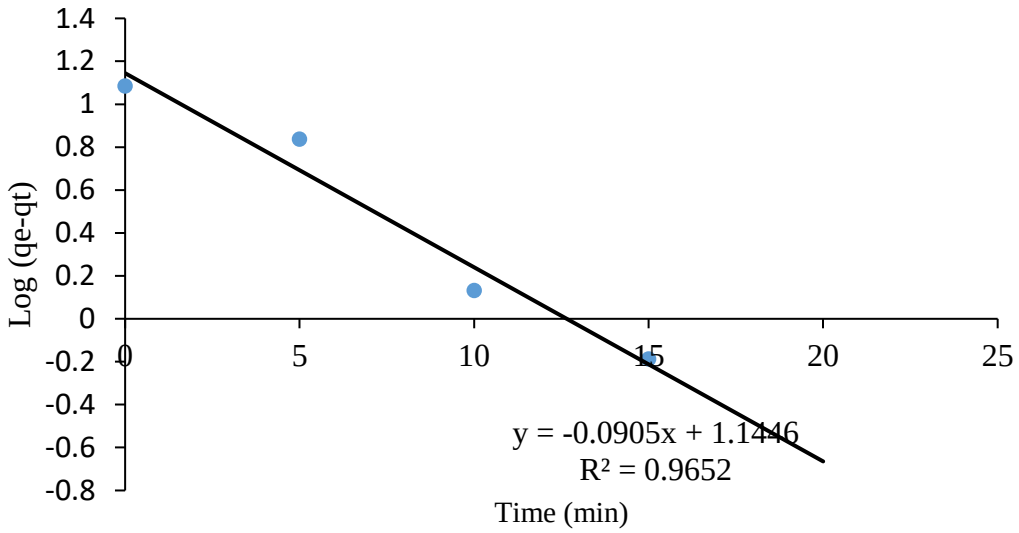

Appendix 8a.iii: Pseudo first order graph for Zinc ions adsorption by activated water hyacinth

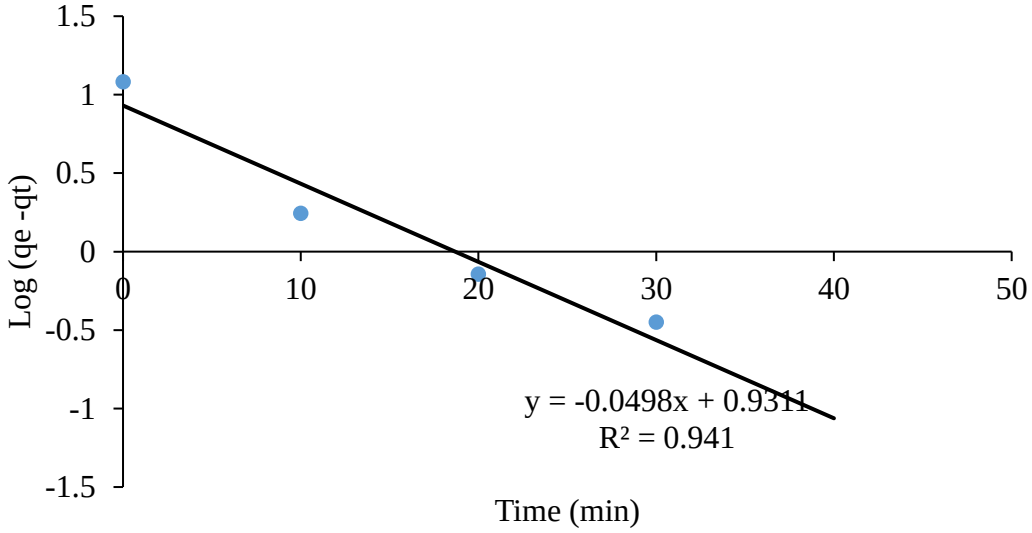

Appendix 8a.iv: Pseudo first order graph for Copper ions adsorption by activated water hyacinth

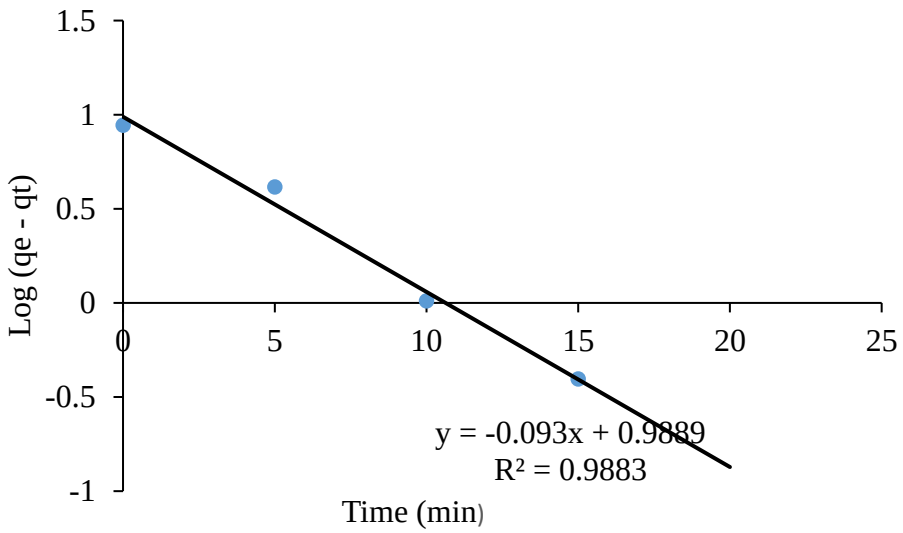

Appendix 8a.v: Pseudo first order graph for Chromium ions adsorption by activated water hyacinth

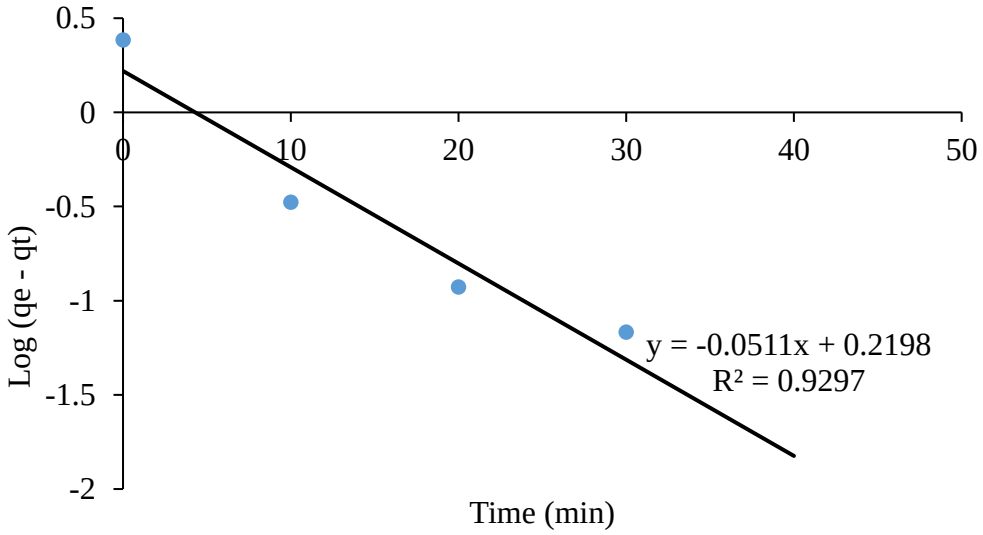

Appendix 8b: Pseudo-second-order graphs

Appendix 8b.i: Pseudo second order graph for Cadmium ions adsorption by activated water hyacinth

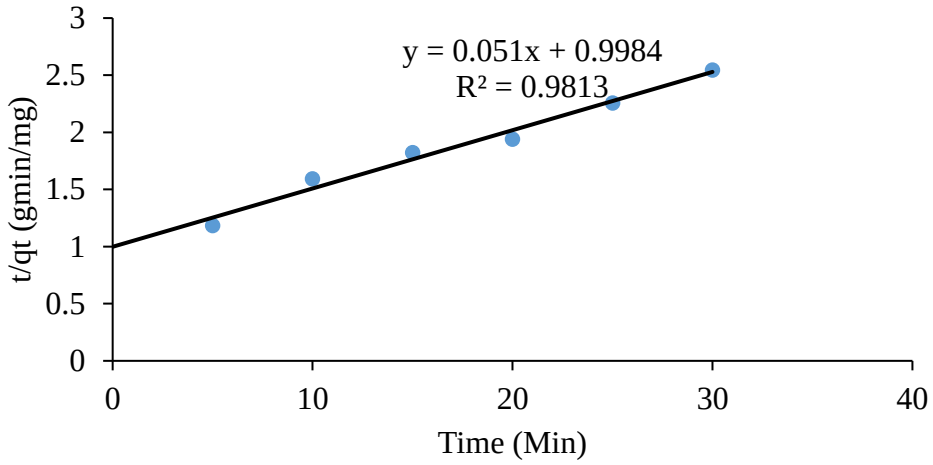

Appendix 8b.ii: Pseudo second order graph for Lead ions adsorption by activated water hyacinth

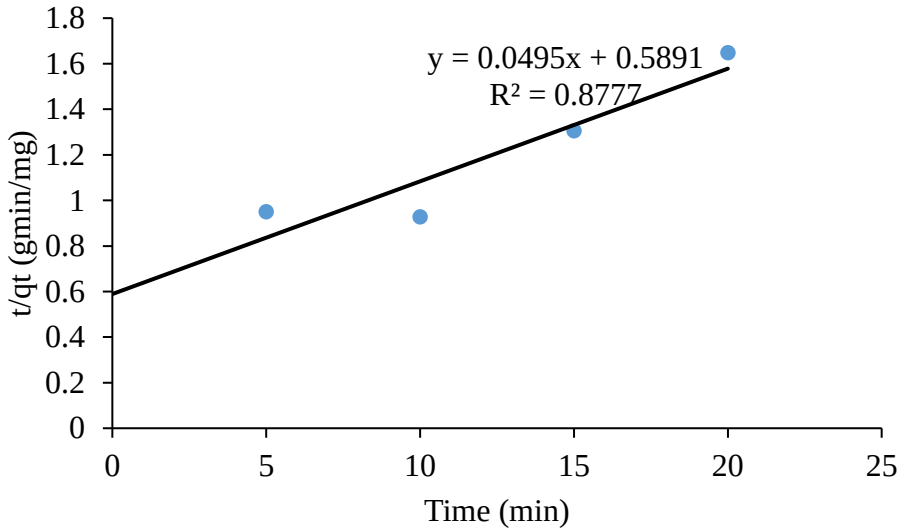

Appendix 8b.iii: Pseudo second order graph for Zinc ions adsorption by activated water hyacinth

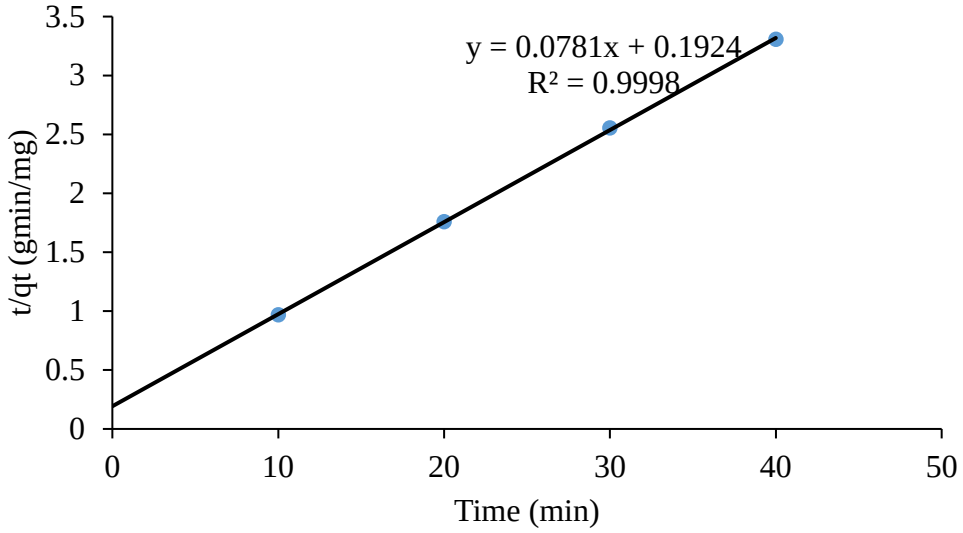

Appendix 8b.iv: Pseudo second order graph for Copper ions adsorption by activated water hyacinth

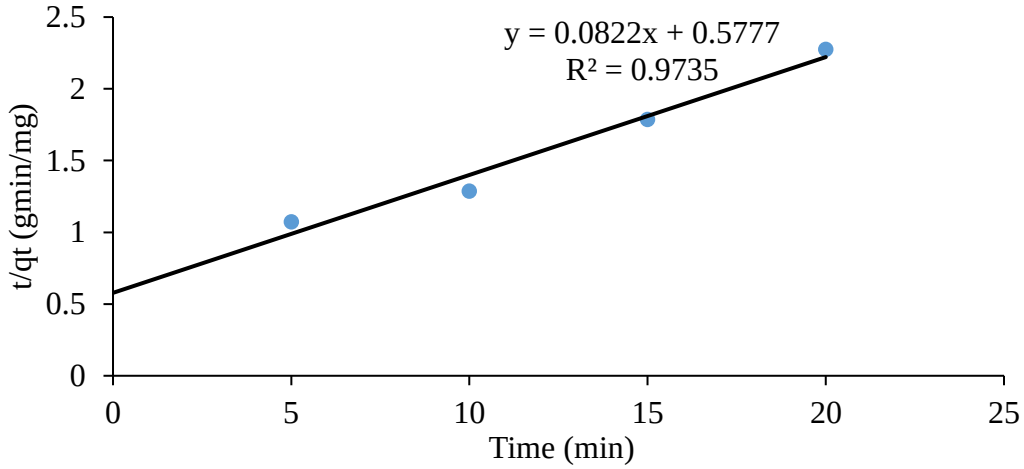

Appendix 8b.v: Pseudo second order graph for Chromium ions adsorption by activated water hyacinth

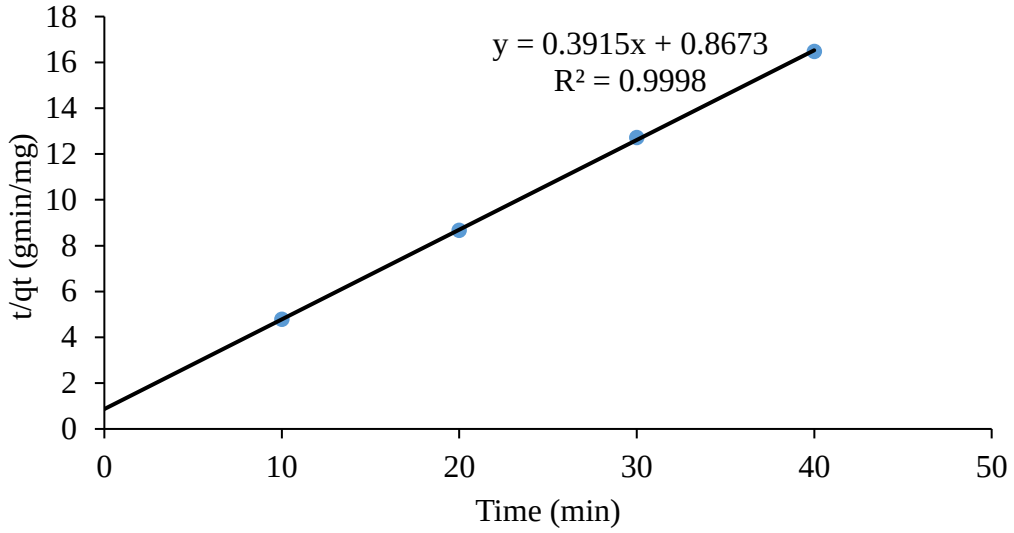

Appendix 9: Equilibrium data for Cd^{2+}, Pb^{2+}, Zn^{2+}, Cu^{2+} and Cr^{3+} ions

Appendix 9a: Equilibrium data for Cd^{2+} ions adsorption

Time	C_0	C_t	M	V	q_t	q_e	$q_e - q_t$	$\log(q_e - q_t)$	$\frac{t}{q_t}$
0	77.13	77.13	0.5	0.1	0	11.78	11.78	1.0711	Error
5	77.13	56.01	0.5	0.1	4.22	11.78	7.56	0.8785	1.1848
10	77.13	45.73	0.5	0.1	6.28	11.78	5.5	0.7404	1.5924
15	77.13	36	0.5	0.1	8.23	11.78	3.55	0.5502	1.8226
20	77.13	25.61	0.5	0.1	10.30	11.78	1.48	0.1703	1.9417
25	77.13	21.79	0.5	0.1	11.07	11.78	0.71	-0.1487	2.2584
30	77.13	18.24	0.5	0.1	11.78	11.78	0.00	Error	2.5467

Appendix 9b: Equilibrium data for Pb^{2+} ions adsorption

Time	C_0	C_t	M	V	q_t	q_e	$q_e - q_t$	$\log(q_e - q_t)$	$\frac{t}{q_t}$
0	93.54	93.54	0.5	0.1	0	12.14	12.14	1.0842	Error
5	93.54	67.2	0.5	0.1	5.268	12.14	6.872	0.8371	0.9491
10	93.54	39.61	0.5	0.1	10.786	12.14	1.354	0.1316	0.9273
15	93.54	36.08	0.5	0.1	11.492	12.14	0.648	-0.1884	1.3053
20	93.54	32.84	0.5	0.1	12.14	12.14	0	Error	1.6474

Appendix 9c: Equilibrium data for Zn^{2+} ions adsorption

Time	C_0	C_t	M	V	q_t	q_e	$q_e - q_t$	$\log(q_e - q_t)$	$\frac{t}{q_t}$
0	84.62	84.62	0.5	0.1	0	12.1	12.1	1.0828	Error
10	84.62	32.9	0.5	0.1	10.344	12.1	1.756	0.2445	0.9667
20	84.62	27.71	0.5	0.1	11.382	12.1	0.718	-0.1439	1.7572
30	84.62	25.9	0.5	0.1	11.744	12.1	0.356	-0.4486	2.5545
40	84.62	24.12	0.5	0.1	12.1	12.1	0	Error	3.3058

Appendix 9d: Equilibrium data for Cu^{2+} ions adsorption

Time	C_0	C_t	M	V	q_t	q_e	$q_e - q_t$	$log(q_e - q_t)$	$\frac{t}{q_t}$
0	54.03	54.03	0.5	0.1	0	8.792	8.792	0.9441	Error
5	54.03	30.7	0.5	0.1	4.666	8.792	4.126	0.6155	1.0716

10	54.03	15.18	0.5	0.1	7.77	8.792	1.022	0.0095	1.2870
15	54.03	12.04	0.5	0.1	8.398	8.792	0.394	-0.4045	1.7861
20	54.03	10.07	0.5	0.1	8.792	8.792	0	Error	2.2748

Appendix 9e: Equilibrium data for Cr^{3+} ions adsorption

Time	C_0	C_t	M	V	q_t	q_e	$q_e - q_t$	$\log(q_e - q_t)$	$\frac{t}{q_t}$
0	13.07	13.07	0.5	0.1	0	2.428	2.428	0.3852	Error
10	13.07	2.6	0.5	0.1	2.094	2.428	0.334	-0.4763	4.775549
20	13.07	1.52	0.5	0.1	2.31	2.428	0.118	-0.9281	8.658009
30	13.07	1.27	0.5	0.1	2.36	2.428	0.068	-1.1675	12.71186
40	13.07	0.93	0.5	0.1	2.428	2.428	0	Error	16.47446

Appendix 10.1: FTIR Spectrum for Water hyacinth biochar (WHB)

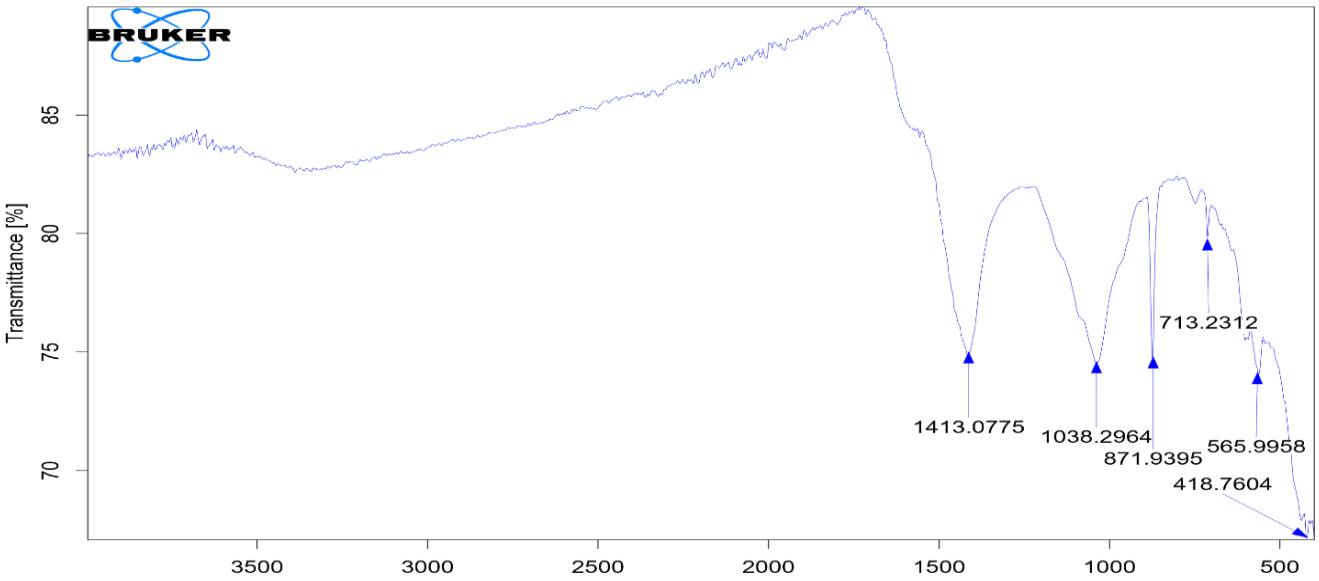

Appendix 10.2: FTIR Spectrum for Eggshell powder treated water hyacinth (EP-WH)

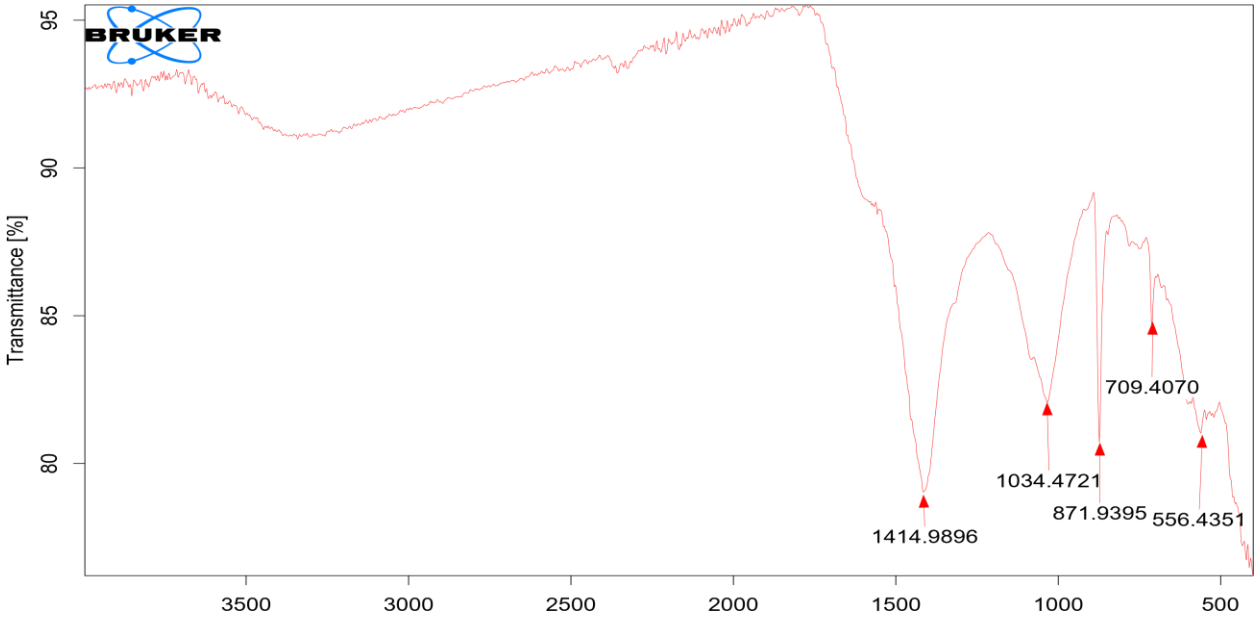

Appendix 10.3: FTIR Spectrum for double-activated water hyacinth (EP-WH-PA)

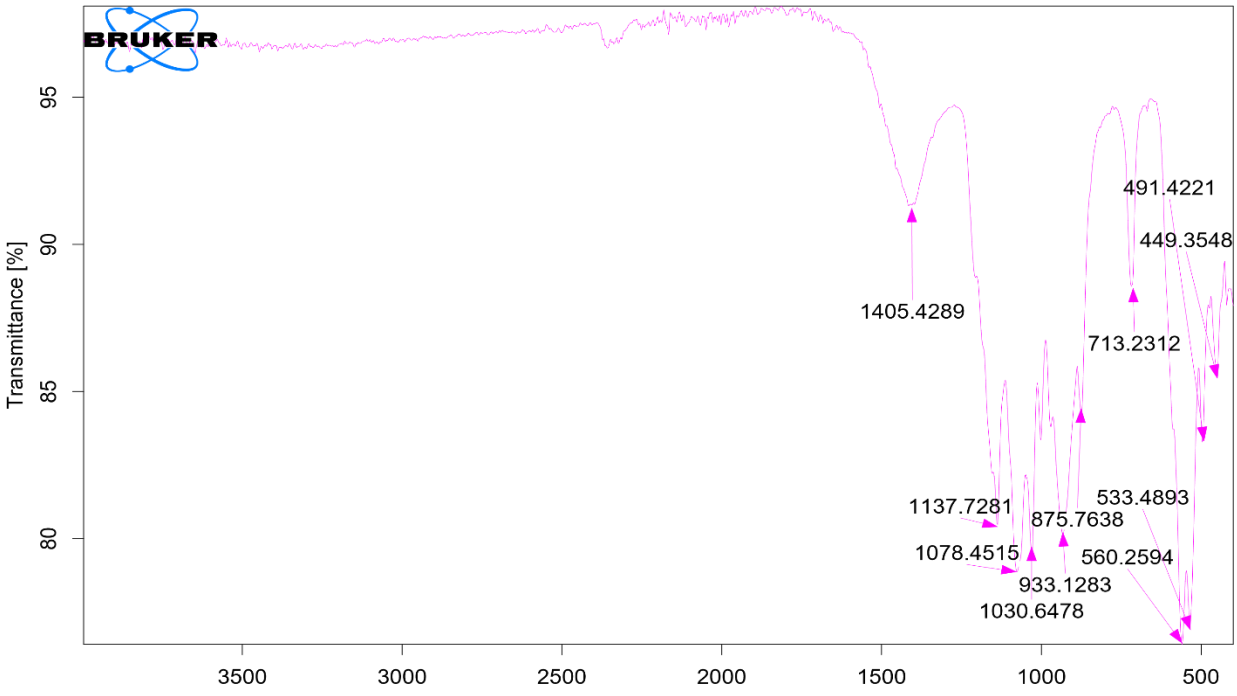

Appendix 10.4: FTIR Spectra after adsorption of selected metal ions